1-1-2012

Three Dimensional Elasticity Analyses for Isotropic and Orthotropic Composite Cylinders

Wenchao Wang

THREE DIMENSIONAL ELASTICITY ANALYSES FOR ISOTROPIC AND ORTHOTROPIC COMPOSITE CYLINDERS

By

Wenchao Wang

A Dissertation
Submitted to the Faculty of
Mississippi State University
in Partial Fulfillment of the Requirements
for the Degree of Doctorate of Philosophy
in Mechanical Engineering
in the Department of Mechanical Engineering

Mississippi State, Mississippi

May 2012

THREE DIMENSIONAL ELASTICITY ANALYSES FOR ISOTROPIC AND

ORTHOTROPIC COMPOSITE CYLINDERS

By

Wenchao Wang

Approved:

Haitham El Kadiri Assistant Professor of Mechanical Engineering Major Professor	Mohamad S. Qatu Professor of Mechanical Engineering Dissertation Director
Rani Warsi Sullivan Associate Professor of Aerospace Engineering Committee	Oliver Myers Assistant Professor of Mechanical Engineering Committee
Youssef Hammi Research Professor of CAVS Committee	
David L. Marcum Professor of Mechanical Engineering Graduate Coordinator	Sarah A. Rajala Professor of Electrical and Computer Engineer Dean of the Bagley College

Name: Wenchao Wang

Date of Degree: May 12, 2012

Institution: Mississippi State University

Major Field: Mechanical Engineering

Major Professor: Dr. Haitham El Kadiri

Title of Study: THREE DIMENSIONAL ELASTICITY ANALYSES FOR ISOTROPIC AND ORTHOTROPIC COMPOSITE CYLINDERS

Pages in Study: 104

Candidate for Degree of Doctorate of Philosophy

The demand for using shell theories comes from its efficiency in computational and analytical cost. On another side, new materials that are orthotropic and/or anisotropic in nature are discovered and broadly used in many fields. Many advanced shell theories are developed for these new materials, particularly in the recent decades. A study about the accuracy of these shell theories is very meaningful to build confidence in them for further applications. This study requires a precise benchmark against which shell theories can be tested. This is the main research subjective in this dissertation: to build a set of solutions using the three dimensional (3D) theory of elasticity against which shell theories can be tested for accuracy. The contents of this dissertation to support this research include a comprehensive literature review for the shell theories and recent usage and to find the gaps which need to be filled. These gaps include, among others, the lack of studies on the accuracy of the theories used and the absence of results using the 3D theory, particularly for orthotropic materials. Some of these studies are conducted here. The deficiency of some commercial finite element packages is discussed here. The reasons for the absence of accurate results are investigated. The 3D theory and analyses

of isotropic and orthotropic materials of hollow cylinders is investigated here for reliable results.

DEDICATION

To my wife Taosha Jiang and my son Logan Wang

ACKNOWLEDGEMENTS

My sincerely gratitude to Dr. Qatu. He is not only my advisor but also my mentor. In these years, he provided a great stage for me to broaden my vision. He devoted many efforts to me. I hope I could be better just for rewarding his support.

My sincerely gratitude to Dr. Yarahmadian.His great personality gives me so many positive impacts. Without his help, I couldn't have made a breakthrough on the power series solution.

TABLE OF CONTENTS

Page

DEDICATION ii

ACKNOWLEDGEMENTS iii

LIST OF TABLES vi

LIST OF FIGURES viii

CHAPTER

I. INTRODUCTION 1

1.1 Background and application 1
1.2 Benchmark and accuracy study 4
1.3 The major contributions of this thesis 6

II. LITERATURE REVIEW 8

2.1 Background and structure of this chapter 8
2.2 Shell theories [147] 10
2.2.1 Three-dimensional elasticity theory 11
2.2.2 Thick shell theory 15
2.2.2.1 Higher order shell theories 22
2.2.2.2 Layer-wise shell theories 22
2.2.3 Thin-shell theory 23
2.2.4 Free vibration 27
2.2.5 Rotating shells 28
2.2.6 Impact loading 29
2.2.7 Dynamic stability 30
2.2.8 General dynamic behavior 31
2.3 Accuracy study for shell theories in vibration study 32

III. 3D ELASTICITY OF ISOTROPIC HOLLOW CYLINDERS AND RELATED STUDIESONTHICK SHELL THEORY AND FEA 35

3.1 Background 35
3.1.1 Mathematical model: the fundamental three equations 36

3.1.2 Boundary conditions and the solution procedures 39
3.2 Finite element analysis 41
3.3 Accuracy study and results comparison 43

IV. 3D ELASTICITY FOR ORTHOTROPIC HOLLOW CYLINDERS AND CORRESPONDING STUDIES 52

4.1 3D elasticity theory of orthotropic hollow cylinder 52
4.2 The general solutions of the Frobenius' Theorem 56
4.2.1 Feasibility 56
4.2.2 Solution procedures 58
4.2.3 Acquiring the natural frequency 63
4.3 Multiple layers orthogonal hollow cylinders 64
4.4 Finite element analyses for orthotropic hollow cylinder 65
4.5 Results and discussion 66
4.5.1 The challenges from indicial roots 66
4.5.2 The normal condition (no repeated roots) 69
4.5.3 The study of the oscillation 74
4.5.3.1 Convergence study 74
4.5.3.2 Oscillation study 77
4.5.4 The comparison with FEA 86
4.5.5 The limitation for material properties of powerseries method 88

V. CONCLUSION 90

5.1 Engineering contributions 90
5.2 Theoretical contribution 91

LIST OF TABLES

TABLE Page

3.1 Frequency parameters for cylindrical thin shells using 3D elasticity solution, R/h = 20, ν = 0.3 44

3.2 Frequency parameters for thick cylinders using 3D elasticity solution (ν 0.3)....44

3.3 A comparison table for frequencies (Hz) of a isotropiccylindrical shell with thickness 0.1 m, R = 1 m, ℓ = 8 m, E = 200 X 10^9 Pa, ν = 0.3....45

3.4 A comparison table for1 m, ℓ = 8 m, E = 200 X 10^9 Pa, ν = 0.3....46

3.5 A comparison table for frequencies (Hz) of a isotropiccylindrical shells, R = 1 m, ℓ = 8 m, E = 200 X 10^9 Pa, ν = 0.3, A 160×124× 4 mesh 48

3.6 A comparison table for frequencies (Hz) of a isotropiccylindrical shells, R = 1 m, ℓ = 8 m, E = 200 X 10^9 Pa, ν = 0.3, A 160×124× 4 mesh 48

3.7 A comparison table for frequencies (Hz) of a isotropiccylindrical shell with thickness 0.1 m, R = 0.95 m, ℓ = 8 m, E = 200 X 10^9 Pa, ν = 0.3 using different shell element options in ABAQUS® 50

3.8 A comparison table for frequencies (Hz) of a isotropiccylindrical shell with thickness 0.2 m, R = 0.9 m, ℓ = 8 m, E = 200 X 10^9 Pa, ν = 0.3 using different shell element options in ABAQUS® 50

4.1 The study of Srinvas' results....70

4.2 The natural frequecy comparison with the hollow cylinder structure: outside radius 1m, inside 0.8m, length 2m....87

4.3 The natural frequecy comparison with the hollow cylinder structure: outside radius 1m, inside 0.7m, length 2m....87

4.4 The natural frequecy comparison with the hollow cylinder structure: outside radius 1m, inside 0.6m, length 2m....87

4.5 The natural frequecy comparison with the hollow cylinder structure: outside radius 1m, inside 0.6m, length 4m.....87

4.6 The natural frequecy comparison with the hollow cylinder structure for the real orthogonal material.....89

LIST OF FIGURES

FIGURE		Page
1.1	Blood vessel	2
1.2	Hollow shafts	2
1.3	Rifle barrel	3
1.4	The accuracy flow for modeling a real problem in Elasticity	5
2.1	Stress in shell coordinates (free outer surfaces).	12
2.2	Lamination parameters in shells	13
2.3	Force resultants in shell coordinates	19
2.4	Moment resultants in shell coordinates	20
3.1	The cylindrical coordinate system for thick hollow cylinder;	36
3.2	Circular cylinder and corresponding coordinates	37
3.3	The dimensions of the 0.1 m thick shell cylinder FEA model	42
3.4	The mode shapes pictures of 0.2 thickness model	43
4.1	The oscillation behavior of results in the first grid table 4.1	71
4.2	The oscillation behavior of results in the second grid table 4.1	72
4.3	The magnified picture of figure 4.2	72
4.4	The oscillation behavior of results in the third grid table 4.1	73
4.5	The magnified picture of figure 4.4	73
4.6	The convergency study	75
4.7	The magnified picture of figure 4.6	75

4.8 The magnified picture of figure 4.7 76
4.9 The convergency study for different parameters....76
4.10 The oscillation behaviors when m=10 77
4.11 The oscillation behaviors when m=9 78
4.12 The oscillation behaviors when m=8 78
4.13 The oscillation behaviors when m=7 79
4.14 The oscillation behaviors when m=6 79
4.15 The oscillation behaviors when m=5 80
4.16 The oscillation behaviors when n=2....80
4.17 The oscillation behaviors when n=3....81
4.18 The oscillation behaviors when n=4....81
4.19 The oscillation behaviors when n=15....81
4.20 The oscillation behaviors when the density ρ=0.5....83
4.21 The oscillation behaviors when the density ρ=1....83
4.22 The oscillation behaviors when the density ρ=2....84
4.23 The oscillation behaviors when the density ρ=4....84
4.24 The oscillation behaviors when the density ρ=9....84
4.25 The oscillation behaviors when the density ρ=15....85
5.1 The illustration for the demanding of advanced shell theories to apply in the FEA 91

CHAPTER I

INTRODUCTION

1.1 Background and application

Cylinders and cylindrical shell-like structures are broadly used in many real world applications and manufactured accordingly. For example, in the biology field, the structure of the micro-organisms are often pipes and cylinders. As shown in Figure 1.1, the blood vessel is a thick, multi-layered cylinder. For other applications, like in the automotive field, the exhaust pipes, the shaft systems (half shafts, drivelines, etc) and many other components and parts are also cylinders or cylindrical structures. Figure 1.2 shows a series of hollow shafts encoders for motors. Another example is the rifle barrel shown in Figure 1.3; which is also a high precision manufacturing thick hollow cylinder. A common characteristic of these examples is that they are thick cylindrical components. The relative thick nature of the tubing system requires special treatment that considers the implications of such a thick tube.

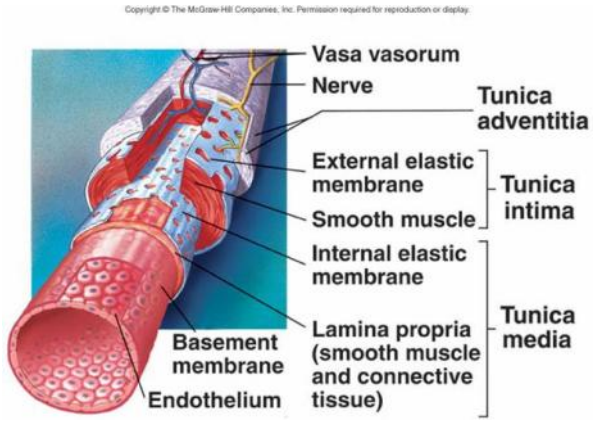

Figure 1.1 Blood vessel

Figure 1.2 Hollow shafts

Figure 1.3 Rifle barrel

For these thick shells, some theories become inaccurate due to the used assumptions. . These include thin shell theories. In addition, many cylindrical structures are made of complex material, like laminated composite or biomaterial, requiring discussion of the existing theories or even developing new ones to obtain a higher level of accuracy. This has been the subject of significant research. The book "VIBRATION OF LAMINATED SHELLS AND PLATES" focusing on research done between 1989 and 2000 yielded approximately 400 papers on composite shell dynamics [1]. Additional surveys showed even more research since then.

Besides mechanics and theoretical development, a method that is more directly used in the analysis of such structures in industrial applications is the finite element analysis (FEA). FEA benefits from the fast-developing computer technology since the 1970s. An advantage to using FEA is its flexibility in treatment of complex structures. FEA can be applied on a vast number of different boundary conditions, external applied conditions, structural geometries and many other different design parameters.

Many commercial packages are developed and broadly used, such as Nastran®, Abaqus®, ANSYS® and others. From all possible theoretical descriptions or mechanics,

FEA element developers usually select one suitable theory to develop the element they are interested in and solve real problems. The question is then raised about the accuracy of the theory chosen and the standards to which the accuracy can be measured. The benchmark to the accuracy of various finite element analyses and various shell theories is highly needed. This need not only come from strong necessity but also from comprehensive apprehension. An example is Kadi's [146] work comparing thin shell theories in his thesis (1970),which was subsequently published in the book "THE VIBRATION OF SHELLS" by Leissa [3] in 1973. This kind of comparison is not only required for developing accurate theories for benchmarking, but is also required to deeply understand other theoretical and numerical methods like FEA. This dissertation could be a prelude to the important benchmarking research work needed on more complex materials and thick shell theories.

1.2 Benchmark and accuracy study

Three-dimensional elasticity is chosen as the benchmark in this study. For a clearer explanation, see Figure 1.4 below.

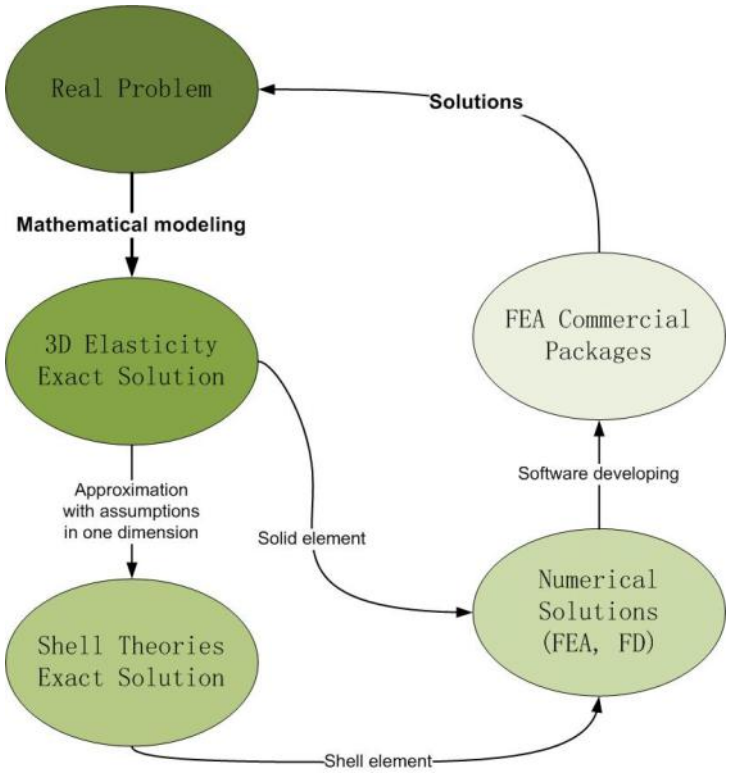

Figure 1.4 The accuracy flow for modeling a real problem in Elasticity

In this figure, the color difference indicates the level of accuracy in the analysis of the real problem (dark green). In other words, the color gradually becoming lighter represents how the inaccuracy grows. To solve the real problem, the first step is theoretical (mathematical) modeling, which converts the physical problem to a mathematical model with controllable parameters. In linear solid mechanics, the fundamental mathematical model is the one developed based on three-dimensional (3D) elasticity theory. It is the classical and original, as well as the most accurate theory for representing the elastic deformation. It is, however, complex and often difficult to use for solving real problems. Subsequently, most solid mechanics theories are developed from this 3D elasticity theory with different approximating assumptions for simplifying it. For example, shell theories assume one of the three dimensions to be small. The necessity for

the simplification comes from the difficulty of obtaining exact solutions from the 3D elasticity equations. These equations are mostly composed of a system of partial differential equations (PDE). However, because of the intrinsic complexity of the PDE system, even with various physical assumptions and mathematical technologies under complex boundary conditions and structures, exact solutions could not be achieved. In this circumstance, numerical methods are used for obtaining numerical solutions for practical use. Examples of numerical methods include the finite difference method (FDM), the Ritz method, the finite element methods (FEM). Of course, numerical solutions are not exact. In solid mechanics, the most successful numerical method appears to be FEM. Different theoretical models are applied in different types of elements (e.g. shell elements). Several commercial FEA packages with solvers of the resulting algebraic equations exist. From the above description, the real physical problem, like NVH (noise, vibration and harshness) problems in automotive industries, could be better modeled by a more accurate mathematical modeling. The accuracy of these solutions will directly impact the quality of solving the industrial problems. In order to benchmark the accuracy of various analyses, the exact solution of 3D elasticity is needed. Under some types of boundary conditions by using crafty mathematical technologies the exact solutioncould be obtained, a special model needs to be built here.

1.3 The major contributions of this thesis

The following contributions are made in this dissertation:

i. A literature review for the 3D elasticity and thick shell theories which have been developed in recent years.

ii. The exact solution of 3D elasticity isotropic hollow cylinders is developed and tested for various parameters.

iii. The exact solution of 3D elasticity isotropic hollow cylinders is used as a benchmark to compare exact results from various shell theories and the commercial FEA package Abaqus®.

iv. The exact solution of 3D elasticity orthotropic hollow cylinders is developed and tested for various parameters.

The content structure will follow the above points. Chapter 2 will present contribution I. Chapter 3 will discuss contributions II and III as for isotropic material. Chapter 4 will exhibit and analyses the contribution IV for the composite material cases. Chapter 5 will summarize these works and show how much progress has been made as a prelude to further research.

CHAPTER II

LITERATURE REVIEW

2.1 Background and structure of this chapter

The increased usage of laminated composite shells in many engineering applications has generated much interest in composite shell behavior. While very little attention was given to composite shell vibration four decades ago [6], a recent article [2] listed about 400 papers on the subject.

When compared to traditional metallic materials, laminated composites offer advantages such as higher strength-to-weight and stiffness-to-weight ratios, improved chemical and environmental resistance, and the ability to tailor properties. Additionally, the advances in composite manufacturing methods have also contributed to the increased usage of laminated composite materials in many modern applications. Composite shells now constitute a large percentage of aerospace, marine and automotive structures. Literature on composite shell vibration research can be found in many of the national and international conferences and journals. Review articles such as those by Qatu [2,4], Kapania [7], Noor and Burton [8,9], and Noor et al. [10] covered much of the research done on the subject prior to the early 1990s. Liew et al. [11] reviewed the literature on shallow shell vibrations. Soldatos [12] reviewed the literature on non-circular cylindrical shells. Computational aspects of the research were covered by Noor et al. [13] and Noor and Venneri [14]. Recently, Carerra [15,16] presented a historical review of zig-zag

theories for multilayered plates and shells and reviewed the theories and finite elements for multilayered, anisotropic, composite plates and shells.

It should be mentioned that several books appeared on the subject of laminated shells during the past decade. Qatu [1] treats the vibrations of laminated shells and plates and Soedel [17] deals with vibrations of composite shells and plates. Reddy [18] focuses on stress analysis and general mechanics of laminated composite plates and shells. Ye [19] and Lee [20] focus on the modeling of composite shells and Shen [21] discusses non-linear analysis of functionally graded materials.

This article aims to present a broad perspective of the recent research (2000-2009) done on the dynamics of composite shells. Different types of dynamic analyses such as free vibrations, transient analysis, impact, shock and other dynamic analyses are included. Additionally, typically used shell theories (thin, or classical, and thick shell theories, including shear deformation and three-dimensional theories, shallow and deep theories, linear and non-linear theories, and others) are reviewed. Most theories are classified based on the thickness ratio of the shell being treated (defined as the ratio of the thickness of the shell to the shortest of the span lengths and/or radii of curvature), its shallowness ratio (defined as the ratio of the shortest span length to one of the radii of curvature) and the magnitude of deformation (compared mainly to its thickness).

The literature is collated and categorized based on various aspects of research. First, a general overview regarding shell theories is presented. Discussion will then focus on shell geometries that are typically used, such as the classical cylindrical, conical and spherical shells of revolution as well as shallow shells.

The second aspect will concentrate on types of analyses which are typically performed: free vibration with various boundary conditions and shell geometries,

rotating shells, transient, impact and shock loading, dynamic stability and general dynamic behavior. The third aspect of this review will focus on material-related complexities, which include piezoelectric materials, viscoelastic or viscoplastic materials with damping, braided materials and shape memory alloys, and thermoplastic or wood material. The fourth category of interest in this paper will focus on structural-related complexities which include stiffened shells, shells with cut-outs, fluid filled or submerged shells and shells with imperfections. Attention will also be given to multi-scale analysis, sensitivity and robustness, and optimization studies that may prove useful to design engineers.

Many articles may be cited more than once in this survey. For example, a research article that uses a shear deformation shell theory to solve a conical shell dynamic problem can be cited under the thick shell theory title of shell theories section, as well as under the conical shells title of the shell geometries section. [147]

2.2 Shell theories [147]

Shells are three-dimensional bodies bounded by two, relatively close, curved surfaces. The three-dimensional equations of elasticity are complicated when written in curvilinear or shell coordinates. Typically, researchers make simplifying assumptions for particular applications. Almost all shell theories (thin and thick, deep and shallow) reduce the three-dimensional (3D) elasticity equations to the two-dimensional (2D) representation. This is done usually by eliminating the coordinate normal to the shell surface in the development of the shell equations. The accuracy of thin and thick shell theories can be established if these theories are compared to the 3D theory of elasticity.

A summary of equations for laminated composite shells is made in this section. In particular, the strain-displacement equations, the stress-strain equations and the equations of motion are described. These equations and the associated boundary conditions constitute a complete set of shell theory equations.

2.2.1 Three-dimensional elasticity theory

A shell is a three-dimensional body confined by two parallel (unless the thickness is varying) surfaces. In general, the distance between those surfaces is small compared with other shell parameters. In this section, the equations from the theory of 3D elasticity in curvilinear coordinates are presented. The literature regarding vibrations of laminated shells using 3D elasticity theory will then be reviewed.

Consider a shell element of thickness h, radii of curvature R_α and R_β(a radius of twist $R_{\alpha\beta}$axial not shown here) (Figure 2.1). Assume that the deformation of the shell is small compared to the shell dimensions. This assumption allows us to neglect non-linear terms in the subsequent derivation. It will also allow us to refer the analysis to the original configuration of the shell. The strain displacement relations can be written as [1]:

$$\varepsilon_\alpha = \frac{1}{(1+z/R_\alpha)}\left(\frac{1}{A}\frac{\partial u}{\partial \alpha}+\frac{v}{AB}\frac{\partial A}{\partial \beta}+\frac{w}{R_\alpha}\right) \tag{2.1}$$

$$\varepsilon_\beta = \frac{1}{(1+z/R_\beta)}\left(\frac{1}{B}\frac{\partial v}{\partial \beta}+\frac{u}{AB}\frac{\partial B}{\partial \alpha}+\frac{w}{R_\beta}\right) \tag{2.2}$$

$$\varepsilon_z = \frac{\partial w}{\partial z} \tag{2.3}$$

$$\gamma_{\alpha\beta} = \frac{1}{(1+z/R_\alpha)}\left(\frac{1}{A}\frac{\partial v}{\partial \alpha}-\frac{u}{AB}\frac{\partial A}{\partial \beta}+\frac{w}{R_{\alpha\beta}}\right)+\frac{1}{(1+z/R_\beta)}\left(\frac{1}{B}\frac{\partial u}{\partial \beta}-\frac{v}{AB}\frac{\partial B}{\partial \alpha}+\frac{w}{R_{\alpha\beta}}\right) \tag{2.4}$$

$$\gamma_{\alpha z} = \frac{1}{A(1+z/R_\alpha)}\frac{\partial w}{\partial \alpha}+A(1+z/R_\alpha)\frac{\partial}{\partial z}\left(\frac{u}{A(1+z/R_\alpha)}\right)-\frac{v}{R_{\alpha\beta}(1+z/R_\alpha)} \tag{2.5}$$

$$\gamma_{\beta z} = \frac{1}{B(1+z/R_\beta)}\frac{\partial w}{\partial \beta} + B(1+z/R_\beta)\frac{\partial}{\partial z}\left(\frac{v}{B(1+z/R_\beta)}\right) - \frac{u}{R_{\alpha\beta}(1+z/R_\beta)} \tag{2.6}$$

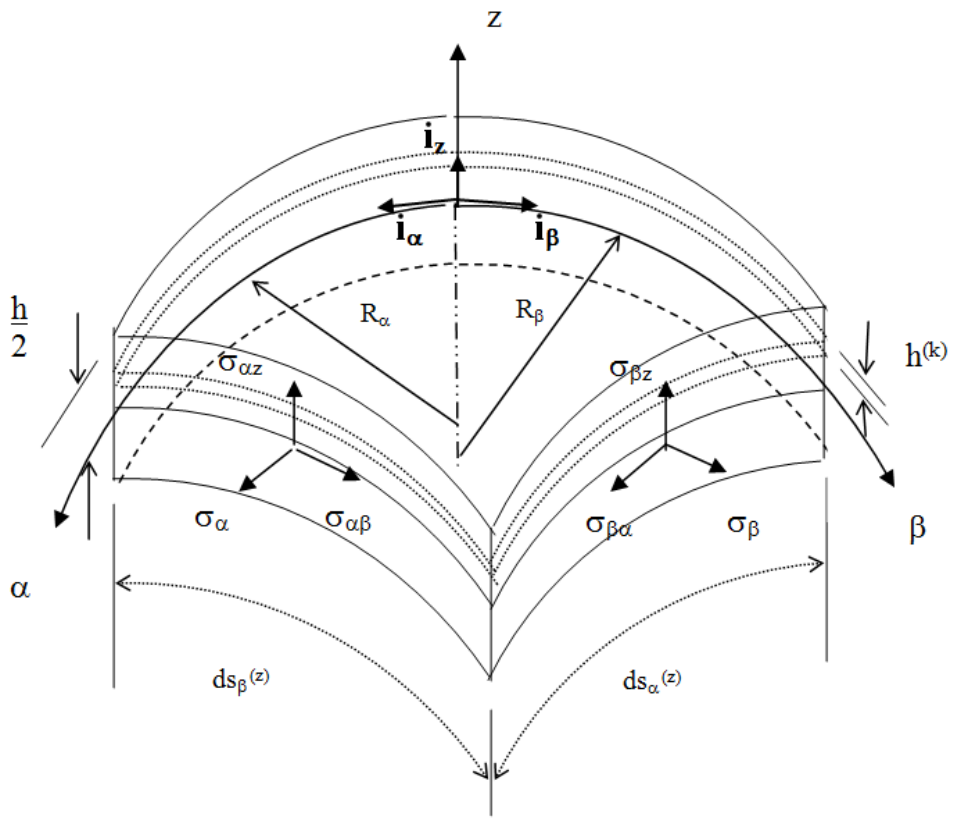

Figure 2.1 Stress in shell coordinates (free outer surfaces).

For the development of the constitutive relations, the laminated composite thin shells are assumed to be composed of plies of unidirectional long fibers embedded in a matrix material such as epoxy resin. On a macroscopic level, each layer may be regarded as being homogeneous and orthotropic. However, the fibers of a typical layer may not be parallel to the coordinates in which the shell equations are expressed. The stress-strain relationship for a typical *n*th lamina (typically called monoclinic) in a laminated composite shell made of N laminas, is shown in Figure2.2 and given by Equation (2.7) [1].

$$\begin{bmatrix} \sigma_\alpha \\ \sigma_\beta \\ \sigma_z \\ \sigma_{\beta z} \\ \sigma_{\alpha z} \\ \sigma_{\alpha\beta} \end{bmatrix} = \begin{bmatrix} \overline{Q}_{11} & \overline{Q}_{12} & \overline{Q}_{13} & 0 & 0 & \overline{Q}_{16} \\ \overline{Q}_{12} & \overline{Q}_{22} & \overline{Q}_{23} & 0 & 0 & \overline{Q}_{26} \\ \overline{Q}_{13} & \overline{Q}_{23} & \overline{Q}_{33} & 0 & 0 & \overline{Q}_{36} \\ 0 & 0 & 0 & \overline{Q}_{44} & \overline{Q}_{45} & 0 \\ 0 & 0 & 0 & \overline{Q}_{45} & \overline{Q}_{55} & 0 \\ \overline{Q}_{16} & \overline{Q}_{26} & \overline{Q}_{36} & 0 & 0 & \overline{Q}_{66} \end{bmatrix} \begin{bmatrix} \varepsilon_\alpha \\ \varepsilon_\beta \\ \varepsilon_z \\ \gamma_{\beta z} \\ \gamma_{\alpha z} \\ \gamma_{\alpha\beta} \end{bmatrix} \tag{2.7}$$

The positive notations of the stresses are shown in Figure 2.1.

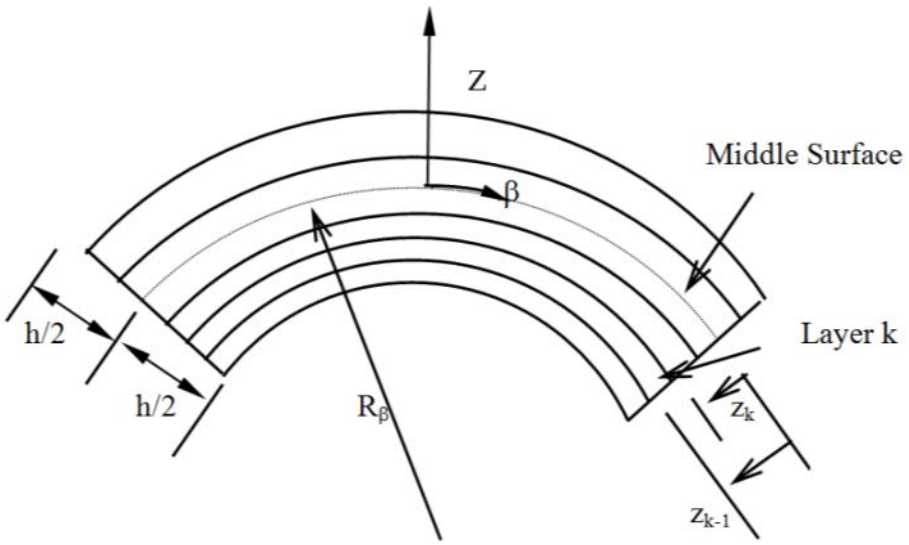

Figure 2.2 Lamination parameters in shells

In order to develop a consistent set of equations, the boundary conditions and the equations of motion will be derived using Hamilton's principle [1]. Substituting the equations for potential energy (U), external work (W) and kinetic energy (T), performing the integration by parts, and setting the coefficients of the displacement variations equal to zero, in a normal manner, yields the equations of motion.

$$\frac{\partial(B\sigma_\alpha)}{\partial\alpha} + \frac{\partial(A\sigma_{\alpha\beta})}{\partial\beta} + \frac{\partial(AB\sigma_{\alpha z})}{\partial z} + \sigma_{\alpha\beta}\frac{\partial A}{\partial\beta} + \sigma_{\alpha z}B\frac{\partial A}{\partial z} - \sigma_\beta\frac{\partial B}{\partial\alpha} + ABq_\alpha = \rho\frac{\partial^2 u}{\partial t^2} \tag{2.8}$$

$$\frac{\partial(B\sigma_{\alpha\beta})}{\partial\alpha} + \frac{\partial(A\sigma_\beta)}{\partial\beta} + \frac{\partial(AB\sigma_{\beta z})}{\partial z} + \sigma_{\beta z}A\frac{\partial B}{\partial z} + \sigma_{\alpha\beta}\frac{\partial B}{\partial\alpha} - \sigma_\alpha\frac{\partial A}{\partial\beta} + ABq_\beta = \rho\frac{\partial^2 v}{\partial t^2} \tag{2.9}$$

$$\frac{\partial\left(B\sigma_{\alpha z}\right)}{\partial\alpha}+\frac{\partial\left(A\sigma_{\beta z}\right)}{\partial\beta}+\frac{\partial\left(AB\sigma_{z}\right)}{\partial z}-\sigma_{\beta}A\frac{\partial B}{\partial z}-\sigma_{\alpha}B\frac{\partial A}{\partial z}+ABq_{z}=\rho\frac{\partial^{2}w}{\partial t^{2}} \tag{2.10}$$

The above equations do not depend on the shell material. Hamilton's principle will also yield boundary terms that are consistent with the other equations (strain-displacement and equilibrium relations). The boundary terms for z = constant are:

$$\sigma_{0z}-\sigma_{z}=0 \qquad or \qquad w^{0}=0 \tag{2.11}$$

$$\sigma_{0\alpha z}-\sigma_{\alpha z}=0 \qquad or \qquad u^{0}=0 \tag{2.12}$$

$$\sigma_{0\beta z}-\sigma_{\alpha z}=0 \qquad or \qquad v^{0}=0 \tag{2.13}$$

whereσ_{0z}, $\sigma_{0\alpha z}$ and $\sigma_{0\beta z}$ are surface tractions and u^0, v^0 and w^0 are displacement functions at z = constant. Similar results are obtained for the boundaries α = constant and β = constant. A three dimensional shell element has six surfaces. With three equations at each surface, a total of 18 equations can be obtained for a single-layered shell.

The above equations are valid for single-layered shells. To use 3D elasticity theory for multi-layered shells (the subject of this study), each layer must be treated as an individual shell. Both displacements and stresses must be continuous between each layer (layer k to layer k+1) in an-ply laminate. These conditions must be met to insure that there are no free internal surfaces (i.e., delamination) between the layers.

$$\begin{aligned}
&u(\alpha,\beta,z=h_k/2)\ \big|_{k=i}=u(\alpha,\beta,z=-h_k/2)\ \big|_{k=i+1}\\
&v(\alpha,\beta,z=h_k/2)\ \big|_{k=i}=v(\alpha,\beta,z=-h_k/2)\ \big|_{k=i+1}\\
&w(\alpha,\beta,z=h_k/2)\ \big|_{k=i}=w(\alpha,\beta,z=-h_k/2)\ \big|_{k=i+1}\\
&\sigma_z(\alpha,\beta,z=h_k/2)\ \big|_{k=i}=\sigma_z(\alpha,\beta,z=-h_k/2)\ \big|_{k=i+1}\\
&\sigma_{\alpha z}(\alpha,\beta,z=h_k/2)\ \big|_{k=i}=\sigma_{\alpha z}(\alpha,\beta,z=-h_k/2)\ \big|_{k=i+1}\\
&\sigma_{\beta z}(\alpha,\beta,z=h_k/2)\ \big|_{k=i}=\sigma_{\beta z}(\alpha,\beta,z=-h_k/2)\ \big|_{k=i+1}\ \text{For k= 1, …, N-1}
\end{aligned} \tag{2.14}$$

The3D theory of elasticity has been used to perform a dynamic analysis of composite shells by Santos et al. [22, 23] in which a finite element model for the free

vibration analysis of 3D axisymmetric laminated shells was developed. Also, Shakeri et al [24] performed dynamic analysis of thick laminated shell panel based on the 3D elasticity solution. Malekzadeh et al [25],conducted a 3D dynamic analysis on composite laminates under a moving load. Saviz et al [26], presented both 3D and 2D solutions of a layerwise theory in the investigation of thick laminated piezoelectric shells subjected to dynamic loading.

2.2.2 Thick shell theory

Thick shells are defined as shells with a thickness smaller by at least one order of magnitude when compared with other shell parameters such as wavelength and/or radii of curvature (thickness is at least $1/10^{th}$of the smallest of the wavelength and/or radii of curvature). The main differentiation between thick shell and thin shell theories is the inclusion of shear deformation and rotary inertia effects. Theories that include shear deformation are referred to as thick shell theories or shear deformation theories.

Thick shell theories are typically based on either a displacement or stress approach. In the former, the midplane shell displacements are expanded in terms of shell thickness, which can be a first order expansion, referred to as first order shear deformation theories. Accurate shell equations based on a first-order shear deformation theoryare now presented.

The 3D elasticity theory is reduced to a 2D theory using the assumption that the normal strains acting upon the plane parallel to the middle surface are negligible compared with other strain components. This assumption is generally valid except within the vicinity of a highly concentrated force (St. Venant's principle). In other words, no stretching is assumed in the z-direction (i.e., $\varepsilon_z=0$). Assuming that normals to the

midsurface strains remain straight during deformation but not normal, the displacements can be written as [1]

$$u(\alpha,\beta,z) = u_0(\alpha,\beta) + z\psi_\alpha(\alpha,B) \tag{2.15}$$

$$v(\alpha,\beta,z) = v_0(\alpha,\beta) + z\psi_\beta(\alpha,B) \tag{2.16}$$

$$w(\alpha,\beta,z) = w_0(\alpha,\beta) \tag{2.17}$$

where u_0, v_0 and $w_0$are midsurface displacements of the shell and ψ_α and ψ_β are midsurface rotations. An alternative derivation can be made with the assumption $\sigma_z = 0$. The subscript ($_0$) will refer to the middle surface in subsequent equations. The above equations describe a typical first-order shear deformation shell theory, and will constitute the only assumption made in this analysis when compared with the 3D theory of elasticity. As a result, strains are written as [1]

$$\varepsilon_\alpha = \frac{1}{(1+z/R_\alpha)}(\varepsilon_{0\alpha} + z\kappa_\alpha) \tag{2.18}$$

$$\varepsilon_\beta = \frac{1}{(1+z/R_\beta)}(\varepsilon_{0\beta} + z\kappa_\beta) \tag{2.19}$$

$$\varepsilon_{\alpha\beta} = \frac{1}{(1+z/R_\alpha)}(\varepsilon_{0\alpha\beta} + z\kappa_{\alpha\beta}) \tag{2.20}$$

$$\varepsilon_{\beta\alpha} = \frac{1}{(1+z/R_\beta)}(\varepsilon_{0\beta\alpha} + z\kappa_{\beta\alpha}) \tag{2.21}$$

$$\gamma_{\alpha z} = \frac{1}{(1+z/R_\alpha)}\left(\gamma_{0\alpha z} - z(\psi_\beta / R_{\alpha\beta})\right) \tag{2.22}$$

$$\gamma_{\beta z} = \frac{1}{(1+z/R_\beta)}\left(\gamma_{0\beta z} - z(\psi_\alpha / R_{\alpha\beta})\right) \tag{2.23}$$

where the midsurface strains are:

$$\varepsilon_{0\alpha} = \frac{1}{A}\frac{\partial u_0}{\partial\alpha} + \frac{v_0}{AB}\frac{\partial A}{\partial\beta} + \frac{w_0}{R_\alpha} \tag{2.24}$$

$$\varepsilon_{0\beta} = \frac{1}{B}\frac{\partial v_0}{\partial\beta} + \frac{u_0}{AB}\frac{\partial B}{\partial\alpha} + \frac{w_0}{R_\beta} \tag{2.25}$$

$$\varepsilon_{0\alpha\beta} = \frac{1}{A}\frac{\partial v_0}{\partial\alpha} - \frac{u_0}{AB}\frac{\partial A}{\partial\beta} + \frac{w_0}{R_{\alpha\beta}} \tag{2.26}$$

$$\varepsilon_{0\beta\alpha} = \frac{1}{B}\frac{\partial u_0}{\partial \beta} - \frac{v_0}{AB}\frac{\partial B}{\partial \alpha} + \frac{w_0}{R_{\alpha\beta}} \tag{2.27}$$

$$\gamma_{0\alpha z} = \frac{1}{A}\frac{\partial w_0}{\partial \alpha} - \frac{u_0}{R_\alpha} - \frac{v_0}{R_{\alpha\beta}} + \psi_\alpha \tag{2.28}$$

$$\gamma_{0\beta z} = \frac{1}{B}\frac{\partial w_0}{\partial \beta} - \frac{v_0}{R_\beta} - \frac{u_0}{R_{\alpha\beta}} + \psi_\beta \tag{2.29}$$

and the curvature and twist changes are:

$$\kappa_\alpha = \frac{1}{A}\frac{\partial \psi_\alpha}{\partial \alpha} + \frac{\psi_\beta}{AB}\frac{\partial A}{\partial \beta} \tag{2.30}$$

$$\kappa_\beta = \frac{1}{B}\frac{\partial \psi_\beta}{\partial \beta} + \frac{\psi_\alpha}{AB}\frac{\partial B}{\partial \alpha} \tag{2.31}$$

$$\kappa_{\alpha\beta} = \frac{1}{A}\frac{\partial \psi_\beta}{\partial \alpha} - \frac{\psi_\alpha}{AB}\frac{\partial A}{\partial \beta} \tag{2.32}$$

$$\kappa_{\beta\alpha} = \frac{1}{B}\frac{\partial \psi_\alpha}{\partial \beta} - \frac{\psi_\beta}{AB}\frac{\partial B}{\partial \alpha} \tag{2.33}$$

The force and moment resultants (Figures 2.3 and 2.4) are obtained by integrating the stresses over the shell thickness considering the (1+z/R) term that appears in the denominator of the stress resultant equations [5]. The stress resultant equations are:

$$\begin{bmatrix} N_\alpha \\ N_\beta \\ N_{\alpha\beta} \\ N_{\beta\alpha} \\ M_\alpha \\ M_\beta \\ M_{\alpha\beta} \\ M_{\beta\alpha} \end{bmatrix} = \begin{bmatrix} \overline{A}_{12} & A_{12} & \overline{A}_{16} & A_{16} & \overline{B}_{11} & B_{12} & \overline{B}_{16} & B_{16} \\ A_{12} & \hat{A}_{22} & A_{26} & A_{26} & B_{12} & \hat{B}_{22} & B_{26} & B_{26} \\ \overline{A}_{16} & A_{26} & \overline{A}_{66} & A_{66} & \overline{B}_{16} & B_{26} & \overline{B}_{66} & B_{66} \\ A_{16} & \hat{A}_{26} & A_{66} & A_{66} & B_{16} & \hat{B}_{26} & B_{66} & B_{66} \\ \overline{B}_{11} & B_{12} & \overline{B}_{16} & B_{16} & \overline{D}_{12} & D_{12} & \overline{D}_{16} & D_{16} \\ B_{12} & \hat{B}_{22} & B_{26} & B_{26} & D_{12} & \hat{D}_{22} & D_{26} & D_{26} \\ \overline{B}_{16} & B_{26} & \overline{B}_{66} & B_{66} & \overline{D}_{16} & D_{26} & \overline{D}_{66} & D_{66} \\ B_{16} & \hat{B}_{26} & B_{66} & B_{66} & D_{16} & \hat{D}_{26} & D_{66} & D_{66} \end{bmatrix} \begin{bmatrix} \varepsilon_{0\alpha} \\ \varepsilon_{0\beta} \\ \varepsilon_{0\alpha\beta} \\ \varepsilon_{0\beta\alpha} \\ \kappa_{0\alpha} \\ \kappa_{0\beta} \\ \kappa_{0\alpha\beta} \\ \kappa_{0\beta\alpha} \end{bmatrix} \tag{2.34}$$

$$\begin{bmatrix} Q_\alpha \\ Q_\beta \\ P_\alpha \\ P_\beta \end{bmatrix} = \begin{bmatrix} \overline{A}_{55} & A_{45} & \overline{B}_{55} & B_{45} \\ A_{45} & \hat{A}_{44} & B_{45} & \hat{B}_{44} \\ \overline{B}_{55} & B_{45} & \overline{D}_{55} & D_{45} \\ B_{45} & \hat{B}_{44} & D_{45} & \hat{D}_{44} \end{bmatrix} \begin{bmatrix} \gamma_{0\alpha z} \\ \gamma_{0\beta z} \\ -\psi_\beta / R_{\alpha\beta} \\ -\psi_\alpha / R_{\alpha\beta} \end{bmatrix} \tag{2.35}$$

where A_{ij}, B_{ij}, D_{ij}, $\overline{A}_{ij}$, $\overline{B}_{ij}$, $\overline{D}_{ij}$ are

$$\left.\begin{aligned} A_{ij} &= \sum_{k=1}^{N} \overline{Q}_{ij}^{(k)} (h_k - h_{k-1}) \\ B_{ij} &= \frac{1}{2} \sum_{k=1}^{N} \overline{Q}_{ij}^{(k)} (h_k^2 - h_{k-1}^2) \\ D_{ij} &= \frac{1}{3} \sum_{k=1}^{N} \overline{Q}_{ij}^{(k)} (h_k^3 - h_{k-1}^3) \end{aligned}\right\} \qquad i, j = 1,2,6 \tag{2.36}$$

$$\left.\begin{aligned} \mathrm{A_{ij}} &= \sum_{\mathrm{k=1}}^{\mathrm{N}} \mathrm{K_i K_j} \overline{\mathrm{Q}}_{\mathrm{ij}}^{(\mathrm{k})} (\mathrm{h_k} - \mathrm{h_{k-1}}) \\ \mathrm{B_{ij}} &= \frac{1}{2} \sum_{\mathrm{k=1}}^{\mathrm{N}} \mathrm{K_i K_j} \overline{\mathrm{Q}}_{\mathrm{ij}}^{(\mathrm{k})} (\mathrm{h_k^2} - \mathrm{h_{k-1}^2}) \\ \mathrm{D_{ij}} &= \frac{1}{3} \sum_{\mathrm{k=1}}^{\mathrm{N}} \mathrm{K_i K_j} \overline{\mathrm{Q}}_{\mathrm{ij}}^{(\mathrm{k})} (\mathrm{h_k^3} - \mathrm{h_{k-1}^3}) \end{aligned}\right\} \qquad \mathrm{i, j = 4,5} \tag{2.37}$$

$$\left.\begin{aligned} \overline{\mathrm{A}}_{\mathrm{ij}} &= \mathrm{A_{ij\alpha}} + \frac{\mathrm{B_{ij\alpha}}}{\mathrm{R_\beta}}, \qquad \hat{\mathrm{A}}_{\mathrm{ij}} = \mathrm{A_{ij\beta}} + \frac{\mathrm{B_{ij\beta}}}{\mathrm{R_\alpha}}, \\ \overline{\mathrm{B}}_{\mathrm{ij}} &= \mathrm{B_{ij\alpha}} + \frac{\mathrm{D_{ij\alpha}}}{\mathrm{R_\beta}}, \qquad \hat{\mathrm{B}}_{\mathrm{ij}} = \mathrm{B_{ij\beta}} + \frac{\mathrm{D_{ij\beta}}}{\mathrm{R_\alpha}}, \\ \overline{\mathrm{D}}_{\mathrm{ij}} &= \mathrm{D_{ij\alpha}} + \frac{\mathrm{E_{ij\alpha}}}{\mathrm{R_\beta}}, \qquad \hat{\mathrm{D}}_{\mathrm{ij}} = \mathrm{D_{ij\beta}} + \frac{\mathrm{E_{ij\beta}}}{\mathrm{R_\alpha}} \end{aligned}\right\} \quad \mathrm{i, j = 1,2,4,5,6} \tag{2.38}$$

where Ki and Kj are shear correction coefficients, typically taken at 5/6, and where

$$\left.\begin{aligned} A_{ijn} &= \sum_{k=1}^{N} \int_{h_{k-1}}^{h_k} \overline{Q}_{ij}^{(k)} \frac{dz}{1 + z/R_n} = R_n \sum_{k=1}^{N} \overline{Q}_{ij}^{(k)} \ln\left(\frac{R_n + h_k}{R_n + h_{k-1}}\right) \\ B_{ijn} &= \sum_{k=1}^{N} \int_{h_{k-1}}^{h_k} \overline{Q}_{ij}^{(k)} \frac{z dz}{1 + z/R_n} = R_n \sum_{k=1}^{N} \overline{Q}_{ij}^{(k)} \left[(h_k - h_{k-1}) - R_n \ln\left(\frac{R_n + h_k}{R_n + h_{k-1}}\right) \right] \\ D_{ijn} &= \sum_{k=1}^{N} \int_{h_{k-1}}^{h_k} \overline{Q}_{ij}^{(k)} \frac{z^2 dz}{1 + z/R_n} \\ &= R_n \sum_{k=1}^{N} \overline{Q}_{ij}^{(k)} \left[\frac{1}{2} \left\{ (R_n + h_k)^2 - (R_n + h_{k-1})^2 \right\} - 2R_n (h_k - h_{k-1}) + R_n^2 \ln\left(\frac{R_n + h_k}{R_n + h_{k-1}}\right) \right] \\ E_{ijn} &= \sum_{k=1}^{N} \int_{h_{k-1}}^{h_k} \overline{Q}_{ij}^{(k)} \frac{z^3 dz}{1 + z/R_n} \\ &= R_n \sum_{k=1}^{N} \overline{Q}_{ij}^{(k)} \left[\begin{aligned} &\frac{1}{3} \left\{ (R_n + h_k)^3 - (R_n + h_{k-1})^3 \right\} - \frac{3}{2} R_n \left\{ (R_n + h_k)^2 - (R_n + h_{k-1})^2 \right\} \\ &+ 3R_n^2 (h_k - h_{k-1}) - R_n^3 \ln\left(\frac{R_n + h_k}{R_n + h_{k-1}}\right) \end{aligned} \right] \end{aligned}\right\} n = \alpha, \beta \tag{2.39}$$

The above equations can be simplified by truncating the 1/(1+z/R) in a Taylor series [1].

$$\left.\begin{aligned} \overline{A}_{ij} &= A_{ij} - c_0 B_{ij}, \qquad \hat{A}_{ij} = A_{ij} + c_0 B_{ij}, \\ \overline{B}_{ij} &= B_{ij} - c_0 D_{ij}, \qquad \hat{B}_{ij} = B_{ij} + c_0 D_{ij} \\ \overline{D}_{ij} &= D_{ij} - c_0 E_{ij}, \qquad \hat{D}_{ij} = D_{ij} + c_0 E_{ij} \end{aligned}\right\} \quad i, j = 1,2,4,5,6 \tag{2.40}$$

Where all terms are as defined in (2.36) to (2.38) and

$$E_{ij} = \frac{1}{4}\sum_{k=1}^{N} \bar{Q}_{ij}^{(k)} \left(h_k^{\,4} - h_{k-1}^{\,4}\right) \qquad i, j = 1,2,6 \tag{2.41}$$

$$c_0 = \left(\frac{1}{R_\alpha} - \frac{1}{R_\beta}\right) \tag{2.42}$$

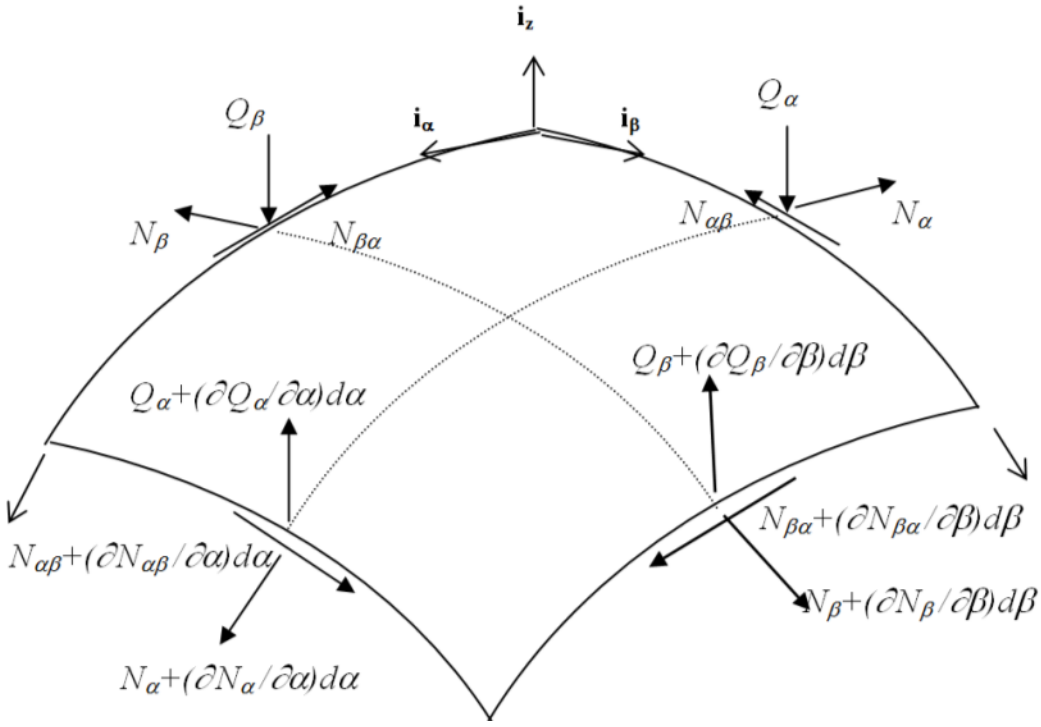

Figure 2.3 Force resultants in shell coordinates

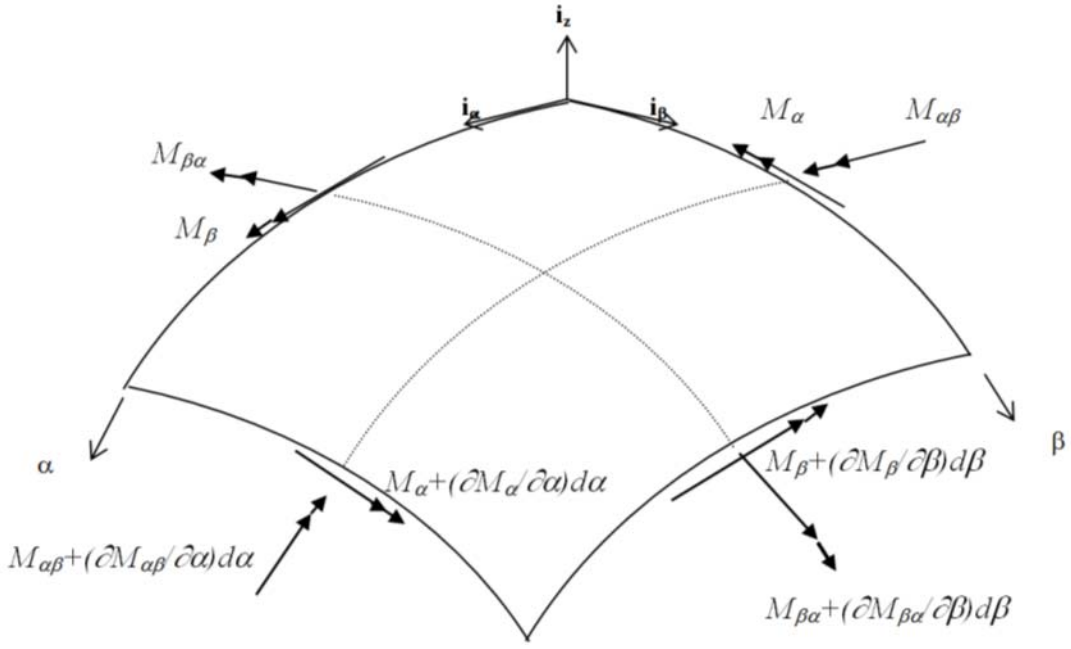

Figure 2.4 Moment resultants in shell coordinates

It has been shown [1,5] that the above equations yield more accurate results when compared with those of plates and those traditionally used for shells [18]. Hamilton's principle can be used to derive the consistent equations of motion and boundary conditions. The equations of motion are [1]:

$$\frac{\partial}{\partial\alpha}\left(BN_\alpha\right)+\frac{\partial}{\partial\beta}\left(AN_{\beta\alpha}\right)+\frac{\partial A}{\partial\beta}N_{\alpha\beta}-\frac{\partial B}{\partial\alpha}N_\beta+\frac{AB}{R_\alpha}Q_\alpha+\frac{AB}{R_{\alpha\beta}}Q_\beta+ABq_\alpha=AB\left(\bar{I}_1\ddot{u}_0+\bar{I}_2\ddot{\psi}_\alpha\right) \tag{2.43}$$

$$\frac{\partial}{\partial\beta}\left(AN_\beta\right)+\frac{\partial}{\partial\alpha}\left(AN_{\alpha\beta}\right)+\frac{\partial B}{\partial\alpha}N_{\beta\alpha}-\frac{\partial A}{\partial\beta}N_\alpha+\frac{AB}{R_\beta}Q_\beta+\frac{AB}{R_{\alpha\beta}}Q_\alpha+ABq_\beta=AB\left(\bar{I}_1\ddot{v}_0+\bar{I}_2\ddot{\psi}_\beta\right) \tag{2.44}$$

$$-AB\left(\frac{N_\alpha}{R_\alpha}+\frac{N_\beta}{R_\beta}+\frac{N_{\alpha\beta}+N_{\beta\alpha}}{R_{\alpha\beta}}\right)+\frac{\partial}{\partial\alpha}\left(BQ_\alpha\right)+\frac{\partial}{\partial\beta}\left(AQ_\beta\right)+ABq_n=AB\left(\bar{I}_1\ddot{w}_0\right) \tag{2.45}$$

$$\frac{\partial}{\partial\alpha}\left(BM_\alpha\right)+\frac{\partial}{\partial\beta}\left(AM_{\beta\alpha}\right)+\frac{\partial A}{\partial\beta}M_{\alpha\beta}-\frac{\partial B}{\partial\alpha}M_\beta-ABQ_\alpha+\frac{AB}{R_{\alpha\beta}}P_\beta+ABm_\alpha=AB\left(\bar{I}_2\ddot{u}_0+\bar{I}_3\ddot{\psi}_\alpha\right) \tag{2.46}$$

$$\frac{\partial}{\partial\beta}\left(AN_\beta\right)+\frac{\partial}{\partial\alpha}\left(AN_{\alpha\beta}\right)+\frac{\partial B}{\partial\alpha}N_{\beta\alpha}-\frac{\partial A}{\partial\beta}N_\alpha+\frac{AB}{R_\beta}Q_\beta+\frac{AB}{R_{\alpha\beta}}Q_\alpha+ABq_\beta=AB\left(\bar{I}_1\ddot{v}_0+\bar{I}_2\ddot{\psi}_\beta\right) \tag{2.47}$$

where the two dots over the terms represent the second derivative of these terms with respect to time, and where:

$$\bar{I}_i = \left(I_i + I_{i+1}\left(\frac{1}{R_\alpha} + \frac{1}{R_\beta} \right) + \frac{I_{i+2}}{R_\alpha R_\beta} \right), \qquad i = 1,2,3 \tag{2.48}$$

$$\left[I_1, I_2, I_3, I_4, I_5 \right] = \sum_{k=1}^{N} \int_{h_{k-1}}^{h_k} \rho^{(k)} \left[1, z, z^2, z^3, z^4 \right] dz \tag{2.49}$$

The boundary terms for the boundaries with α =constant are

$$N_{0\alpha} - N_\alpha = 0 \qquad or \qquad u_0 = 0 \tag{2.50}$$

$$N_{0\alpha\beta} - N_{\alpha\beta} = 0 \qquad or \qquad v_0 = 0 \tag{2.51}$$

$$Q_{0\alpha} - Q_\alpha = 0 \qquad or \qquad w_0 = 0 \tag{2.52}$$

$$M_{0\alpha} - M_\alpha = 0 \qquad or \qquad \psi_\alpha = 0 \tag{2.53}$$

$$M_{0\alpha\beta} - M_{\alpha\beta} = 0 \qquad or \qquad \psi_\beta = 0 \tag{2.54}$$

Similar equations can be obtained for β = constant.

Shear deformation theories have been used by many authors. Qatu [5] used it to solve the free vibration problem of simply supported shells. Toorani and Lakis [27] discussed shear deformation in dynamic analysis of laminated open cylindrical shells interacting with a flowing fluid. Dong and Wang [28] analyzed the effect of transverse shear and rotary inertia on wave propagation in laminated piezoelectric cylindrical shells. Ribeiro [29] investigated the influence of membrane inertia and shear deformation on nonlinear vibrations of open, cylindrical, laminated clamped shells. Qatu [30] used the shear deformation shell theory described here to study the free vibration of laminated cylindrical and barrel thick shells. Wang et al. [31] were interested in the wave propagation of stresses in orthotropic laminated thick-walled spherical shells. Ding [32] employed a shear deformation theory to study the thermoelastic dynamic response of thick closed laminated shells. Ganapathi and Haboussi [33] studied the free vibrations of

thick laminated anisotropic non-circular cylindrical shells. Other studies using thick shell theories will be reviewed in other sections.

2.2.2.1 Higher order shell theories

The equations derived earlier for thick shells are called first- order shear deformation theory because in Equation 2.15 to Equation 2.17, only the first-order expansion is performed across the thickness for in-plane displacements. If third-order terms are retained, the resulting theory will be a third-order deformation theory. The group of theories that are based on a cubic or higher expansion of the in-plane displacements in terms of the thickness is referred to as higher order theories.

Ganapathi et al. [34] used a higher order theory to perform dynamic analysis of laminated cross-ply composite noncircular thick cylindrical shells. Khare and Rode [35] utilized a higher order theory to develop closed-form solutions for vibrations of thick shells. Balah and AI-Ghemady [36] employed a third-order theory to develop an energy momentum conserving algorithm for non- linear dynamics of laminated shells. Pinto Correia et al. [37] studied dynamics and statics of laminated conical shell structures using higher order models. Qian et al. [38] studied active vibration control of laminated shells using higher order layer-wise theory. Lam et al. [39] combined displacements from transverse shear forces and from thin-shell theory to modify a higher order theory to study the vibration response of thick laminated cylindrical shells.

2.2.2.2 Layer-wise shell theories

Other thick shell theories, such as layer-wise theories have also been utilized. These theories typically reduce a 3D problem to a 2D problem by expanding the 3D displacement field in terms of a 2D displacement field and the through-the-shell

thickness. Braga and Rivas [40] used a layer-wise theory to study the high-frequency response of cylindrical shells made of isotropic and laminated materials. Basar and Omurtag [41] used a layer-wise model to investigate free vibrations of shell structures. Other research involving layer-wise shell theories include Lee et al. [42] who studied the dynamic behavior of cylindrical composite structures with viscoelastic layers, Moreira et al. [43] who used a layer-wise theory to formulate shell finite elements for dynamic modeling of composite laminates and Oh, who used layer-wise mechanics to investigate dynamic response [44], damping characteristics [45], and vibration characteristics [46] of cylindrical laminates. Qian used a higher order theory for studying composite laminated shells underactive vibration control [38], Saravanan et al. [47] studied active damping in a laminated shell and Saravanos and Christoforou [48] investigated impacts of composite shells. Other works utilizing layer based techniques include Shin et al. [49] who investigated aeroelastic analysis using zig-zag layer-wise theory, Varelis and Saravanos [50] who studied the non-linear response of doubly curved composite shells using a shear layer-wise shell theory, and Wang et al. [51] who investigated the dynamic response of laminated shells.

2.2.3 Thin-shell theory

If the shell thickness is less than $1/20^{th}$ of the wavelength of the deformation mode and/or radii of curvature, a thin shell theory, where shear deformation and rotary inertia are negligible, is generally acceptable. Depending on various assumptions made during the derivation of the strain-displacement relations, stress-strain relations, and the equilibrium equations, various thin shell theories can be derived. Among the most common of these are Love's, Reissner's, Naghdy's, Sander's and Flugge's shell theories.

Descriptions of these and other thin shell theories can be found [5]. All these theories were initially derived for isotropic shells and expanded later for laminated composite shells by applying the appropriate integration through laminas, and stress-strain relations. For very thin shells, the following additional assumptions simplify the shell equations and their order.

i. The shell is thin such that the ratio of the thickness compared to any of the shell's radii or any other shell parameter, i.e., width or length, is negligible when compared to unity.

ii. The normals to the middle surface remain straight and normal when the shell undergoes deformation.

The first assumption assures that certain parameters in the shell equations (including the z/R) term mentioned earlier in the thick shell theory can be neglected. Due to the second assumption, the shear deformation can be neglected in the kinematic equations and this allows the in-plane displacement to vary linearly through the shell's thickness as given by

$$\varepsilon_\alpha = \varepsilon_{0\alpha} + z\kappa_\alpha \tag{2.55}$$

$$\varepsilon_\beta = \varepsilon_{0\beta} + z\kappa_\beta \tag{2.56}$$

$$\gamma_{\alpha\beta} = \gamma_{0\alpha\beta} + z\tau_{\alpha\beta} \tag{2.57}$$

where the midsurface strains, curvature and twist changes are

$$\varepsilon_{0\alpha} = \frac{1}{A}\frac{\partial u_0}{\partial \alpha} + \frac{v_0}{AB}\frac{\partial A}{\partial \beta} + \frac{w_0}{R_\alpha} \tag{2.58}$$

$$\varepsilon_{0\beta} = \frac{1}{B}\frac{\partial v_0}{\partial \beta} + \frac{u_0}{AB}\frac{\partial B}{\partial \alpha} + \frac{w_0}{R_\beta} \tag{2.59}$$

$$\gamma_{0\alpha\beta} = \frac{1}{A}\frac{\partial v_0}{\partial \alpha} - \frac{u_0}{AB}\frac{\partial A}{\partial \beta} + \frac{1}{B}\frac{\partial u_0}{\partial \beta} - \frac{v_0}{AB}\frac{\partial B}{\partial \alpha} + 2\frac{w_0}{R_{\alpha\beta}} \tag{2.60}$$

$$\kappa_\alpha = \frac{1}{A}\frac{\partial \psi_\alpha}{\partial \alpha} + \frac{\psi_\beta}{AB}\frac{\partial A}{\partial \beta} \tag{2.61}$$

$$\kappa_\beta = \frac{1}{B}\frac{\partial \psi_\beta}{\partial \beta} + \frac{\psi_\alpha}{AB}\frac{\partial B}{\partial \alpha} \tag{2.62}$$

$$\tau = \frac{1}{A}\frac{\partial \psi_\beta}{\partial \alpha} - \frac{\psi_\alpha}{AB}\frac{\partial A}{\partial \beta} + \frac{1}{B}\frac{\partial \psi_\alpha}{\partial \beta} - \frac{\psi_\beta}{AB}\frac{\partial B}{\partial \alpha} \tag{2.63}$$

and where

$$\psi_\alpha = \frac{u}{R_\alpha} + \frac{v_0}{R_{\alpha\beta}} - \frac{1}{A}\frac{\partial w}{\partial \alpha} \tag{2.64}$$

$$\psi_\beta = \frac{v}{R_\beta} + \frac{u_0}{R_{\alpha\beta}} - \frac{1}{A}\frac{\partial w}{\partial \beta} \tag{2.65}$$

Applying Kirchhoff hypothesis of neglecting shear deformation and the assumption that εz is negligible, the stress-strain equations for an element of material in the kth lamina may be written as [1]

$$\begin{bmatrix} \sigma_\alpha \\ \sigma_\beta \\ \sigma_{\alpha\beta} \end{bmatrix}_k = \begin{bmatrix} Q_{11} & Q_{12} & Q_{16} \\ Q_{12} & Q_{22} & Q_{26} \\ Q_{16} & Q_{26} & Q_{66} \end{bmatrix}_k \begin{bmatrix} \varepsilon_\alpha \\ \varepsilon_\beta \\ \gamma_{\alpha\beta} \end{bmatrix}_k \tag{2.66}$$

where σα and σβ are normal stress components, ταβ is the in-plane shear stress component [1],εα and εβ are the normal strains, and γαβis the in-plane engineering shear strain. The terms Qij are the elastic stiffness coefficients for the material. If the shell coordinates (α,β) are parallel or perpendicular to the fibers, then the terms Q16 and Q26 are both zero. Stresses over the shell thickness (h) are integrated to get the force and moment resultants as given by

$$\begin{bmatrix} N_\alpha \\ N_\beta \\ N_{\alpha\beta} \\ M_\alpha \\ M_\beta \\ M_{\alpha\beta} \end{bmatrix} = \begin{bmatrix} A_{11} & A_{12} & A_{16} & B_{11} & B_{12} & B_{16} \\ A_{12} & A_{22} & A_{26} & B_{12} & B_{22} & B_{26} \\ A_{16} & A_{26} & A_{66} & B_{16} & B_{26} & B_{66} \\ B_{11} & B_{12} & B_{16} & D_{11} & D_{12} & D_{16} \\ B_{12} & B_{22} & B_{26} & D_{12} & D_{22} & D_{26} \\ B_{16} & B_{26} & B_{66} & D_{16} & D_{26} & D_{66} \end{bmatrix} \begin{bmatrix} \varepsilon_{0\alpha} \\ \varepsilon_{0\beta} \\ \gamma_{0\alpha\beta} \\ k_\alpha \\ k_\beta \\ \tau \end{bmatrix} \tag{2.67}$$

where Aij , Bij , and Dij are the stiffness coefficients arising from the piecewise integration over the shell thickness (Equation2.41, 2.42). For shells which are laminated

symmetrically with respect to their midsurfaces, all the Bij terms become zero. Note that the above equations are the same as those for laminated plates, which are also valid for thin laminated shells. Using Hamilton's principle yields the following equations of motion.

$$\frac{\partial}{\partial\alpha}\left(BN_\alpha\right)+\frac{\partial}{\partial\beta}\left(AN_{\beta\alpha}\right)+\frac{\partial A}{\partial\beta}N_{\alpha\beta}-\frac{\partial B}{\partial\alpha}N_\beta+\frac{AB}{R_\alpha}Q_\alpha+\frac{AB}{R_{\alpha\beta}}Q_\beta+ABq_\alpha=AB\left(\bar{I}_1\ddot{u}_0\right) \tag{2.68}$$

$$\frac{\partial}{\partial\beta}\left(AN_\beta\right)+\frac{\partial}{\partial\alpha}\left(AN_{\alpha\beta}\right)+\frac{\partial B}{\partial\alpha}N_{\beta\alpha}-\frac{\partial A}{\partial\beta}N_\alpha+\frac{AB}{R_\beta}Q_\beta+\frac{AB}{R_{\alpha\beta}}Q_\alpha+ABq_\beta=AB\left(\bar{I}_1\ddot{v}_0\right) \tag{2.69}$$

$$-AB\left(\frac{N_\alpha}{R_\alpha}+\frac{N_\beta}{R_\beta}+\frac{N_{\alpha\beta}+N_{\beta\alpha}}{R_{\alpha\beta}}\right)+\frac{\partial}{\partial\alpha}\left(BQ_\alpha\right)+\frac{\partial}{\partial\beta}\left(AQ_\beta\right)+ABq_n=AB\left(\bar{I}_1\ddot{w}_0\right) \tag{2.70}$$

where

$$ABQ_\alpha=\frac{\partial}{\partial\alpha}\left(BM_\alpha\right)+\frac{\partial}{\partial\beta}\left(AM_{\beta\alpha}\right)+\frac{\partial A}{\partial\beta}M_{\alpha\beta}-\frac{\partial B}{\partial\alpha}M_\beta \tag{2.71}$$

$$ABQ_\beta=\frac{\partial}{\partial\beta}\left(AM_\beta\right)+\frac{\partial}{\partial\alpha}\left(BM_{\alpha\beta}\right)+\frac{\partial B}{\partial\alpha}M_{\beta\alpha}-\frac{\partial A}{\partial\beta}M_\alpha \tag{2.72}$$

The following boundary conditions can be obtained for thin shells for α = constant (similar equations can be obtained for β = constant).

$$N_{0\alpha}-N_\alpha=0 \qquad or \qquad u_0=0 \tag{2.73}$$

$$\left(N_{0\alpha\beta}-\frac{N_{0\alpha\beta}}{R_\beta}\right)-\left(N_{\alpha\beta}-\frac{N_{\alpha\beta}}{R_\beta}\right)=0 \qquad or \qquad v_0=0 \tag{2.74}$$

$$\left(Q_{0\alpha}-\frac{1}{B}\frac{\partial M_{0\alpha\beta}}{\partial\beta}\right)-\left(Q_\alpha-\frac{1}{B}\frac{\partial M_{\alpha\beta}}{\partial\beta}\right)=0 \qquad or \qquad w_0=0 \tag{2.75}$$

$$M_{0\alpha}-M_\alpha=0 \qquad or \qquad \psi_\alpha=0 \tag{2.76}$$

$$M_{0\alpha\beta}w\ \Big]_{\beta_1}^{\beta_2}=0 \tag{2.77}$$

The equations presented thus far are complete in the sense that the number of equations is equal to the number of unknowns for each of the theories presented. The number of equations using 3D elasticity theory is 15 written in three coupled variables (α, β and z). Other shell theories use only two variables (α, and β). For 3D elasticity theory, three boundary conditions must be satisfied at each of the six external boundaries, leading

to a total of 18 conditions whereas for thin shell theory, five conditions (four along the edges and one for the corners) at each of the four edges of the shell are required.

Much research using thin shell theory has been performed. Ray and Reddy [52] studied control of thin circular cylindrical laminated composite shells using active constrained layer damping treatment. Evseev and Morozov [53] discussed the aeroelastic interaction of shock waves with thin-walled composite shells. The transient vibration of a composite cylindrical shell due to an underwater shock wave was studied by Li and Hua [54]. Ruotolo [55] determined the natural frequencies of stiffened shells and compared the results obtained from Donnell's, Love's, Sanders' and Flugge's thin shell theories.

Numerous studies dealing with modal analysis on laminated composite shells using thin shell theory appear in the literature. Free vibration analyses based on Love's thin shell theory have been performed by Civalek [56,57] for laminated conical and cylindrical shells. Free vibration analyses have also been performed by Sakiyama et al [58] and Hu et al [59] who considered composite conical shells with twist and by Lee et al [60] who determined the vibration characteristics of a laminated cylindrical shell with an interior rectangular plate. Other free vibration studies have been conducted by Kim and Lee [61] on the modal response of ring-stiffened laminated cylindrical shells, and by Shang [62] on composite cylindrical shells with hemispherical end caps.

2.2.4 Free vibration

Santos et al. [22] performed vibration analysis of 3D axisymmetric laminated shells with piezoelectric actuators. Ganapathiand Haboussi [33] studied the free vibrations of thick laminated anisotropic non-circular cylindrical shells. Civalek [57]

numerically solved the free vibrations of laminated composite conical and cylindrical shells using discrete singular convolution. Lee et al. [60] analyzed the free vibrations of laminated composite cylindrical shells with an interior rectangular plate. Korhevskaya and Mikhasev [63] studied the free vibrations of a laminated cylindrical shell subjected to nonuniformly distribute axial forces. Toorani and Lakis [64] analyzed the free vibrations of nonuniform composite cylindrical shells. Umur and Varlik [65] studied the free vibrations of bonded single lap joints in composite shell panels whereas Singh [66] studied the non-linear vibrations of fiber reinforced laminated shallow shells. Hu and Ou [67] maximized the fundamental frequency of laminated truncated conical shells with respect to fiber orientation. Timarchi and Soldatos [68] analyzed the vibrations of angle-ply laminated circular cylindrical shells with different edge boundary conditions. Topal [69] performed a mode-frequency analysis of laminated spherical shells. Tizzi [70] presented a Ritz procedure for optimization of cylindrical shells with a nearly symmetric angle-ply composite laminate. Ferreira et al. [71] presented natural frequencies of cross-ply composite shells by multiquadrics using a shear deformation shell theory. Iqbal and Qatu [72] studied the transverse bending vibration of circular two-segment composite shafts. Tetsuya [73] simplified the analytical method for calculation of natural frequencies of laminated composite cylindrical shells using equivalent curvature.

2.2.5 Rotating shells

Zhang [74] used a wave propagation approach to study the frequency of rotating composite cylindrical shells. Zhao et al. [75] studied the vibrations of rotating cross-ply circular cylindrical shells with ring stiffeners. Hua and Lam [76] researched the orthotropic influence on frequency characteristics of a rotating laminated conical shell

by the differential quadrature method. Gong and Lam [77] studied the transient response of rotating multilayer cylindrical shells to impact loading. Shi et al. [78] studied the effects of dynamic characteristics (centrifugal force, Transverse shear force, etc.) on the natural frequencies of a rotating composite shell.

2.2.6 Impact loading

Krishnamurthy et al. [123,124] performed a parametric study of the impact response of laminated cylindrical shells. Huang and Lee [79] studied composite shells subjected to low-velocity impact loads. Kim et al. [80] investigated the behavior of laminated composite shells under transverse impact loading. Saravanos and Christoforou [48] studied the low-energy impact of adaptive cylindrical piezoelectric-composite shells. johnson and Holzapfel [81] investigated the response of laminated composite shells to soft body impacts such as bird strikes on aircraft surfaces and continued their study by investigating high velocity impacts [82]. johnson et at. [83] reviewed recent developments regarding the impact response of composite structures. Other research on composite shells under impact loading includes studies by Kim et al. [84,85] who characterized the response and resulting damage from impact on curved composite shells, Krishnamurthy et al. [123,124] who used finite elements to investigate impact response and damage, and Lee et al. [86], who used neural networks to investigate impact loading parameters on composite shells. Low- velocity impact of composite shells was also investigated by Rastorguev and Snisarenko [87], Smojver et al. [88] (impact damage modeling), Tiberka k et al. [89] (impact damage prediction), and Zhao and Cho [90-92] (impact damage analysis and prediction). Wan et al. [93], studied the failure behavior of filament wound cylindrical shells subjected to axial impact loading.

Yang et al. [94], performed penetration experiments on laminated composite shells to determine penetration characteristics of various stacking sequences.

2.2.7 Dynamic stability

Sahu and Datta [95] reviewed recent research activity on the dynamic stability behavior of plates and shells. Zhou and Wang [127] presented a theory of non-linear dynamic stability for laminated composite cylindrical shells. Liew et al. [125] applied the mesh-free kp-Ritz method to perform a dynamic stability analysis on composite cylindrical shells subjected to periodic axial forces. Yang and Fu [126] analyzed the dynamic stability for composite laminated cylindrical shells with delaminations. Birman and Simitses [96] studied cylindrical sandwich shells subjected to periodic lateral pressure; Darabi et al. [97] and Ng et al. [98] analyzed functionally graded cylindrical shells subjected to periodic axial loading; Darvizeh et al. [99] investigated the general dynamic behavior of circular cylindrical shells including both shear deformation and rotary inertia terms. Ganapathi [128] studied the dynamic behavior of functionally graded shallow spherical shells; Kamat et al. [100] investigated the dynamic instability of a joined conical and cylindrical composite shell undergoing a periodic in-plane load; Kasuya and Yamagishi [101] studied the behavior of cross-ply laminated cylindrical shells subjected to impact hydrostatic pressure; the dynamic stability under an external pressure loading on composite cylindrical shells was also investigated by Nemoto et a!. [102]. Dynamic stability analysis was performed by Park and Lee [129] on composite spherical shells subjected to in-plane pulsating forces and by Peng et al. [103] on cylindrical shells under axially harmonic loads. Sofiyev [104] studied the dynamic stability of cross-ply laminated cylindrical shells with a focus on torsional

buckling and also investigated the dynamic stability of functionally graded conical shells under external pressure [130].

2.2.8 General dynamic behavior

Several other studies have addressed the general dynamic behavior of laminated composite shells. Pinto Correiaa et al. [108] presented a finite element model for the dynamic analysis of laminated axisymmetric shells. Wu and Lo [109] discussed an asymptotic theory for dynamic response of laminated piezoelectric shells. Prusty and Satsangi [110] performed finite element transient dynamic analysis of laminated stiffened shells. Park et al. [111] conducted a linear static and dynamic analysis of laminated composite plates and shells using finite elements. Fares et al. [112] studied the dynamic response of laminated doubly curved composite shells for optimization. Yang and Shen [113] performed dynamic instability analysis of laminated piezoelectric shells. Sahuand Datta [114] discussed parametric resonance characteristics of laminated composite shells subjected to nonuniform loading. Sofiyev [105] investigated the dynamic loading and its impact on the torsional buckling of cross-ply laminated orthotropic cylindrical shells. Tetsuya et al. [115] studied the vibration characteristics of laminated composite cylindrical shells. Lee [116] presented a dynamic variational asymptotic procedure for laminated composite shells. Tzou et al. [131] investigated the dynamics of conical shells laminated with full and diagonal actuators. Vu-Quoc and Tan [117] used optimal solid shells for non-linear dynamic analysis of laminated composites. Birman et al. [118] studied the dynamic behavior of composite spherical shells reinforced with active piezoelectric composite stiffeners. Lee and Hodges [119] performed a low frequency vibration analysis of laminated composite shells and

Tetsuya [120] determined the resonant frequencies and deformations of composite cylindrical shells. Ip and Tse [121] located damage in circular cylindrical composite shells based on frequency sensitivities and mode shapes. Ribeiro and Jansen [122] studied the non-linear vibrations of laminated cylindrical shallow shells under thermo mechanical loading. Jansen [123] investigated the effects of static loading and imperfections on the non-linear vibrations of laminated cylindrical shells. Li and Hua [54] studied the transient vibrations of laminated composite cylindrical shells exposed to underwater shock waves.

2.3 Accuracy study for shell theories in vibration study

As is shown here, the articles that are dedicated to obtaining experimental results and experimental verification and correlation are limited. In order to test and verify the shell theories, many current publications for analytical methods and theories are comparing their results with previous publications or FEA results obtained from the commercial packages.

For the thin and thick shell theories, it is justifiable to do this type of comparison. An argument the author found during dialogue with researchers at conferences is that the theory is developed at the 2D's level of accuracy. Subsequently, the argument is unnecessary and inaccurate to compare them to 3D theories. The newly developed shell theories claim to be close to the previous 2D's level of accuracy, but not necessarily better. Of course, the accuracy may not be the emphasis of the proposed research but it is necessary for verification. To do the FEA comparison is even more suspicious, unless the accuracy level of the FEA results could be tested and verified for certain commercial package.

Another practical problem that makes it necessary to do the comparison with 3D elasticity is the difficulty to find the appropriate results. Because of the complexity and limitations from the 3D elasticity solution, it is difficult and often impossible to obtain detailed solutions, these need to be studied. Only with solved or clarified detail solutions, could the 3D theory become a benchmark against which other theories can truly be verified.

A good example is Kadi's dissertation [147] (1970) on the free vibration of isotropic hollow cylinders to build a benchmark to evaluate many thin shell theories as described by Leissa's book [3] vibration of shells. In the book, Leissa compares almost all thin shell theories before 1970s. The 3D elasticity theory is used to study the free vibration of isotropic hollow cylinders. He starts by establishing the study of axi-symmetric cylinders (Herrmann and Mirsky [138]), and then investigating wave propagation in cylinders by using 3D elasticity (Gazis [139]) and (Mirsky [140]). This work was later finalized as a published book by Armenãkas, Gazis, and Herrmann [132] in 1969 that included plentiful frequency results. The exact solutions are obtained using separation of variables. Trigonometric functions are assumed in the time and space domains. In the space domain, the assumed functions are required to satisfy the different boundary conditions. Subsequently, Bessel Functions are applied to solve the resulting system of equations.

Because of the virtue of the 3D elasticity, Kadi's work could be used as the benchmark to compare the thick shell theories for isotropic hollow cylinders. However, although many thick shell theories have been developed, as shown in previous sections, the accuracy study is not to be found.

For the free vibration study of the composite hollow cylinders, the more general power series method (by using Frobenius method) is suggested by Mirsky [141] (1967) for composite materials and later applied and developed by Chou and Achenbach [142] (1970), and then being used by Sirinvas [148] for multiple layers (1972). Recently Yuan [143] expanded the power series solutions for the anisotropic cylinders(1992) and Shuvalov [149] developed the theory for the inhomogeneous elastic materials(2003). However, no detailed results of the 3D elasticity of the composite cylinders are found. For the orthotropic material, the only results found by the author in reference[148] will be proven to have mistakes. Understanding the difficulties of achieving the results is important in order to build the benchmark to compare the thin or thick composite shell theories.

Chapter I showed the importance of this research area. The purpose of doing the literature review is to find the research gaps which in this area. Two gaps will be summarized here:

i. Although many shell theories and FEA elements are established and developed, limited studies on their accuracy could be found.
ii. As an important benchmark for the accuracy studies, the exact solution of orthotropic hollow cylinders was not achieved.

CHAPTER III

3D ELASTICITY OF ISOTROPIC HOLLOW CYLINDERS AND RELATED STUDIESONTHICK SHELL THEORY AND FEA

The model that is being studied in this Chapter is the isotropic cylinder. Shear diaphragm simple support type of boundaries at both ends allow exact solutions for both the 3D theory of elasticity and shell theories. Accuracy study for different element types of Abaqus® and one advance shell theory will be discussed and analyzed by using the exact solutions of the 3D theory.

3.1 Background

The 3D elasticity theory in cylindrical coordinates could be found in many classical elasticity books [134, 135]. The three basic sets of equations used in 3D elasticity are equilibrium equations, kinematic equations, and constitutive equations. These equations could be found in the aforementioned books. Many efforts have been made by researches to solve this system of partial differential equations (PDEs) early on. The exact solutions are obtained using separation of variables. Trigonometric functions are assumed in the time and space domains. In the space domain, the assumed functions are required to satisfy the different boundary conditions. Subsequently, Bessel Functions are applied to solve the resulting system of equations.

3.1.1 Mathematical model: the fundamental three equations

The coordinate system of a thick circular cylinder is shown in Figure 3.1. The origin, polar axis, and longitudinal axis are shown as o, r, and x respectively. The u, v, and w represent the displacement parameters in the x, θ, and r directions, which represent the longitudinal, circumferential, and radial directions respectively. The total length, inner radius, and outer radius of the thick hollow cylinder are ℓ, Ri, and Ro.

The equilibrium equations (Equation 3.1 to 3.3) are the 3D equations of elastic motion in cylindrical coordinates with the tensor direction shown in Figure 3.2. σ and τ are the normal and shear stress tensors with different directional suffixes. The couple stresses with higher order differential divisor are neglected.

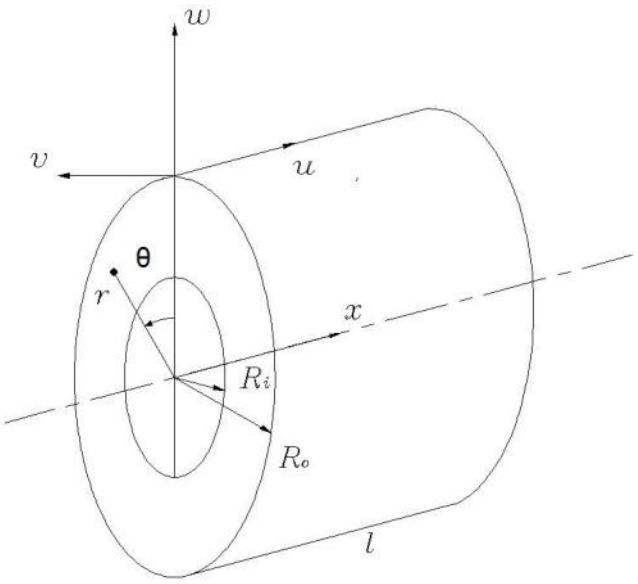

Figure 3.1 The cylindrical coordinate system for thick hollow cylinder;

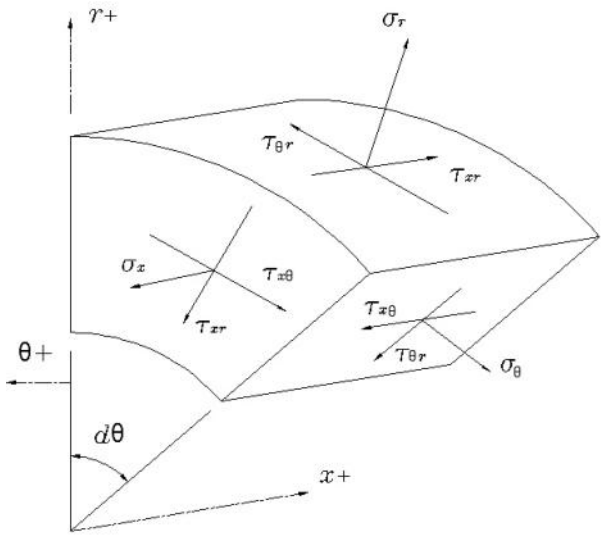

Figure 3.2 Circular cylinder and corresponding coordinates

The equilibrium equations are [134]:

$$\frac{\partial}{\partial x}\sigma_x + \frac{1}{r}\cdot\frac{\partial}{\partial \theta}\tau_{x\theta} + \frac{\partial}{\partial r}\tau_{xr} + \frac{\tau_{xr}}{r} = \rho\cdot\frac{\partial^2}{\partial t^2}u \tag{3.1}$$

$$\frac{\partial}{\partial x}\tau_{rx} + \frac{1}{r}\cdot\frac{\partial}{\partial \theta}\tau_{r\theta} + \frac{\partial}{\partial r}\sigma_r + \frac{\sigma_r - \sigma_\theta}{r} = \rho\cdot\frac{\partial^2}{\partial t^2}w \tag{3.2}$$

$$\frac{\partial}{\partial x}\tau_{x\theta} + \frac{1}{r}\cdot\frac{\partial}{\partial \theta}\sigma_\theta + \frac{\partial}{\partial r}\tau_{\theta r} + \frac{2\tau_{\theta r}}{r} = \rho\cdot\frac{\partial^2}{\partial t^2}v \tag{3.3}$$

The kinematic equations (Equation 3.4 to 3.9) are the strain-displacement equations in terms of cylindrical coordinates:

$$e_x = \frac{\partial}{\partial x}u \tag{3.4}$$

$$e_\theta = \frac{w}{r} + \frac{1}{r}\cdot\frac{\partial}{\partial \theta}v \tag{3.5}$$

$$e_r = \frac{\partial}{\partial r}w \tag{3.6}$$

$$\gamma_{x\theta} = \gamma_{\theta x} = \frac{\partial}{\partial x}v + \frac{1}{r}\cdot\frac{\partial}{\partial \theta}u \tag{3.7}$$

$$\gamma_{xr} = \gamma_{rx} = \frac{\partial}{\partial x}w + \frac{\partial}{\partial r}u \tag{3.8}$$

$$\gamma_{r\theta} = \gamma_{\theta r} = \frac{\partial}{\partial r} v + \frac{1}{r} \cdot \frac{\partial}{\partial \theta} w - \frac{v}{r} \tag{3.9}$$

The constitutive equations (Equation 3.10 to 3.11) are the general Hooke's law for the isotropic material in index notations:

$$e_i = \frac{1}{E} \cdot \left[\sigma_i - \upsilon \cdot \left(\sigma_j + \sigma_k \right) \right] \tag{3.10}$$

$$\gamma_{ij} = \frac{2(1+\upsilon)}{E} \cdot \sigma_{ij} \tag{3.11}$$

E and ν are the Young's modulus and Poisson's ratio respectively.

Substituting constitutive equations into kinematic equations and combining with equilibrium equations, one obtains the governing equations:

$$L_{11} \cdot u + L_{12} \cdot v + L_{13} \cdot w = \delta^2 \cdot \frac{\partial^2}{\partial t^2} u \tag{3.12}$$

$$L_{21} \cdot u + L_{22} \cdot v + L_{23} \cdot w = \delta^2 \cdot \frac{\partial^2}{\partial t^2} v \tag{3.13}$$

$$L_{31} \cdot u + L_{32} \cdot v + L_{33} \cdot w = \delta^2 \cdot \frac{\partial^2}{\partial t^2} w \tag{3.14}$$

where $L_{11} \ldots L_{33}$ are the differential operators which are

$$\delta^2 = 2(1+\upsilon)(1-2\upsilon)\frac{\rho}{E} \tag{3.15}$$

$$L_{11} = (1-2\upsilon)\left(\frac{\partial^2}{\partial r^2} + \frac{1}{r} \cdot \frac{\partial^2}{\partial r^2} + \frac{1}{r^2} \cdot \frac{\partial^2}{\partial \theta^2} \right) + 2(1-\upsilon) \cdot \frac{1}{r} \cdot \frac{\partial^2}{\partial x^2} \tag{3.16}$$

$$L_{12} = L_{21} = \frac{1}{r} \cdot \frac{\partial}{\partial \theta} \frac{\partial}{\partial x} \tag{3.17}$$

$$L_{13} = \frac{\partial}{\partial r} \frac{\partial}{\partial x} + \frac{1}{r} \cdot \frac{\partial}{\partial x} \tag{3.18}$$

$$L_{22} = (1-2\upsilon)\left(\frac{\partial^2}{\partial r^2} + \frac{1}{r} \cdot \frac{\partial^2}{\partial r^2} - \frac{1}{r^2} + \frac{\partial^2}{\partial x^2} \right) + 2(1-\upsilon) \cdot \frac{1}{r} \cdot \frac{\partial^2}{\partial \theta^2} \tag{3.19}$$

$$L_{23} = \frac{1}{r} \cdot \frac{\partial}{\partial \theta} \frac{\partial}{\partial r} + (3-4\upsilon) \cdot \frac{1}{r} \cdot \frac{\partial^2}{\partial \theta^2} \tag{3.20}$$

$$L_{31} = \frac{\partial}{\partial r} \frac{\partial}{\partial x} \tag{3.21}$$

$$L_{32} = \frac{1}{r}\cdot\frac{\partial}{\partial\theta}\frac{\partial}{\partial r}\blacksquare - (3-4\upsilon)\cdot\frac{1}{r}\cdot\frac{\partial^2}{\partial\theta^2}\blacksquare \tag{3.22}$$

$$L_{33} = 2(1-\upsilon)\left(\frac{\partial^2}{\partial r^2}\blacksquare + \frac{1}{r}\cdot\frac{\partial}{\partial r}\blacksquare - \frac{1}{r^2}\right) + (1-2\upsilon)\cdot\frac{1}{r}\cdot\left(\frac{\partial^2}{\partial x^2}\blacksquare + \frac{1}{r^2}\cdot\frac{\partial^2}{\partial\theta^2}\blacksquare\right) \tag{3.23}$$

The PDE system (Equation 3.12 to 3.14) is the final mathematical model for the isotropic hollow cylinders, which also called governing equations. Notice that this model could be used for any isotropic structures in cylindrical coordinates. Without the geometry boundary conditions, the hollow cylinder structure hasn't been built up yet.

3.1.2 Boundary conditions and the solution procedures

As mentioned previously, the shear diaphragm boundary conditions at both ends (abbreviation as SD-SD) are applied on the mathematical model derived at last section. What is the shear diaphragm boundary condition? From the physical point of view, the SD-SD could be understood as two very thin and flat plate covers rigidly attached on the both ends. In their own planes (r-θ plane), the stiffness is extremely high, but in the x direction transverse to the r-θ plane, because of the virtue of thinness, the stiffness is considerable low. Consequently, the displacement components v and w in the r-θ plane are constrained and the bending moment M_x and longitudinal membrane force N_x can't be effectively generated. The mathematical formulation could be written as Equation 3.24:

$$\sigma_x = M_x = N_x = v = w = 0 \text{at} x = 0, \ell \tag{3.24}$$

The main benefit from this boundary condition is capable to use separation variable method to find the exact solution.

Assuming the solutions of the PDE system in the form:

$$u = U(r,\theta)\cdot\cos(\lambda\cdot x)\cdot\cos(\omega\cdot t) \tag{3.25}$$

$$v = V(r,\theta)\cdot\sin(\lambda\cdot x)\cdot\cos(\omega\cdot t) \tag{3.26}$$

$$w = W(r,\theta)\cdot\sin(\lambda\cdot x)\cdot\cos(\omega\cdot t) \tag{3.27}$$

where$\lambda = m\pi/\ell$, m is the longitudinal mode number. These solutions satisfy the shear diaphragms boundary conditions at both ends, which are:

Submitting the solutions to the governing equations and using the displacement potential functions as suggested by Mirsky [141] to the U, V, and W functions deduce the governing equations to the Bessel function pattern. Then, the closed form solutions of the displacement functions can be obtained. In course of the deduction, the circumferential mode number n is used in the θ direction.

Substituting the displacement functions into the strain-displacement equations and the general Hooke's law equations, the stress functions are achieved. Then, the boundary conditions of $\sigma_r = \tau_{rx} = \tau_{r\theta} = 0$ at the inner and outer surfaces $r = R_i,\ and\ R_o$ can be applied.It should be noted that this yields six homogeneous equations with frequency function parameters. To avoid the trivial solution, the determinant of the resulting matrix must be set to zero.

$$\left|a_{ij}\right| = 0, \quad (i,j = 1,\ldots,6) \tag{3.28}$$

where these parameters a_{ij} are:

$$a_{11}(\omega) = 0.5\cdot\left[2n\cdot(n-1) + \left(\lambda^2 - p_2(\omega)^2\right)\cdot R_o^{\,2}\right]\cdot Z_{1o}(n,\omega) + \xi_1\cdot q_1(\omega)\cdot R_o\cdot Z_{1o}(n+1,\omega) \tag{3.29}$$

$$a_{12}(\omega) = 0.5\cdot\left[2n\cdot(n-1) + \left(\lambda^2 - p_2(\omega)^2\right)\cdot R_o^{\,2}\right]\cdot Zb_{1o}(n,\omega) + q_1(\omega)\cdot R_o\cdot Zb_{1o}(n+1,\omega) \tag{3.30}$$

$$a_{13}(\omega) = \left[n\cdot(n-1) - p_2(\omega)^2\cdot R_o^{\,2}\right]\cdot Z_{2o}(n,\omega) + \xi_2\cdot q_2(\omega)\cdot R_o\cdot Z_{2o}(n+1,\omega) \tag{3.31}$$

$$a_{14}(\omega) = \left[n\cdot(n-1) - p_2(\omega)^2\cdot R_o^{\,2}\right]\cdot Zb_{2o}(n,\omega) + q_2(\omega)\cdot R_o\cdot Zb_{2o}(n+1,\omega) \tag{3.32}$$

$$a_{15}(\omega) = n\cdot(n-1)\cdot Z_{2o}(n,\omega) - \xi_2\cdot n\cdot q_2(\omega)\cdot R_o\cdot Z_{2o}(n+1,\omega) \tag{3.33}$$

$$a_{16}(\omega) = n\cdot(n-1)\cdot Zb_{2o}(n,\omega) - n\cdot q_2(\omega)\cdot R_o\cdot Zb_{2o}(n+1,\omega) \tag{3.31}$$

$$a_{22}(\omega) = -n\cdot(n-1)\cdot Zb_{1o}(n,\omega) + n\cdot q_1(\omega)\cdot R_o\cdot Zb_{1o}(n+1,\omega) \tag{3.32}$$

$$a_{23}(\omega) = -n\cdot(n-1)\cdot Z_{2o}(n,\omega) + \xi_2\cdot n\cdot q_2(\omega)\cdot R_o\cdot Z_{2o}(n+1,\omega) \tag{3.33}$$

$$a_{24}(\omega) = -n\cdot(n-1)\cdot Zb_{2o}(n,\omega) + n\cdot q_2(\omega)\cdot R_o\cdot Zb_{2o}(n+1,\omega) \tag{3.34}$$

$$a_{25}(\omega) = -\left(n^2 - n - \frac{p_2(\omega)^2 \cdot R_o{}^2}{2}\right) \cdot Z_{2o}(n,\omega) - \xi_2 \cdot q_2(\omega) \cdot R_o \cdot Z_{2o}(n+1,\omega) \tag{3.35}$$

$$a_{26}(\omega) = -\left(n^2 - n - \frac{p_2(\omega)^2 \cdot R_o{}^2}{2}\right) \cdot Zb_{2o}(n,\omega) - q_2(\omega) \cdot R_o \cdot Zb_{2o}(n+1,\omega) \tag{3.36}$$

$$a_{31}(\omega) = \lambda \cdot R_o \cdot \left(n \cdot Z_{1o}(n,\omega) - \xi_1 \cdot q_1(\omega) \cdot R_o \cdot Z_{1o}(n+1,\omega)\right) \tag{3.37}$$

$$a_{32}(\omega) = \lambda \cdot R_o \cdot \left(n \cdot Zb_{1o}(n,\omega) - q_1(\omega) \cdot R_o \cdot Zb_{1o}(n+1,\omega)\right) \tag{3.38}$$

$$a_{33}(\omega) = \frac{R_o}{2 \cdot \lambda} \cdot \left(\lambda^2 - p_2(\omega)^2\right) \cdot \left(n \cdot Z_{2o}(n,\omega) - \xi_2 \cdot q_2(\omega) \cdot R_o \cdot Z_{2o}(n+1,\omega)\right) \tag{3.39}$$

$$a_{34}(\omega) = \frac{R_o}{2 \cdot \lambda} \cdot \left(\lambda^2 - p_2(\omega)^2\right) \cdot \left(n \cdot Zb_{2o}(n,\omega) - q_2(\omega) \cdot R_o \cdot Zb_{2o}(n+1,\omega)\right) \tag{3.40}$$

$$a_{35}(\omega) = \frac{\lambda \cdot R_o}{2} \cdot n \cdot Z_{2o}(n,\omega) \tag{3.41}$$

$$a_{36}(\omega) = \frac{\lambda \cdot R_o}{2} \cdot n \cdot Zb_{2o}(n,\omega) \tag{3.42}$$

The other 18 coefficient functions of the determinant are the same mathematical formulation patterns as above instead R_i of R_o. This can be solved for the frequencies and their associated natural modes.

3.2 Finite element analysis

Two kinds of thick cylinder FEA models with different thicknesses are tested. Other dimensions are shown in Figure 3.3 The cylinders are 8 meters long and have a 2 meters mean diameter. The material is linear elastic and isotropic with 200 GPa Young's modules, 0.3 Poisson's Ratio and 7860 kg/m^3 density. The mesh size for each element of the model in Figure 3.3 is 0.025m×0.025m×0.025m (i.e. 4 elements through the thickness are used when the thickness is 0.1 m).

Figure 3.4 shows the mode shapes of the thicker shell (with the thickness of 0.2 meter). Two breathing modes are shown in the first picture of the second raw and the last picture of the fourth row. An extensional mode is shown as the first picture of third row. The first bending mode is shown as the first picture in the first row (the lowest frequency)

and the second bending mode is given in the second picture of the second row. Other higher shell modes (n>1) are also shown. This shows the complexity of the vibration problems for shells in general.

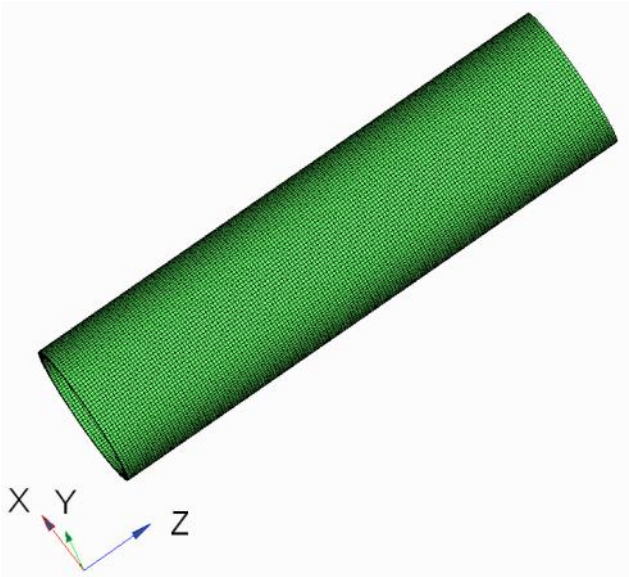

Figure 3.3 The dimensions of the 0.1 m thick shell cylinder FEA model

Different mesh sizes of the same cylinders are tested. A convergence study is conducted with both shell and solid element meshes until convergence is obtained and the required fine mesh size is determined.

Both linear and quadratic element types for solid and shell element are used and discussed. The improvement options for thick shell element in ABAQUS® are tested and compared.

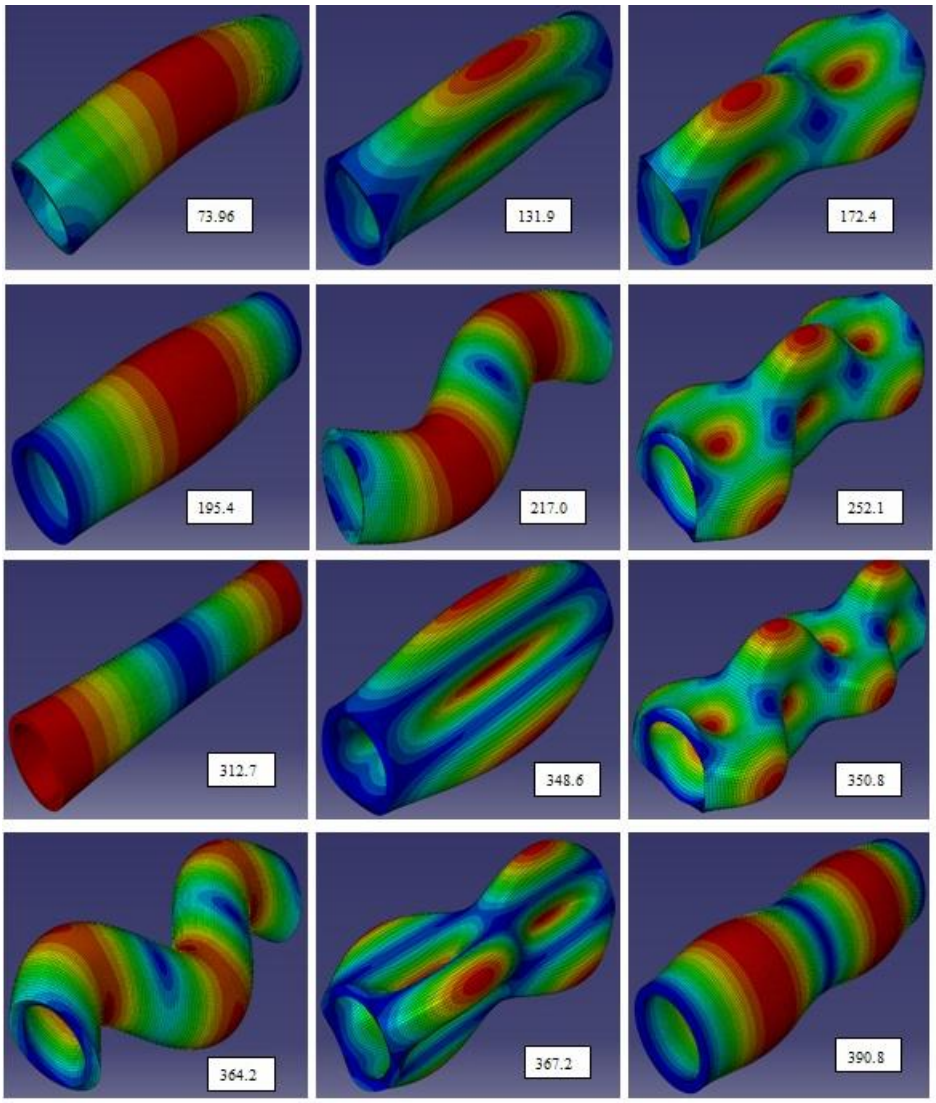

Figure 3.4 The mode shapes pictures of 0.2 thickness model

3.3 Accuracy study and results comparison

Nondimensional frequency parameters are shown in Equation 3.43, were the r_m is the mean radius (or half of the outer radius plus the inner radius). All angular frequency results are presented using the same dimensions and material properties with two different thickness values of the hollow cylinders as mentioned in the previous section.

$$\Omega = \sqrt{\frac{\rho \cdot (1-\nu^2) \cdot r_m^2 \cdot \omega^2}{E}} \tag{3.43}$$

Table 3.1 shows results obtained using the 3D elasticity for thin cylindricalshells (with a thickness ratio h/R of 1/20) which agrees to the 6th decimal with results obtained by Leissa [3].

Table 3.1 Frequency parameters for cylindrical thin shells using 3D elasticity solution, R/h = 20, ν = 0.3

ℓ/mr	n	present	ℓ/mr	n	present
1	0	0.958082810	4	0	0.464645920
	1	0.856413695		1	0.257011376
	2	0.675486335		2	0.121248730
	3	0.539294096		3	0.129881418
	4	0.492342930		4	0.219097491

Other thicker shell results [132, 144] are compared in Table 3.2 with the authors' results for further verification. The longitudinal mode parameter ℓ/mR is 1 in Table 3.2. Since a different expression is used for the nondimensional parameters, they were converted to our parameter described in (3.10). The conversion equation is shown as

$$\Omega = \frac{r_m \cdot \Omega_A}{\ell}\sqrt{(1-\upsilon)} \tag{3.44}$$

The Ω_A is non-dimension results from Armenãkas [132] (and Soldatos [144])

Table 3.2 Frequency parameters for thick cylinders using 3D elasticity solution (ν 0.3)

	h/R = 0.1			h/R =0.2			h/R = 0.3		
n	Soldatos (1990)	Armenakas (1969)	Present	Soldatos (1990)	Armenakas (1969)	Present	Soldatos (1990)	Armenakas (1969)	Present
1	1.06238	1.06226	1.062321	1.18908	1.18889	1.188896	1.33761	1.33727	1.337315
2	0.88260	0.88233	0.882490	1.10121	1.10092	1.100931	1.32371	1.32335	1.323354
3	0.80963	0.80925	0.809424	1.19793	1.19755	1.197546	1.52805	1.52764	1.527672
4	0.89905	0.89877	0.898778	1.48975	1.48933	1.489362	1.92695	1.92660	1.926662

The present results compare very closely to those of Armenakas. The difference can be due to round-off errors in the computations done by different machine and the

amount of precision. Results by Soldatos are slightly off (less than 0.1%) because of assumption made by Soldatos. With the confidence built in the accuracy of the arithmetic in the current analysis, several 3D solutions will be described here for possible use in future research on the accuracy of various shell theories and the development of more accurate shell elements.

Tables 3.3 and 3.4 present the frequencies of cylindrical shells using FEA solid and shell elements, and exact 3D elasticity theory for a shell having a thickness of 0.1 m (where a thick shell theory is applicable). The accuracy of FEA solid element C3D8R (which is the linear 8 nodes brick element) is investigated by testing the convergence with an increasing mesh size.

Table 3.3 A comparison table for frequencies (Hz) of a isotropiccylindrical shell with thickness 0.1 m, R = 1 m, ℓ = 8 m, E = 200 X 10^9 Pa, ν = 0.3

Mesh Size	H=0.1m	320×252	160×248×2	80×62×2	160×248×4	320×248×4	320×248×4	Present
m	n	Shell S4R	Continuum Shell	Solid C3D8R	Solid C3D8R	Solid C3D8R	Solid C3D20R	3D results
Breath.		195.62	195.52	195.3	195.49	195.49	195.52	195.522
1	1	73.608	73.659	73.6	73.67	73.67	73.677	73.677
	2	71.964	71.957	64.117	70.212	70.212	72.137	72.137
	3	184.77	185.46	161.7	179.61	179.61	185.23	185.225
2	1	216.42	216.60	216.5	216.59	216.59	216.62	216.623
	2	120.67	120.5	115.06	119.48	119.48	120.91	120.913
	3	199.05	199.58	175.7	193.92	193.92	199.65	199.648
3	1							
	2	204.28	204.15	199.5	203.32	203.32	204.57	204.569
	3	231.64	232.02	208.44	226.64	226.64	232.40	232.400
4	1							
	2							
	3	282.90	283.19	259.6	277.90	277.91	283.75	283.744

As Table 3.3 shows, when the mesh size in the longitudinal, circumferential, and thickness directions is 320, 248, and 4 elements, respectively (i.e., each element size is 0.25×0.25×0.25 meters), the results have converged. Interestingly, they did not converge

to the exact solution as obtained by the 3D elasticity. Noting the difference between the 320X248X4 solution using C3D8R and the exact 3D elasticity solution is about 2 % for m = 1, n = 2 and 3% for m =1 and n = 3.

Table 3.4 A comparison table for1 m, ℓ = 8 m, E = 200 X 10^9 Pa, ν = 0.3

Mesh Size	H=0.2m	320×252	160×124×4	160×248×8	160×124×4	160×124× 4	present
m	n	Shell S4R	Solid C3D8R	Solid C3D8R	Continuum Shell	Solid C3D20R	
Breath.		195.89	195.4	195.48	195.52	195.52	195.523
1	1	73.727	73.97	73.978	73.983	73.987	73.987
	2	133.34	130.85	133.81	133.98	134.73	134.734
	3	351.86	348.6	353.61	354.84	356.02	356.019
2	1	217.10	217	217.86	217.90	217.90	217.896
	2	173.28	172.44	174.24	173.47	175.16	175.155
	3	370.04	367.2	372.42	373.01	375	374.992
3	1	363.2	364.2	364.37	364.52	364.51	364.505
	2	252.56	252	253.99	252.76	254.93	254.927
	3						
4	1						
	2	351.37	350.83	353.01	351.77	354.14	354.137
	3						
other	Exten.	312.77	312.7	312.73			

The continuum shell element is an advanced shell element provided by ABAQUS® which is described in the ABAQUS® manual as: “Continuum shell elements discretize an entire three-dimensional body. The thickness is determined from the element nodal geometry. From a modeling point of view continuum shell elements look like three-dimensional continuum solids, but their kinematic and constitutive behavior is similar to conventional shell elements”. It could be understood as a 3D-2D combined model. As the results shown from the Table 3.3 to Table 3.6, it could achieve to the 2th ~ 5th decimal place agreement accuracy, where the disagreement happens when n increases. The time costs is around 5 times than shell elements (around 15 mins) for the same mesh, however still much less than the quadratic solid elements.

The quadratic 20 noded solid element C3D20R is also tested using the same mesh. The quadratic element provides very accurate results (as compared with the authors' 3D program). Results between FEM using this element and those obtained using the 3D elasticity theory agreed to the 5^{th} decimal place. However, the very large size of the mesh used in this model (using C3D20R element) resulted in spending more than 70 hours on a 4 processors workstation. This is to be compared with solutions obtained using shell elements that took minutes on the same machine. This shows that while the solid element C3D20R can be excellent for benchmarking purposes, it is impractical in industrial applications.

Further comparisons are shown for larger thickness ratios in Tables 3.5 and 3.6 for much thicker shells. A mesh of 160 element in the longitudinal dimension, 124 in the circumferential direction and 4 in the thickness direction are used. Results for thickness ratios of 0.3 and 0.4 are shown first in Table 3.5. Increasing the thickness has minimal impact on breathing mode. Or the modes m =1 and n = 1 (i.e. bending mode). This can be due to the fact that increasing the thickness increases both the inertia and stiffness with the same degree for this mode. Increasing the thickness, however has a significant impact on the higher shell mode with m = 1 and n = 2.

Table 3.5 A comparison table for frequencies (Hz) of a isotropiccylindrical shells, R = 1 m, ℓ = 8 m, E = 200 X 10^9 Pa, ν = 0.3, A 160×124× 4 mesh

m	n	H = 0.3 m		H = 0.4 m	
		C3D20R FEM	Present/ 3D	C3D20R FEM	Present/ 3D
1	1	74.496	74.49618618	75.196	75.19610770
	2	195.19	195.18842500	251.31	251.30811987
	0 (Breathing 1)	195.52	195.52184759	195.52	195.52000000
2	1	219.96	219.95565686	222.71	222.71466583
	2	234.6	234.59857585	291.57	291.57084477
	0 (Breathing 2)	391.05	391.04687826	391.05	391.04369518
3	1	369.95	369.95054891	376.97	376.97054921
	2	315.13	315.12496561	374.61	374.60611329
4	1				
	2	421.9	421.89767218	488.58	488.58088092
Extension		312.72		312.68	
Shear		499.71		501.06	

Table 3.6 A comparison table for frequencies (Hz) of a isotropiccylindrical shells, R = 1 m, ℓ = 8 m, E = 200 X 10^9 Pa, ν = 0.3, A 160×124× 4 mesh

m	n	H = 0.5 m		H = 0.6 m	
		C3D20R FEM	Present/ 3D	C3D20R FEM	Present/ 3D
1	1	76.074	76.07430818	77.116	77.11611100
	2	302.46	302.46123051	348.67	348.66819312
	0	195.52	195.52264336	195.52	195.52184918
2	1	226.07	226.06649692	229.89	229.89463367
	2	343.66	343.66410075	390.34	390.33915691
	0	391.05	391.04528673	291.05	391.04369518
3	1	385.11	385.11181845	393.94	393.94182014
	2	429.16	429.15780137	477.58	477.57772760
4	1	537.46	537.46390965	554.42	554.41647557
Extension		312.64		312.58	
Shear		502.7		504.56	

It is also observed in these tables that the solid elements used here gave solutions that agreed with the 3D elasticity solution to the fifth decimal place for most cases. This is important because it builds confidence in using this kind of 3D solid FEM for other boundary conditions (e.g. a cantilevered or completely clamped cylinder) where a 3D

exact solution simply does not exist. We have kept 10 or more significant figured in the 3D exact solution here to allow for accurate future benchmarking.

In addition, we did provide results for higher thickness values to tests shell theories that can be applicable for higher values of thickness like higher order shell theories.

For the shell element, more options and parameters could be selected. These options which could influence the homogeneous linear problem are tested as shown in Tables 3.7 and 3.8 for different thicknesses [145]:

i. The 4 noded linear elements S4R for thin and thick shell (shear deformation included).
ii. The 8 noded quadratic elements S8R for thick shell.
iii. Under S4R element, second order accuracy could be selected for improvement.
iv. Under S4R element, membrane strains could be specified as finite (default) or small deformation.
v. Thickness integration method could be chosen as Simpson or Gauss. Different quantity of thickness integration points could be specified. 2 points for Gauss and 3 points for Simpson are suggested for linear problem. 8 points for Gauss and 9 points for Simpson are suggested.
vi. Transverse Shear Stiffness could be specified.

Table 3.7 A comparison table for frequencies (Hz) of a isotropiccylindrical shell with thickness 0.1 m, R = 0.95 m, ℓ = 8 m, E = 200 X 10^9 Pa, ν = 0.3 using different shell element options in ABAQUS®

Mesh Size	H= 0.1m	160×124	320×252	320*252	320*252	320*252
m	n	S4R	S4R [1]	S4R [1,2]	S8R	S8R [3]
Breathing (n=0)		175.9	176.24	177.26	177.03	179.68
1	1	69.7	69.776	69.871	69.84	70.130
	2	76.5	76.506	76.525	76.496	76.969
	3	199	198.62	198.65	198.48	201.09
2	1	204.2	204.54	205.13	204.91	206.82
	2	121.3	121.32	121.54	121.45	122.34
	3	212.2	211.82	211.9	211.7	214.60
3	1					
	2	200	200.07	200.75	200.5	202.51
	3	242	241.61	241.85	241.59	245.06
4	1					
	2					
	3	288.9	288.43	289.13	288.75	293.17

Table 3.8 A comparison table for frequencies (Hz) of a isotropiccylindrical shell with thickness 0.2 m, R = 0.9 m, ℓ = 8 m, E = 200 X 10^9 Pa, ν = 0.3 using different shell element options in ABAQUS®

Mesh Size	H= 0.2m	160×124	320*252	320*252	320*252	320*252	Present
m	n	S4R	S4R [1]	S4R [1,2]	S8R[4]	S8R[3]	3D results
Breathing (n=0)		156.6	156.65	160.21	160.08	163.51	195.523
1	1	65.7	65.784	66.265	66.23	66.64	73.987
	2	152	151.95	152.03	151.95	155.61	134.734
	3	393	392.05	392.26	391.75	408.69	354.631
2	0	312.62	312.62	319.67	319.09	326.56	
	1	191.4	191.36	194.33	194.04	196.85	217.896
	2	184.6	184.45	185.3	185.1	189.48	175.155
	3						374.992
3	1	319.3	319.23	325.44	324.63	331.17	364.505
	2	250.8	250.66	253.43	252.96	259.12	254.927
	3						

From the parametric studies performed and the results shown in the Table 3.7 and 3.8, we conclude that the difference between various choices (Gauss and Simpsons integration points, accuracy order, the transverse shear coefficient) did not show clear

improvements. It should be noted here that the S8R element model costs 10 times the time needed for calculations with the S4R element.

CHAPTER IV

3D ELASTICITY FOR ORTHOTROPIC HOLLOW CYLINDERS AND CORRESPONDING STUDIES

In this Chapter, the model is the hollow cylinder of orthotropic materials. SD-SD boundary conditions are applied on the cylinder ends. This boundary condition allows us to make separation of variables for the PDE mathematical model. The exact solution of 3D elasticity for natural frequencies is used to test the accuracy of the Abaqus® solid and shell elements and advance shell theories for the orthotropic material.

4.1 3D elasticity theory of orthotropic hollow cylinder

In the same cylindrical coordinate system used in Chapter III, the equilibrium and kinematic equations are the same as those for isotropic cylinders. These were discussed in last chapter. Here, the capital U, V, and W represent the displacement parameters in the x, θ, and r directions, which in turn represent the longitudinal, circumferential, and radial directions; respectively. The total length, inner radius, and outer radius of the thick hollow cylinder are ℓ, R_i, and R_o. σ and τ are the normal and shear stress tensors with different directions suffixes. ε and γ are the normal and shear strain tensors with corresponding directions suffixes. The couple stresses with higher order differential divisor are neglected.

The constitutive equations are different between isotropic material model and orthotropic material model. For the isotropic material, two elasticity parameters (Young's modulus E and Poisson's ratio ν) are enough to show the elastic stress-strain relationships

in Equation 3.10 to 3.11. However for orthotropic material, 9 independent elasticity parameters are required, which is shown as constants C with suffixes in the elastic stiffness matrix equation 4.1. Here the index notations follow the ABAQUS® definition [145] for the further comparison:

$$\begin{bmatrix}\sigma_{rr}\\ \sigma_{\theta\theta}\\ \sigma_{xx}\\ \tau_{r\theta}\\ \tau_{rx}\\ \tau_{\theta x}\end{bmatrix}=\begin{bmatrix}C_{11} & C_{12} & C_{13} & & & \\ & C_{22} & C_{23} & & 0 & \\ & & C_{33} & & & \\ & & & C_{44} & & \\ & SYM & & & C_{55} & \\ & & & & & C_{66}\end{bmatrix}\begin{bmatrix}\varepsilon_{rr}\\ \varepsilon_{\theta\theta}\\ \varepsilon_{xx}\\ \Upsilon_{r\theta}\\ \Upsilon_{rx}\\ \Upsilon_{\theta x}\end{bmatrix} \tag{4.1}$$

Although the 9 elasticity parameters increase the complexity of the mathematical model, there is a great virtue of orthotropic materials: no coupling between the normal stress/strain and shear strain/stress parameters. From the equation 4.1, σ are independent ofΥ and τ are independent ofε. These independencies ensure the separation of variables (Equation 3.25 to 3.27) still works.

However, these 9 elasticity parameters can't be directly obtained from testing. For composite materials, the engineering constants E, G and ν associating with the material's principal directions are more commonly reported. The engineering constitutive relationships are presented as:

$$\begin{bmatrix}\varepsilon_{rr}\\ \varepsilon_{\theta\theta}\\ \varepsilon_{xx}\\ \Upsilon_{r\theta}\\ \Upsilon_{rx}\\ \Upsilon_{\theta x}\end{bmatrix}=\begin{bmatrix}1/E_r & -\nu_{\theta r}/E_\theta & -\nu_{xr}/E_x & & & \\ -\nu_{r\theta}/E_r & 1/E_\theta & -\nu_{x\theta}/E_x & & 0 & \\ -\nu_{rx}/E_r & -\nu_{\theta x}/E_\theta & 1/E_x & & & \\ & & & 1/G_{r\theta} & 0 & 0\\ & 0 & & 0 & 1/G_{rx} & 0\\ & & & 0 & 0 & 1/G_{\theta x}\end{bmatrix}\begin{bmatrix}\sigma_{rr}\\ \sigma_{\theta\theta}\\ \sigma_{xx}\\ \sigma_{r\theta}\\ \sigma_{rx}\\ \sigma_{\theta x}\end{bmatrix} \tag{4.2}$$

The relationships between the engineering constants and the elasticity parameters are shown as :

$$C_{11}=E_r(1-\nu_{\theta x}\nu_{x\theta})\Upsilon \tag{4.3}$$
$$C_{22}=E_\theta(1-\nu_{rx}\nu_{xr})\Upsilon \tag{4.4}$$
$$C_{33}=E_x(1-\nu_{r\theta}\nu_{\theta r}) \tag{4.5}$$

$$C_{12} = E_r(\nu_{\theta r} + \nu_{xr}\nu_{\theta x})\Upsilon = E_\theta(\nu_{r\theta} + \nu_{x\theta}\nu_{rx})\Upsilon \quad (4.6)$$
$$C_{13} = E_r(\nu_{xr} + \nu_{\theta r}\nu_{x\theta})\Upsilon = E_x(\nu_{rx} + \nu_{r\theta}\nu_{\theta x})\Upsilon \quad (4.7)$$
$$C_{23} = E_\theta(\nu_{x\theta} + \nu_{r\theta}\nu_{xr})\Upsilon = E_x(\nu_{\theta x} + \nu_{\theta r}\nu_{rx})\Upsilon \quad (4.8)$$
$$C_{44} = G_{r\theta} \quad (4.9)$$
$$C_{55} = G_{rx} \quad (4.10)$$
$$C_{66} = G_{\theta x} \quad (4.11)$$
$$\Upsilon = {}^{1}/_{(1 - \nu_{r\theta}\nu_{\theta r} - \nu_{\theta x}\nu_{x\theta} - \nu_{xr}\nu_{rx} - 2\nu_{\theta r}\nu_{x\theta}\nu_{rx})} \quad (4.12)$$

Substituting the constitutive equations into the kinematic equations and combining with the equilibrium equations, the equilibrium relationships equation 4.13 to 4.15in terms of displacements are obtained in a manner similar to governing equations for isotropic material:

$$L_{11} \cdot U + L_{12} \cdot V + L_{13} \cdot W = \frac{\partial^2}{\partial t^2} U \quad (4.13)$$
$$L_{21} \cdot U + L_{22} \cdot V + L_{23} \cdot W = \frac{\partial^2}{\partial t^2} V \quad (4.14)$$
$$L_{31} \cdot U + L_{32} \cdot V + L_{33} \cdot W = \frac{\partial^2}{\partial t^2} W \quad (4.15)$$

where L11 … L33 are the differential operators which are given below

$$L_{11} = C_{55}\frac{\partial^2}{\partial r^2} + C_{55}\frac{1}{r}\frac{\partial}{\partial r} + C_{66}\frac{1}{r^2}\frac{\partial^2}{\partial \theta^2} + C_{33}\frac{\partial^2}{\partial x^2} \quad (4.16)$$
$$L_{12} = (C_{23} + C_{66})\frac{1}{r}\frac{\partial^2}{\partial \theta\, \partial x} \quad (4.17)$$
$$L_{13} = (C_{13} + C_{55})\frac{\partial^2}{\partial r\, \partial x} + (C_{55} + C_{23})\frac{1}{r}\frac{\partial}{\partial x} \quad (4.18)$$
$$L_{21} = (C_{23} + C_{66})\frac{1}{r}\frac{\partial^2}{\partial \theta\, \partial x} \quad (4.19)$$
$$L_{22} = C_{44}\frac{\partial^2}{\partial r^2} + C_{44}\frac{1}{r}\frac{\partial}{\partial r} + C_{22}\frac{1}{r^2}\frac{\partial^2}{\partial \theta^2} - C_{44}\frac{1}{r^2} + C_{66}\frac{\partial^2}{\partial x^2} \quad (4.20)$$
$$L_{23} = (C_{12} + C_{44})\frac{1}{r}\frac{\partial^2}{\partial r\, \partial \theta} + (C_{44} + C_{22})\frac{1}{r^2}\frac{\partial}{\partial \theta} \quad (4.21)$$
$$L_{31} = (C_{13} + C_{55})\frac{\partial^2}{\partial r\, \partial x} + (C_{13} - C_{23})\frac{1}{r}\frac{\partial}{\partial x} \quad (4.22)$$
$$L_{32} = (C_{12} + C_{44})\frac{1}{r}\frac{\partial^2}{\partial r\, \partial \theta} - (C_{44} + C_{22})\frac{1}{r^2}\frac{\partial}{\partial \theta} \quad (4.23)$$
$$L_{33} = C_{11}\frac{\partial^2}{\partial r^2} + C_{11}\frac{1}{r}\frac{\partial}{\partial r} + C_{44}\frac{1}{r^2}\frac{\partial^2}{\partial \theta^2} - C_{22}\frac{1}{r^2} + C_{55}\frac{\partial^2}{\partial x^2} \quad (4.24)$$

Assuming the solutions in the form below

$$U = u(r) \cdot \cos(n \cdot \theta) \cdot \cos(\lambda \cdot x) \cdot \cos(\omega \cdot t) \quad (4.25)$$
$$V = v(r) \cdot \sin(n \cdot \theta) \cdot \sin(\lambda \cdot x) \cdot \cos(\omega \cdot t) \quad (4.26)$$
$$W = w(r) \cdot \cos(n \cdot \theta) \cdot \sin(\lambda \cdot x) \cdot \cos(\omega \cdot t) \quad (4.27)$$
$$\lambda = m\pi/\ell \quad (4.28)$$

where m and n are the longitudinal and circumferential mode numbers; respectively. The shear diaphragms boundary conditions at both ends (referred to as SD-SD) are satisfied by these solutions.

Substituting the solutions equations(4.25 to 4.28) to equation (4.13 to 4.15), the right sides of equations goes to zero, and the differential operators of the left sides would change to:

$$L_{11} = C_{55}\frac{\partial^2}{\partial r^2} + C_{55}\frac{1}{r}\frac{\partial}{\partial r} - C_{66}\frac{1}{r^2}n^2 - C_{33}\lambda^2 + \rho\omega^2 \tag{4.29}$$

$$L_{12} = (C_{23} + C_{66})\frac{1}{r}n \cdot \lambda \tag{4.30}$$

$$L_{13} = (C_{13} + C_{55})\frac{\partial}{\partial r}\lambda + (C_{55} + C_{23})\frac{1}{r}\lambda \tag{4.31}$$

$$L_{21} = (C_{23} + C_{66})\frac{1}{r}n \cdot \lambda \tag{4.32}$$

$$L_{22} = C_{44}\frac{\partial^2}{\partial r^2} + C_{44}\frac{1}{r}\frac{\partial}{\partial r} - C_{22}\frac{1}{r^2}n^2 - C_{44}\frac{1}{r^2} - C_{66}\lambda^2 + \rho\omega^2 \tag{4.33}$$

$$L_{23} = -(C_{12} + C_{44})\frac{1}{r}\frac{\partial}{\partial r}n - (C_{44} + C_{22})\frac{1}{r^2}n \tag{4.34}$$

$$L_{31} = -(C_{13} + C_{55})\frac{\partial}{\partial r}\lambda - (C_{13} - C_{23})\frac{1}{r}\lambda \tag{4.35}$$

$$L_{32} = (C_{12} + C_{44})\frac{1}{r}\frac{\partial}{\partial r}n - (C_{44} + C_{22})\frac{1}{r^2}n \tag{4.36}$$

$$L_{33} = C_{11}\frac{\partial^2}{\partial r^2} + C_{11}\frac{1}{r}\frac{\partial}{\partial r} - C_{44}\frac{1}{r^2}n^2 - C_{22}\frac{1}{r^2} - C_{55}\lambda^2 + \rho\omega^2 \tag{4.37}$$

Here, from the mathematical point of view, the previous partial differential system changes to a linear homogeneous ordinary differential system in radius direction, if the frequency ω is treated as constants. And because the studying subjective is the hollow cylinder where the interval Ro>r>Ri>0 avoids the singularity points r=0, then all coefficient functions are continuous in the interval. This continuity is an essential property for the existence of solutions. As been discussed in Chapter 2, Frobenius method (or Power series method) was suggested to solve this ordinary differential system.

The power series method is a “root” level method to solve the differential equations, (for example, Bessel functions are developed from the power series method). Although the primary property broadens the range of the equations to be possibly solved, the feasibility of the Frobenius method still should be discussed in order to understand the

least requirements. On the other hand, the barbaric method significantly increases the complexity of the solution procedures and the solution itself. For example, as the Bessel functions successfully solved the isotropic case in Chapter 3, it is very difficult to obtain the natural frequency solutions or even the displacement general solution functions for isotropic material (similar with transversely isotropic materials) by the power series method. The reasons for it, especially for obtaining the natural frequency, will be discussed in later sections.

4.2 The general solutions of the Frobenius' Theorem

At first, some notation announcements will help read this section.

i. The lower case u, v and w are used instead the u(r), v(r) and w(r).

ii. Using the subscript instead of the derivates. For example the first and secondary derivates in w directions are expressed as w_r and $w_{rr.}$

4.2.1 Feasibility

In order to make the derivation easier to express, use Greek letter α and Ω with subscripts to stand for the constant equations are defined as shown below:

$$\alpha_1 = \frac{-C_{66}\cdot n^2}{C_{55}} \tag{4.38}$$

$$\alpha_2 = \frac{(C_{23}+C_{66})\cdot n\cdot\lambda}{C_{55}} \tag{4.39}$$

$$\alpha_3 = \frac{(C_{13}+C_{55})\cdot\lambda}{C_{55}} \tag{4.40}$$

$$\alpha_4 = \frac{(C_{23}+C_{55})\cdot\lambda}{C_{55}} \tag{4.41}$$

$$\alpha_5 = \frac{(C_{23}+C_{66})\cdot n\cdot\lambda}{C_{44}} \tag{4.42}$$

$$\alpha_6 = \frac{-(C_{22}\cdot n^2+C_{44})}{C_{44}} \tag{4.43}$$

$$\alpha_7 = \frac{-(C_{12}+C_{44})\cdot n}{C_{44}} \tag{4.44}$$

$$\alpha_8 = \frac{-(C_{22}+C_{44})\cdot n}{C_{44}} \tag{4.45}$$

$$\alpha_9 = \frac{-(C_{13}+C_{55})\cdot\lambda}{C_{11}} \tag{4.46}$$

$$\alpha_{10} = \frac{-(C_{13}-C_{23})\cdot\lambda}{C_{11}} \tag{4.47}$$

$$\alpha_{11} = \frac{(C_{12}+C_{44})\cdot n}{C_{11}} \tag{4.48}$$

$$\alpha_{12} = \frac{-(C_{22}+C_{44})\cdot n}{C_{11}} \tag{4.49}$$

$$\alpha_{13} = \frac{-(C_{44}\cdot n^2+C_{22})}{C_{11}} \tag{4.50}$$

$$\Omega_1 = \frac{\rho\cdot\omega^2-C_{33}\cdot\lambda^2}{C_{55}} \tag{4.51}$$

$$\Omega_2 = \frac{\rho\cdot\omega^2-C_{66}\cdot\lambda^2}{C_{44}} \tag{4.52}$$

$$\Omega_3 = \frac{\rho\cdot\omega^2-C_{55}\cdot\lambda^2}{C_{11}} \tag{4.53}$$

After these simplifying procedures, the ordinary differential equations system would be written as the following equations:

$$u_{rr} + \frac{1}{r}u_r + \alpha_3 w_r + \left(\frac{\alpha_1}{r^2} + \Omega_1\right)u + \frac{\alpha_2}{r}v + \frac{\alpha_4}{r}w = 0 \tag{4.54}$$

$$v_{rr} + \frac{1}{r}v_r + \frac{\alpha_7}{r}w_r + \frac{\alpha_5}{r}u + \left(\frac{\alpha_6}{r^2} + \Omega_2\right)v + \frac{\alpha_8}{r^2}w = 0 \tag{4.55}$$

$$w_{rr} + \alpha_9 u_r + \frac{\alpha_{11}}{r}v_r + \frac{1}{r}w_r + \frac{\alpha_{10}}{r}u + \frac{\alpha_{12}}{r^2}v + \left(\frac{\alpha_{13}}{r^2} + \Omega_3\right)w = 0 \tag{4.56}$$

and could be rewriten in the matrix form as followed:

$$\begin{bmatrix}1 & 0 & 0\\ 0 & 1 & 0\\ 0 & 0 & 1\end{bmatrix}\begin{bmatrix}u_{rr}\\ v_{rr}\\ w_{rr}\end{bmatrix} + \begin{bmatrix}\frac{1}{r} & 0 & \alpha_3\\ 0 & \frac{1}{r} & \frac{\alpha_7}{r}\\ \alpha_9 & \frac{\alpha_{11}}{r} & \frac{1}{r}\end{bmatrix}\begin{bmatrix}u_r\\ v_r\\ w_r\end{bmatrix} + \begin{bmatrix}\frac{\alpha_1}{r^2}+\Omega_1 & \frac{\alpha_2}{r} & \frac{\alpha_4}{r}\\ \frac{\alpha_5}{r} & \frac{\alpha_6}{r^2}+\Omega_2 & \frac{\alpha_8}{r^2}\\ \frac{\alpha_{10}}{r} & \frac{\alpha_{12}}{r^2} & \frac{\alpha_{13}}{r^2}+\Omega_3\end{bmatrix}\begin{bmatrix}u\\ v\\ w\end{bmatrix} = 0 \tag{4.57}$$

Simplifying the above equations:

$$\mathbf{I}\cdot\mathbf{D_{rr}} + \mathbf{M_1}\cdot\mathbf{D_r} + \mathbf{M_2}\cdot\mathbf{D} = \mathbf{0} \tag{4.58}$$

Expanding u, v, and w at r = 0 which is a regular singular point. The regular singular point is the feasibility requirement for Frobenius' Theorem, which are [133]:

$$r > 0$$

For the matrix$\mathbf{M_1}\cdot r$, $\mathbf{M_2}\cdot r^2$ are analytic at r=0.

When satisfying the feasibility requirements, at least one solution could be found for each of the three displacements.

4.2.2 Solution procedures

First of all, we assume the solutions for respectively three directions as the following expanding power series with series constants a_p, b_p, and c_p. z is a power constant which could be achieved later:

$$u = \sum_{p=0}^{\infty} a_p r^{p+z} \tag{4.59}$$
$$v = \sum_{p=0}^{\infty} b_p r^{p+z} \tag{4.60}$$
$$w = \sum_{p=0}^{\infty} c_p r^{p+z} \tag{4.61}$$

Then we calculate the first and second derivates of assumed solutions:

$$u_r = \sum_{p=0}^{\infty} a_p (p+z) r^{p+z-1} \tag{4.62}$$
$$v_r = \sum_{p=0}^{\infty} b_p (p+z) r^{p+z-1} \tag{4.63}$$
$$w_r = \sum_{p=0}^{\infty} c_p (p+z) r^{p+z-1} \tag{4.64}$$
$$u_{rr} = \sum_{p=0}^{\infty} a_p (p+z)(p+z-1) r^{p+z-2} \tag{4.65}$$
$$v_{rr} = \sum_{p=0}^{\infty} b_p (p+z)(p+z-1) r^{p+z-2} \tag{4.66}$$
$$w_{rr} = \sum_{p=0}^{\infty} c_p (p+z)(p+z-1) r^{p+z-2} \tag{4.67}$$

We then substitute these expressions to ordinary differential equations (ODE). The ODE system convert to the power series express as below:

$$\sum_{p=0}^{\infty}\Big\{\big[a_p(p+z)(p+z-1) + a_p(p+z) + \alpha_1 a_p\big] r^{p+z-2} + \big[\alpha_3 c_p(p+z) + \alpha_2 b_p + \alpha_4 c_p\big] r^{p+z-1} + \Omega_1 a_p r^{p+z}\Big\} = 0 \tag{4.68}$$

$$\sum_{p=0}^{\infty}\Big\{\big[b_p(p+z)(p+z-1) + b_p(p+z) + \alpha_6 b_p + \alpha_7 c_p(p+z) + \alpha_8 c_p\big] r^{p+z-2} + \alpha_5 a_p r^{p+z-1} + \Omega_2 b_p r^{p+z}\Big\} = 0 \tag{4.69}$$

$$\sum_{p=0}^{\infty}\Big\{\big[c_p(p+z)(p+z-1) + c_p(p+z) + \alpha_{13} c_p + \alpha_{11} b_p(p+z) + \alpha_{12} b_p\big] r^{p+z-2} + [\alpha_9 a_p(p+z) + \alpha_{10} a_p] r^{p+z-1} + \Omega_3 c_p r^{p+z}\Big\} = 0 \tag{4.70}$$

For combining the variable power series terms r^{p+z-2}, $r^{p+z-1}$and r^{p+z}, we move the indices of coefficient functions and powers of r^{p+z-2}, r^{p+z-1} to r^{p+z} as followed:

$$\sum_{p=-2}^{\infty} a_{p+2}[(p+z+2)^2 + \alpha_1] r^{p+z} + \sum_{p=-1}^{\infty}\big\{c_{p+1}[\alpha_3(p+z+1) + \alpha_4] + \alpha_2 b_{p+1}\big\} r^{p+z} + \sum_{p=0}^{\infty} \Omega_1 a_p r^{p+z} = 0 \tag{4.71}$$

$$\sum_{p=-2}^{\infty}\big\{b_{p+2}[(p+z+2)^2 + \alpha_6] + c_{p+2}[\alpha_7(p+z+2) + \alpha_8]\big\} r^{p+z} + \sum_{p=-1}^{\infty} \alpha_5 a_{p+1} r^{p+z} + \sum_{p=0}^{\infty} \Omega_2 b_p r^{p+z} = 0 \tag{4.72}$$

$$\sum_{p=-2}^{\infty}\big\{c_{p+2}[(p+z+2)^2 + \alpha_{13}] + b_{p+2}[\alpha_{11}(p+z+2) + \alpha_{12}]\big\} r^{p+z} + \sum_{p=-1}^{\infty} a_{p+1}[\alpha_9(p+z+1) + \alpha_{10}] r^{p+z} + \sum_{p=0}^{\infty} \Omega_3 c_p r^{p+z} = 0 \tag{4.73}$$

Then we combine the summation terms of r^{p+z} from zero to infinity, in the same time, several terms with the indices p<0 will be rejected from the infinite summation. The

coefficient functions of these terms are called indices equations. After the combination, the above equations deduce to:

$$a_0[z^2+\alpha_1]\cdot r^{z-2}+\{a_1[(z+1)^2+\alpha_1]+c_0[\alpha_3 z+\alpha_4]+\alpha_2 b_0\}\cdot r^{z-1}+\sum_{p=0}^{\infty}\{a_{p+2}[(p+z+2)^2+\alpha_1]+c_{p+1}[\alpha_3(p+z+1)+\alpha_4]+\alpha_2 b_{p+1}+\Omega_1 a_p\}r^{p+z}=0 \quad (4.74)$$

$$\{b_0[z^2+\alpha_6]+c_0[\alpha_7 z+\alpha_8]\}r^{z-2}+\{b_1[(z+1)^2+\alpha_6]+c_1[\alpha_7(z+1)+\alpha_8]+\alpha_5 a_0\}r^{z-1}+\sum_{p=0}^{\infty}\{b_{p+2}[(p+z+2)^2+\alpha_6]+c_{p+2}[\alpha_7(p+z+2)+\alpha_8]+\alpha_5 a_{p+1}+\Omega_2 b_p\}r^{p+z}=0 \quad (4.75)$$

$$\{c_0[z^2+\alpha_{13}]+b_0[\alpha_{11}z+\alpha_{12}]\}r^{z-2}+\{c_1[(z+1)^2+\alpha_{13}]+b_1[\alpha_{11}(z+1)+\alpha_{12}]+a_0[\alpha_9 z+\alpha_{10}]\}r^{z-1}+\sum_{p=0}^{\infty}\{c_{p+2}[(p+z+2)^2+\alpha_{13}]+b_{p+2}[\alpha_{11}(p+z+2)+\alpha_{12}]+a_{p+1}[\alpha_9(p+z+1)+\alpha_{10}]+\Omega_3 c_p\}r^{p+z}=0 \quad (4.76)$$

In this ODE systems, the indicial equations are the six coefficient equations before the $r^{z-2}$and r^{z-1}. Note that

i. r is not zero.

ii. The different power indicial terms such as the r^{z-2} andr^{z-1} are linear independent.

So these coefficient equations have to be zero as showing below:

$$a_0[z^2+\alpha_1]=0 \quad (4.77)$$

$$b_0[z^2+\alpha_6]+c_0[\alpha_7 z+\alpha_8]=0 \quad (4.78)$$

$$c_0[z^2+\alpha_{13}]+b_0[\alpha_{11}z+\alpha_{12}]=0 \quad (4.79)$$

$$a_1[(z+1)^2+\alpha_1]+c_0[\alpha_3 z+\alpha_4]+\alpha_2 b_0=0 \quad (4.80)$$

$$b_1[(z+1)^2+\alpha_6]+c_1[\alpha_7(z+1)+\alpha_8]+\alpha_5 a_0=0 \quad (4.81)$$

$$c_1[(z+1)^2+\alpha_{13}]+b_1[\alpha_{11}(z+1)+\alpha_{12}]+a_0[\alpha_9 z+\alpha_{10}]=0 \quad (4.82)$$

Rewriting the first three indices equations of (Equation 4.77 to 4.79) into matrix form yields:

$$\begin{bmatrix} z^2+\alpha_1 & 0 & 0 \\ 0 & z^2+\alpha_6 & \alpha_7 z+\alpha_8 \\ 0 & \alpha_{11}z+\alpha_{12} & z^2+\alpha_{13} \end{bmatrix}\begin{bmatrix} a_0 \\ b_0 \\ c_0 \end{bmatrix}=0 \quad (4.83)$$

The a_0, b_0 and c_0 can not be all zero, otherwise a_p, b_p and c_p will all become zero and u, v, w become zero as well yielding the trivial solutions. So the determinant of

the left side 3X3 matrix has to be zero and the a_0, b_0 or c_0 could be arbitrary. From the zero determinant, six roots of z could be achieved as:

$$z(1) = \sqrt{-\alpha_1} \tag{4.84}$$

$$z(2) = -\sqrt{-\alpha_1} \tag{4.85}$$

$$z(3) = \sqrt{\frac{-B+\sqrt{B^2-4C}}{2}} \tag{4.86}$$

$$z(4) = -\sqrt{\frac{-B+\sqrt{B^2-4C}}{2}} \tag{4.87}$$

$$z(5) = \sqrt{\frac{-B-\sqrt{B^2-4C}}{2}} \tag{4.88}$$

$$z(6) = -\sqrt{\frac{-B-\sqrt{B^2-4C}}{2}} \tag{4.89}$$

where $B = \alpha_6 + \alpha_{13} - \alpha_7\alpha_{11}$

$C = \alpha_6\alpha_{13} - \alpha_8\alpha_{12}$

Six roots of z indicate six power series for each u, v and w, which are six solutions of u, v and w respectively. For the second order three variables ODE system is obtained. The general solutions for each of the variables are generated from six (2X3) linear independent solutions. For satisfying the linear independence, the simple situation is not repeated solutions. For the power series solutions here, no repeated solutions mean that the six roots of z are different and the differences with each one are not an integer. The special of the integer difference is because if the difference is integer the different power series are the same series for an infinitely long cylinder. In this case, we don't need to build the new linear independent solutions from the repeated solutions. The simplest situation is the real (none repeated) solutions. And the simplest one is also best for the benchmark sought here because it is more stable, No new functions and potential singularities need to be introduced into the power series.

So under this simplest situation, the coefficient series a_p, b_p and c_p could be calculated according to the following steps.

First, obtain the a_0, b_0 and c_0; a_1, b_1 and c_1 from the indices equations. Two routes of calculation by different roots of z are required and explained as below:

i. Pick up the roots z(1) and z(2) to substitute into indices equations:

   a. $a_0$is arbitrary, for example setting as 1.

   b. $b_0$andc_0 have to be zero. The reason is:

   $$\left|\begin{bmatrix} z^2+\alpha_6 & \alpha_7 z+\alpha_8 \\ \alpha_{11}z+\alpha_{12} & z^2+\alpha_{13} \end{bmatrix}\right| \neq 0$$

   c. Substitute the a_0, b_0 and c_0 into other three indicial equations so that a_1, b_1 and c_1 could be achieved, which are (as $a_0 = 1$):

   $$a_1 \quad = 0 \begin{bmatrix} b_1 \\ c_1 \end{bmatrix} =$$

   $$\begin{bmatrix} (z+1)^2+\alpha_6 & \alpha_7(z+1)+\alpha_8 \\ \alpha_{11}(z+1)+\alpha_{12} & (z+1)^2+\alpha_{13} \end{bmatrix}^{-1} \begin{bmatrix} -\alpha_5 \\ -[\alpha_9 z+\alpha_{10}] \end{bmatrix}$$

ii. Pick up the other roots to apply in the indices equations:

   a. $b_0$orc_0 could be arbitrary, for example setting both as $b_0 = 1$, then $c_0 = \frac{-z^2-\alpha_6}{\alpha_7 z+\alpha_8}$.

   b. $a_0$has to be zero. The reason is: $z^2 + \alpha_1 \neq 0$

   c. Same as route I to achieve a_1, b_1 and c_1 from other indices equations while as $b_0 = 1$

   $$b_1 = 0, c_1 = 0 a_1 = \frac{-\alpha_2}{(z+1)^2+\alpha_1} + \frac{-z^2-\alpha_6}{\alpha_7 z+\alpha_8} \cdot \frac{-\alpha_3 z-\alpha_4}{(z+1)^2+\alpha_1}$$

With the initial six constants achieved from above two routes, other constants of certain z could be obtained by the three recurrence equations below which come from the coefficient functions of power series in equation:

$$a_{p+2}[(p+z+2)^2+\alpha_1] + c_{p+1}[\alpha_3(p+z+1)+\alpha_4] + \alpha_2 b_{p+1} + \Omega_1 a_p = 0 \quad (4.90)$$

$$b_{p+2}[(p+z+2)^2+\alpha_6] + c_{p+2}[\alpha_7(p+z+2)+\alpha_8] + \alpha_5 a_{p+1} + \Omega_2 b_p = 0 \quad (4.91)$$

$$c_{p+2}[(p+z+2)^2+\alpha_{13}]+b_{p+2}[\alpha_{11}(p+z+2)+\alpha_{12}]+a_{p+1}[\alpha_9(p+z+1)+\alpha_{10}]+\Omega_3 c_p=0 \tag{4.92}$$

Noticing here, for route I: The constants a_{2p+1}, b_{2p} and c_{2p} are always zero; for case II: The constants a_{2p}, b_{2p+1} and c_{2p+1} are always zero. Rewrite the recurrence equations as the following equations for easily achieving new constants and subsequent programming:

$$a_{p+2} \leftarrow K_1 a_p + K_2 b_{p+1} + K_3 c_{p+1} \tag{4.93}$$
$$b_{p+2} \leftarrow K_4 a_{p+1} + K_5 b_p + K_6 c_p \tag{4.94}$$
$$c_{p+2} \leftarrow K_7 a_{p+1} + K_8 b_p + K_9 c_p \tag{4.95}$$

where

$$K_1 = \frac{-\Omega_1}{(p+z+2)^2+\alpha_1} \tag{4.96}$$
$$K_2 = \frac{-\alpha_2}{(p+z+2)^2+\alpha_1} \tag{4.97}$$
$$K_3 = \frac{-[\alpha_3(p+z+1)+\alpha_4]}{(p+z+2)^2+\alpha_1} \tag{4.98}$$
$$K_4 = \frac{-\frac{\alpha_9(p+z+1)+\alpha_{10}}{(p+z+2)^2+\alpha_{13}}+\frac{\alpha_5}{\alpha_7(p+z+2)+\alpha_8}}{\frac{\alpha_{11}(p+z+2)+\alpha_{12}}{(p+z+2)^2+\alpha_{13}}-\frac{(p+z+2)^2+\alpha_6}{\alpha_7(p+z+2)+\alpha_8}} \tag{4.99}$$
$$K_5 = \frac{\frac{\Omega_2}{\alpha_7(p+z+2)+\alpha_8}}{\frac{\alpha_{11}(p+z+2)+\alpha_{12}}{(p+z+2)^2+\alpha_{13}}-\frac{(p+z+2)^2+\alpha_6}{\alpha_7(p+z+2)+\alpha_8}} \tag{4.100}$$
$$K_6 = \frac{-\frac{\Omega_3}{(p+z+2)^2+\alpha_{13}}}{\frac{\alpha_{11}(p+z+2)+\alpha_{12}}{(p+z+2)^2+\alpha_{13}}-\frac{(p+z+2)^2+\alpha_6}{\alpha_7(p+z+2)+\alpha_8}} \tag{4.101}$$
$$K_7 = \frac{-\frac{\alpha_9(p+z+1)+\alpha_{10}}{\alpha_{11}(p+z+2)+\alpha_{12}}+\frac{\alpha_5}{(p+z+2)^2+\alpha_6}}{\frac{(p+z+2)^2+\alpha_{13}}{\alpha_{11}(p+z+2)+\alpha_{12}}-\frac{\alpha_7(p+z+2)+\alpha_8}{(p+z+2)^2+\alpha_6}} \tag{4.102}$$
$$K_8 = \frac{\frac{\Omega_2}{(p+z+2)^2+\alpha_6}}{\frac{(p+z+2)^2+\alpha_{13}}{\alpha_{11}(p+z+2)+\alpha_{12}}-\frac{\alpha_7(p+z+2)+\alpha_8}{(p+z+2)^2+\alpha_6}} \tag{4.103}$$
$$K_9 = \frac{-\frac{\Omega_3}{\alpha_{11}(p+z+2)+\alpha_{12}}}{\frac{(p+z+2)^2+\alpha_{13}}{\alpha_{11}(p+z+2)+\alpha_{12}}-\frac{\alpha_7(p+z+2)+\alpha_8}{(p+z+2)^2+\alpha_6}} \tag{4.104}$$

After this point, the general solutions of each three directions could be achieved as follows:

$$u = \sum_{i=1}^{6} A_i \sum_{p=0}^{\infty} a_{p,i} r^{p+z(i)} \tag{4.105}$$
$$v = \sum_{i=1}^{6} A_i \sum_{p=0}^{\infty} b_{p,i} r^{p+z(i)} \tag{4.106}$$
$$w = \sum_{i=1}^{6} A_i \sum_{p=0}^{\infty} c_{p,i} r^{p+z(i)} \tag{4.107}$$

In the general solutions, i indicate which root of z we have. Accordingly, the power series constants a, b and c have six different sets for different root of z(i). A_i is the arbitrary constant which has to be the same for all u, v and w, because the linear operations only validly work on the same group of solutions for the ODE system. In other words, as the matrix form of ODE system in equation 4.57, the u, v and w compose a vector. For keeping the same vector space (the solutions space), if linear operations add on one element of the vector, the same operations need to be added on other elements as well.

4.2.3 Acquiring the natural frequency

For free vibration of hollow cylinders, the stress in the radial direction would be zero at the free edges where r= R_i and R_o. These stress constraint are the boundary conditions here, which are:

$$\sigma_r = \tau_{rx} = \tau_{r\theta} = 0 \tag{4.108}$$

Rewrite these stresses as the stress-displacement relationship:

$$\sigma_r = C_{11}\frac{\partial}{\partial r}W + C_{12}\frac{W}{r} + C_{12}\frac{1}{r}\frac{\partial}{\partial \theta}V + C_{13}\frac{\partial}{\partial x}U \tag{4.109}$$

$$\tau_{r\theta} = C_{44}\left(\frac{\partial}{\partial r}V + \frac{1}{r}\frac{\partial}{\partial \theta}W - \frac{V}{r}\right) \tag{4.110}$$

$$\tau_{rx} = C_{55}\left(\frac{\partial}{\partial x}W + \frac{\partial}{\partial r}U\right) \tag{4.111}$$

Apply the separation variable procedure as suggested in equations 4.25 to 4.27:

$$\sigma_r = \left(C_{11}w_r + C_{12}\frac{w}{r} + C_{12}\frac{1}{r}v \cdot n - C_{13}u \cdot \lambda\right) \cdot \cos(n \cdot \theta) \cdot \sin(\lambda \cdot x) \cdot \cos(\omega \cdot t) \tag{4.112}$$

$$\tau_{r\theta} = C_{44}\left(v_r - \frac{1}{r}w \cdot n - \frac{v}{r}\right) \cdot \sin(n \cdot \theta) \cdot \sin(\lambda \cdot x) \cdot \cos(\omega \cdot t) \tag{4.113}$$

$$\tau_{rx} = C_{55}(\lambda \cdot w + u_r) \cdot \cos(n \cdot \theta) \cdot \cos(\lambda \cdot x) \cdot \cos(\omega \cdot t) \tag{4.114}$$

Define the $m(r, \omega, i)$, $n(r, \omega, i)$ and $l(r, \omega, i)$ as below.

$$m(r, \omega, i) = C_{11}w(i)_r + C_{12}\frac{w(i)}{r} + C_{12}\frac{1}{r}v(i) \cdot n - C_{13}u(i) \cdot \lambda \tag{4.115}$$

$$n(r, \omega, i) = v(i)_r - \frac{1}{r}w(i) \cdot n - \frac{v(i)}{r} \tag{4.116}$$

$$l(r, \omega, i) = \lambda \cdot w(i) + u(i)_r \tag{4.117}$$

where i is from 1 to 6 and indicates the six solution respectively with the indicial roots z(i). Substitute the achieved general solutions of u, v and w in last section:

$$m(r,\omega,i) = A_i M(r,\omega,i) \quad (4.118)$$
$$n(r,\omega,i) = A_i N(r,\omega,i) \quad (4.119)$$
$$l(r,\omega,i) = A_i L(r,\omega,i) \quad (4.120)$$

Apply the boundary conditions, when $r = R_i$ or R_o, the m, n and l functions are zero:

$$\begin{bmatrix} M(R_i,\omega,1) & M(R_i,\omega,2) & M(R_i,\omega,3) & M(R_i,\omega,4) & M(R_i,\omega,5) & M(R_i,\omega,6) \\ N(R_i,\omega,1) & N(R_i,\omega,2) & N(R_i,\omega,3) & N(R_i,\omega,4) & N(R_i,\omega,5) & N(R_i,\omega,6) \\ L(R_i,\omega,1) & L(R_i,\omega,2) & L(R_i,\omega,3) & L(R_i,\omega,4) & L(R_i,\omega,5) & L(R_i,\omega,6) \\ M(R_o,\omega,1) & M(R_o,\omega,2) & M(R_o,\omega,3) & M(R_o,\omega,4) & M(R_o,\omega,5) & M(R_o,\omega,6) \\ N(R_o,\omega,1) & N(R_o,\omega,2) & N(R_o,\omega,3) & N(R_o,\omega,4) & N(R_o,\omega,5) & N(R_o,\omega,6) \\ L(R_o,\omega,1) & L(R_o,\omega,2) & L(R_o,\omega,3) & L(R_o,\omega,4) & L(R_o,\omega,5) & L(R_o,\omega,6) \end{bmatrix} \begin{bmatrix} A_1 \\ A_2 \\ A_3 \\ A_4 \\ A_5 \\ A_6 \end{bmatrix} = 0 \quad (4.121)$$

For avoiding the trivial solutions, A_i can't be all zeros. So the determinant has to be zero. The roots that satisfy the resulting zero determinant equations are natural frequencies.

4.3 Multiple layers orthogonal hollow cylinders

For free vibrations, and to obtain the natural frequency of multiple layered cylinders, the boundary conditions on the interface need to be added. Without delaminating, the displacement and the stress in radius direction should be the same from both side materials on the interface. The mathematical equations of these boundary conditions are:

$$u(j) - u(j+1) = 0 \quad (4.122)$$
$$v(j) - v(j+1) = 0 \quad (4.123)$$
$$w(j) - w(j+1) = 0 \quad (4.124)$$
$$\sigma_r(j) - \sigma_r(j+1) = 0 \quad (4.125)$$
$$\tau_{r\theta}(j) - \tau_{r\theta}(j+1) = 0 \quad (4.126)$$
$$\tau_{rx}(j) - \tau_{rx}(j+1) = 0 \quad (4.127)$$

where the j is the number of the layers.

The similar matrix could be built up from the below matrix to obtain the natural frequencies as the left matrix in the equation 4.128. The matrix needs to be filled with

zeros to make the correct dimension for matrix product. The j^* represent only the first and last layers. We then substitute the general solutions into this matrix. The arbitrary constant A_i needs to change to $A_i(j)$ for representing the different layers' general solutions. For avoiding trivial solutions, $A_i(j)$ can't be all zero. The determinant of the new matrix has to be zero. A function with only frequency variable is derived. We then solve the function for the roots. The roots are the natural frequencies.

$$\begin{bmatrix} \sigma_r(j^*) \\ \tau_{r\theta}(j^*) \\ \tau_{rx}(j^*) \\ u(j) - u(j+1) \\ v(j) - v(j+1) \\ w(j) - w(j+1) \\ \sigma_r(j) - \sigma_r(j+1) \\ \tau_{r\theta}(j) - \tau_{r\theta}(j+1) \\ \tau_{rx}(j) - \tau_{rx}(j+1) \end{bmatrix} A_i(j) = 0 \tag{4.128}$$

4.4 Finite element analyses for orthotropic hollow cylinder

For the orthotropic hollow cylinders, the geometries, mesh sizes and element types are similar as the isotropic cylinders. The detail numbers of these similar parameters will be listed in the result discussion section. Besides them, some new parameters need to be considered:

i. The material orientation.

ii. Meshing method

iii. Material stability requirement. As in Abaqus® help document request, "the linear elastic materials must satisfy the conditions of material or Drucker stability[145]". Material stability requires for orthotropic material as in engineering constants:

$$E_x, E_\theta, E_r, G_{r\theta}, G_{rx}, G_{\theta x}, \Upsilon > 0 \tag{4.129}$$

$$|\nu_{r\theta}| < (E_r/E_\theta)^{1/2} \tag{4.130}$$

$$|\nu_{rx}| < \left(\frac{E_r}{E_x}\right)^{\frac{1}{2}} \tag{4.131}$$

$$|\nu_{\theta x}|<\left(\frac{E_\theta}{E_x}\right)^{\frac{1}{2}} \quad (4.132)$$

in elasticity parameters:

$$C_{11}, C_{22}, C_{33}, C_{12}, C_{13}, C_{23} > 0 \quad (4.134)$$

$$|C_{44}|<(C_{11}C_{22})^{\frac{1}{2}} \quad (4.135)$$

$$|C_{55}|<(C_{11}C_{33})^{\frac{1}{2}} \quad (4.136)$$

$$|C_{66}|<(C_{22}C_{33})^{1/2} \quad (4.137)$$

$$\det(C_{\text{matrix}}) > 0 \quad (4.138)$$

4.5 Results and discussion

As been mentioned in Chapter II, although many publications discussed the theoretical foundation, the detailed results like the natural frequency of a certain mode shape are hard to find in the literature. We will address here the challenges that face researchers and how to solve it.

4.5.1 The challenges from indicial roots

The indicial root z is the core for solving the ODE system with the regular singular point by power series method. The properties of the indicial roots will directly impact the final detailed solution. Some challenges are faced from the repeated indicial roots z (here "repeated" means same number or multiple numbers with integer difference), which are listed as below:

i. Under some special modes, the natural frequency results couldn't be directly achieved. Examples are the first longitudinal, breathing, torsion, and elongation modes.

ii. Under some material properties including isotropic properties, the frequency results couldn't directly be obtained using the power series method.

iii. Material and mode shape mixed cases, as $n * \sqrt{G_{rx}/G_{\theta x}}$is integer.

Under all of the above three conditions, one or more repeated roots (solutions) could be found. The case of isotropic material will produce 6 (maximum) solutions. Some mathematical techniques could be used to solve these problems in the power series method, such as adding logarithmic functions to build a new linear independent solution[133]:

If one solution is

$$Y_1 = \sum_{p=0}^{\infty} A_p r^{p+z(1)} \tag{4.139}$$

Another linear independent solution that can be used then becomes :

$$Y_2 = C\,Y_1 \ln(r) + \sum_{p=0}^{\infty} B_p r^{p+z(1)} \tag{4.140}$$

where $z(1) \geq z(2)$; $A_0 \neq 0$; C=1 when z(1)=z(2); $B_0 \neq 0$ when z(1)-z(2) is integer.

However; the complexity of the solution series will dramatically increase, which will create much more difficulties to obtain the natural frequencies. An easier way to solve these problems is to use other methods. For example, creating potential functions can be used to convert the ODE to a Bessel functions pattern similar to the isotropic problem in Chapter III. The simplified two dimensional theories like shell theories and FEA are much easier to cater to the requirements like material properties and geometries.

Another challenge will be the complex solution of indicial roots z. Although no previous publication appeared on this problem, this situation is quite possible to be generated by the use of composite materials and their properties. Because even for one layer of composite material, the fiber angles could be oriented in any direction, which means different constitutive parameters that are not zero. For example, A graphite/epoxy material can have the following properties: E_1=138*10^9 Pa; E_2=8.96*10^9 Pa; E_3=5*10^9 Pa; G_{12}=7.1*10^9 Pa; G_{13}=3.44*10^9 Pa; G_{23}=3.64*10^9 Pa; v_{12}=0.49; v_{13}=0.33; v_{23}=0.33.

If 1 indicates the x direction, 3 for the r direction, the indicial root of z will be a real number. If one turns the fibers 90 degree with the θ axial (1-r; 3-x), the indicial root of z will change to complex number. To solve this problem, a small lemma is developed here:

i. z(1) and z(2) can't be complex number. Because the $-\alpha_1$ is always larger than zero. This insures the route 1 of the recurrence staying the same.

ii. The other four indicial roots will be $c \pm di$, $e \pm fi$. Four real number power series solutions could be written as:

$$c = \sum_{p=0}^{\infty} A_p r^{p+c} \cos(d \ln(r)) \quad (4.141)$$

$$d = \sum_{p=0}^{\infty} A_p r^{p+c} \sin(d \ln(r)) \quad (4.142)$$

$$e = \sum_{p=0}^{\infty} B_p r^{p+e} \cos(f \ln(r)) \quad (4.143)$$

$$f = \sum_{p=0}^{\infty} B_p r^{p+e} \cos(f \ln(r)) \quad (4.144)$$

The proof of the second part can be to done first. We rewrite the solution Y in the form Y_1+i*Y_2, or

$$\sum_{p=0}^{\infty} A_p r^{p+c+di} = \sum_{p=0}^{\infty} A_p r^{p+c} e^{d(\ln(r))i} = \sum_{p=0}^{\infty} A_p r^{p+c} \left(\cos(d \ln(r)) - i \sin(d \ln(r))\right)$$

$$= \sum_{p=0}^{\infty} A_p r^{p+c} \cos(d \ln(r)) - i \sum_{p=0}^{\infty} A_p r^{p+c} \sin(d \ln(r)) \quad (4.145)$$

Then one can prove that the Y_1 and Y_2 are also two solutions for the second order homogeneous ODE,

$$P(r)Y'' + Q(r)Y' + R(r)Y = 0 \quad (4.146)$$

$$P(r)(Y_1 + i\,Y_2)'' + Q(r)(Y_1 + i\,Y_2)' + R(r)(Y_1 + i\,Y_2) = 0 \quad (4.147)$$

$$P(r){Y_1}'' + Q(r){Y_1}' + R(r)Y_1 + i\,(P(r){Y_2}'' + Q(r){Y_2}' + R(r)Y_2) = 0 \quad (4.148)$$

Both real and imaginary parts have to be zero. Our proof ends here.

With this lemma, the <u>complex</u> indicial roots solutions could be converted to <u>real</u> indicial roots solutions, and then the problem could be solved by previous discussions.

4.5.2 The normal condition (no repeated roots)

After the above discussion of the special cases of the indicial roots, one needs to address the most normal condition where we get real and no repeated indicial roots. Let's study the only detailed solution the author found in reference [148]. The model is a three layer hollow cylinder with two orthotropic materials. The material properties areC_{11}=0.08*C_{33}; C_{22}=0.19*C_{33}; C_{12}=0.05*C_{33}; C_{13}=0.07*C_{33};C_{23}=0.32*C_{33}; C_{44}=0.03*C_{33}; C_{55}=0.04*C_{33}; C_{66}=0.34*C_{33}.

With this ratio of material properties, the indicial roots are under the most normal condition. For the top and bottom layers, C_{33}=20, and for the middle layer C_{33} = 1. The reference suggested a non-dimensional natural frequency expression as:

$$\omega^* = \omega R_o \left[\frac{\sum_{j=1}^{3} \rho\left(R_{j+1}{}^2 - R_j{}^2\right)}{\sum_{j=1}^{3} C33_j\left(R_{j+1}{}^2 - R_j{}^2\right)}\right]^{0.5} \tag{4.149}$$

where j is the number of the layer which counts from inside to outside; R4 is Ro; R1 is Ri. The dimensional natural frequency could be calculated from the above equation.

For the thick shell, where R1=0.8, R2=0.82, R3=0.98, R4=1, the length is 16, and the density is 1. The **dimensional** natural angle frequency results (ω) are shown in Table 4.1, for studying the results, the determinant of the final matrix which should be zero listed on the right side column.

Table 4.1 is split as three big grid m=16, m=8 and m=2. The determinant calculated by the author from the natural frequency reported in the reference by Srinivas are the bold numbers in Table 4.1, which are interestingly not zero especially for the first grid (m=16).

Firstly, we study the procedures for numerical evaluation from the reference by Srinivas (Page 38):

i. Set a starting value of the natural frequency.

ii. Calculate the final determinant.

iii. Adjust the starting value (example, take the original value + 0.01 or – 0.01) to find two values making two final determinants one positive, one negative.

iv. Using linear interpolation and Regula Falsi technique to achieve the natural frequency with the desired accuracy.

Table 4.1 The study of Srinvas' results

n	m	Srinivas (natural freq.)	Operations	Determinant (found here)
2	16	1.01865441		**-1.468559403030325e+011**
			+0.01	-8.995010968534168e+010
			-0.01	2.589411075785058e+011
3		1.11525076		**2.550241380807452e+020**
			+0.01	9.129009909419222e+020
			-0.0099999	-3.883934278667399e+020
4		1.15308744		**-1.476669469674072e+017**
			+0.0100003	-7.966297113533057e+017
			-0.01	4.279223259220539e+016
2	8	0.74374151		**-2.230800350258182e+004**
3		0.61561825		**-2.169382484916956e+006**
4		0.7245274		**-1.360129170409474e+008**
2	2	0.1922068		**-9.056072517608495e+002**
			0.169500253379415	-5.903480550019523e-010
3		0.40441643		**-1.349479041302209e+005**
			0.394589434345435	-5.824026022845884e-008
4		0.62694515		**-9.155489624979297e+006**
			0.620826316101041	-1.943306650805638e-006

.

So for checking the linear interpolation operation in step iv, the author added two small value steps (one positive, one negative) to the frequency values in the first grid. One positive determinant and one negative determinant are found. This means that for linear interpolation there should be one zero point for the determinant between them.

However, between them, at the frequency value, there is another big number (in absolute sense) for the determinant, where the linear interpolation failed. It is showing that in this small range more than one solution for the determinant can be found (equal to zero). In another word, there exists large oscillation. The figure below is showing the oscillation for the first grid (m=16) as n=3.

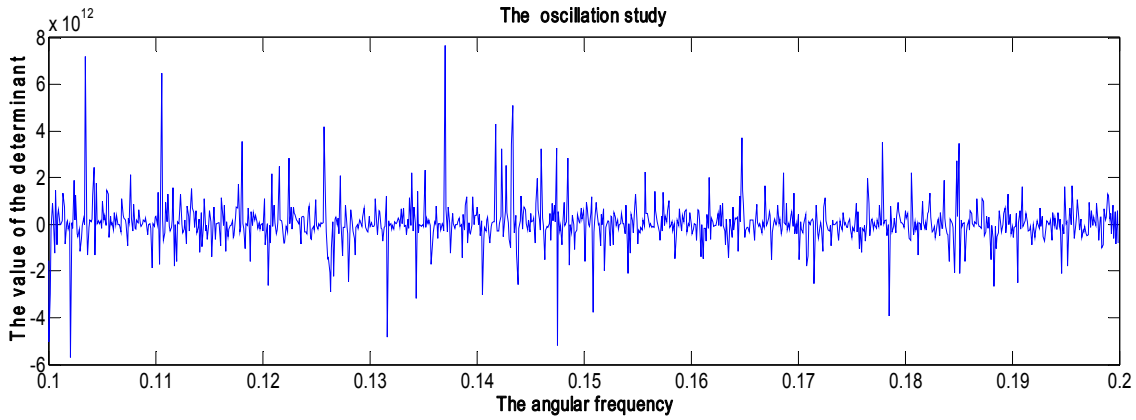

Figure 4.1 The oscillation behavior of results in the first grid table 4.1

In Figure 4.1, even in the big span from 0.1 to 0.2 and only 1000 sampling points, the oscillation is showing as random noise. It indicates any achieved frequency can't be trusted even if the determinant is exactly zero. And if the large oscillation permanently exists, the power series method to solve this problem is a failed method from a practical point of view. Fortunately it is not. For other two grids of the table 4.1, the "oscillation" figures for the determinant as a result of eigen-value variation are shown below.

For the grid: m=8 and n=3Span from 0.45 to 0.55, sampling points 1000.

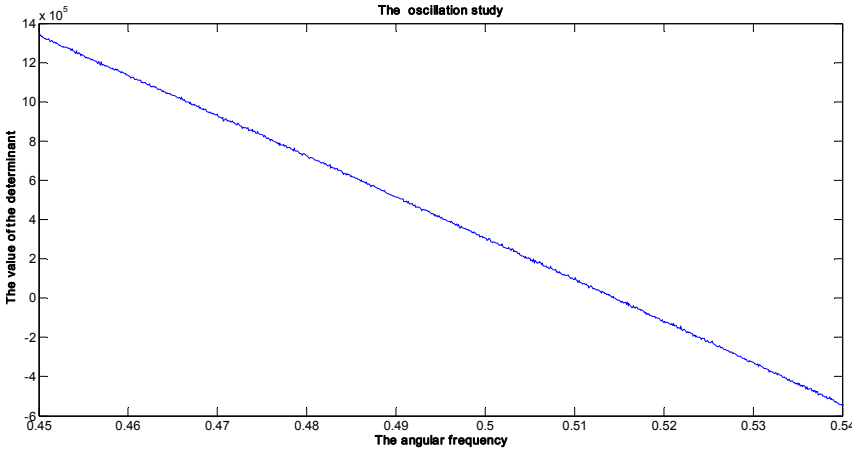

Figure 4.2 The oscillation behavior of results in the second grid table 4.1

Span from 0.513 to 0.523, sampling points 10000.

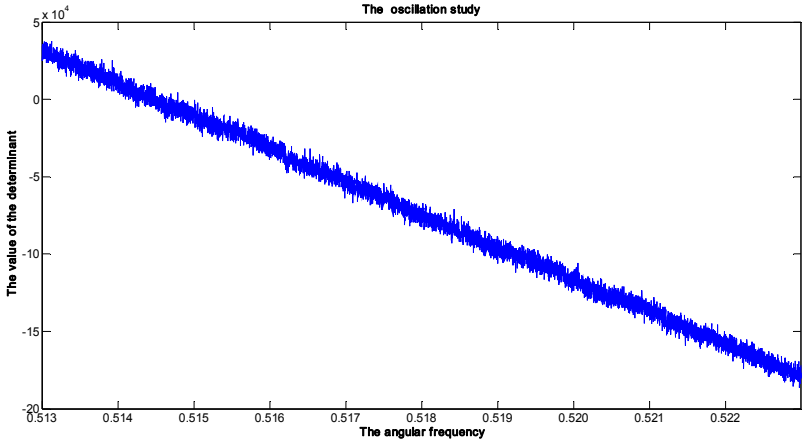

Figure 4.3 The magnified picture of figure 4.2

For the grid: m=2 and n=3, Span from 0.35 to 0.45, sampling points 1000.

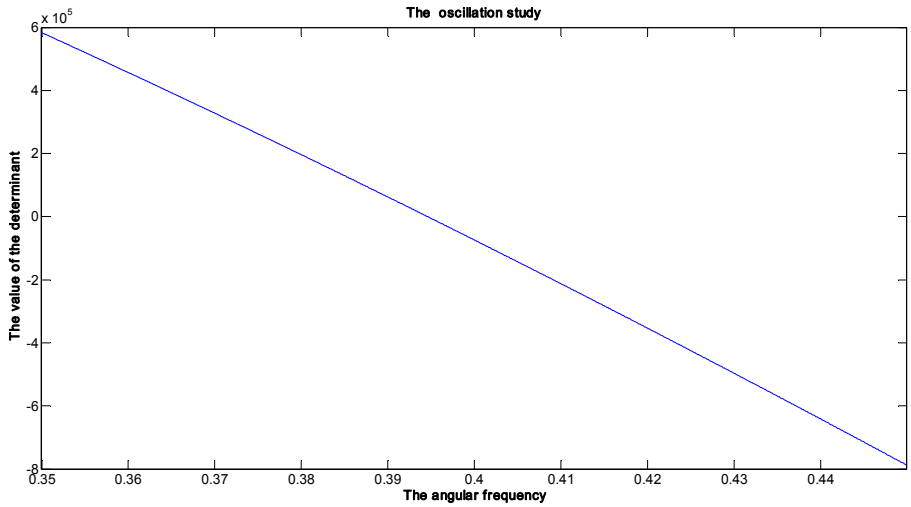

Figure 4.4 The oscillation behavior of results in the third grid table 4.1 Span from 0.39 to 0.40, sampling points 10000.

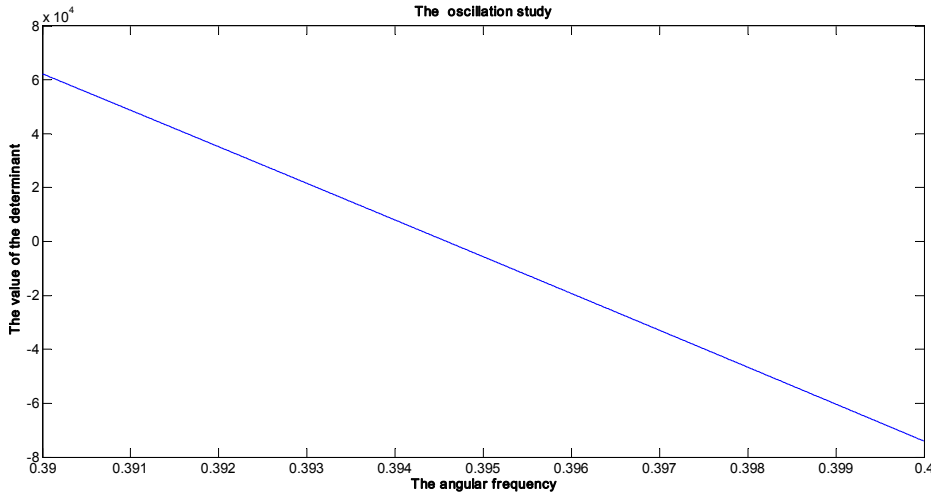

Figure 4.5 The magnified picture of figure 4.4

From the above figures, the "oscillation" is weakening with the increase in m. When m=8, the "oscillation" is acceptable for predicting the curve trend. But when magnifying it with higher sampling rate and a smaller sampling span range, the oscillation is still obvious. When m=2, the curve is almost perfectly smooth even within

higher sampling rates and smaller sampling span range. The obtained natural frequency (Table 4.1) results from m=2 in the figure match well with the reference by Sirnivas. From these figures, it is concluded that the "oscillation" could be controlled or avoided. And for further using it as benchmarking, the study of the "oscillation" is required.

4.5.3 The study of the oscillation

For simplifying the situation, the study of the oscillation will only focus on one layer problem with the same material ratio as described in the last section as C_{33}=1.

4.5.3.1 Convergence study

Before the oscillation study is made, if the power series solution was not convergent, the whole study would be meaningless. And even it is convergent, how large the least number of loops is needed for the desirable convergence to occur will be also important to know.

Take the example of a thin cylinder with a thickness ratio of 25. Testing with so thin of a thickness makes it harder to converge as was found by the reference [Srinvas; page 38].However, the author here doesn't agree. Because the convergence of the power-series method solution only depends on if the absolute value of the coefficients of the power series solutions, like a_n, b_n and c_n in the equation 4.93 to 4.95, will become zero with n going to infinity. These coefficients are independent of the radius. The radius will influence only the convergence speed of the final matrix determinant. This is important for obtaining the natural frequency. The thickness could influence the accuracy of obtaining the natural frequency because if the thickness is too small the linear independency of the final matrix would become vague for any frequency number.

However this problem will happen for many other 3D elasticity solutions like the Bessel function method discussed earlier in Chapter 3 and it is not a problem of convergence.

When m=1, n=2, ω=0, length=2 the loop from 1:200:

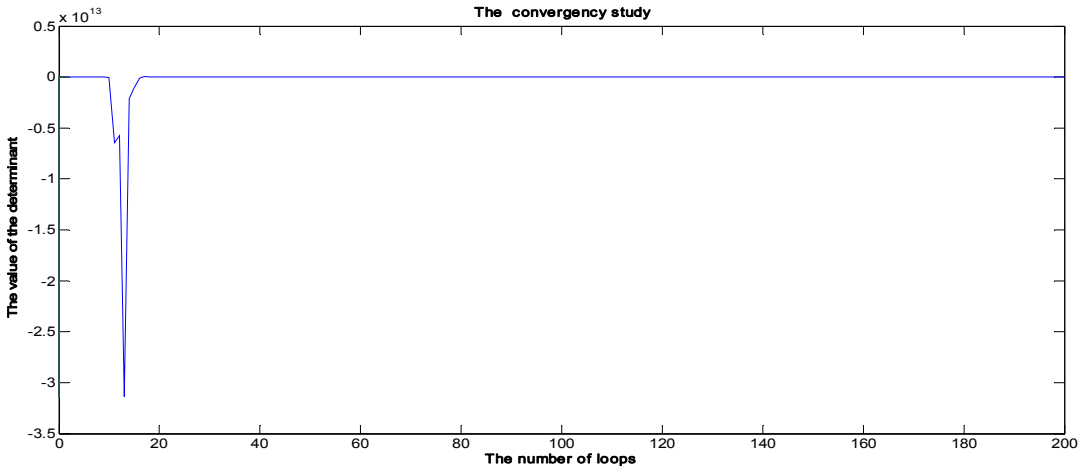

Figure 4.6 The convergency study

Magnify the range from 40 to 200

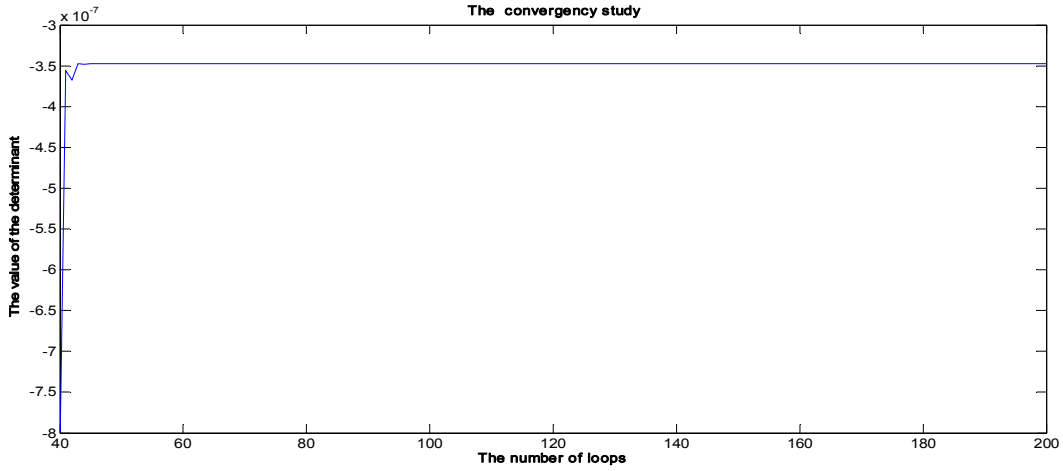

Figure 4.7 The magnified picture of figure 4.6

Magnify the range from 100 to 200

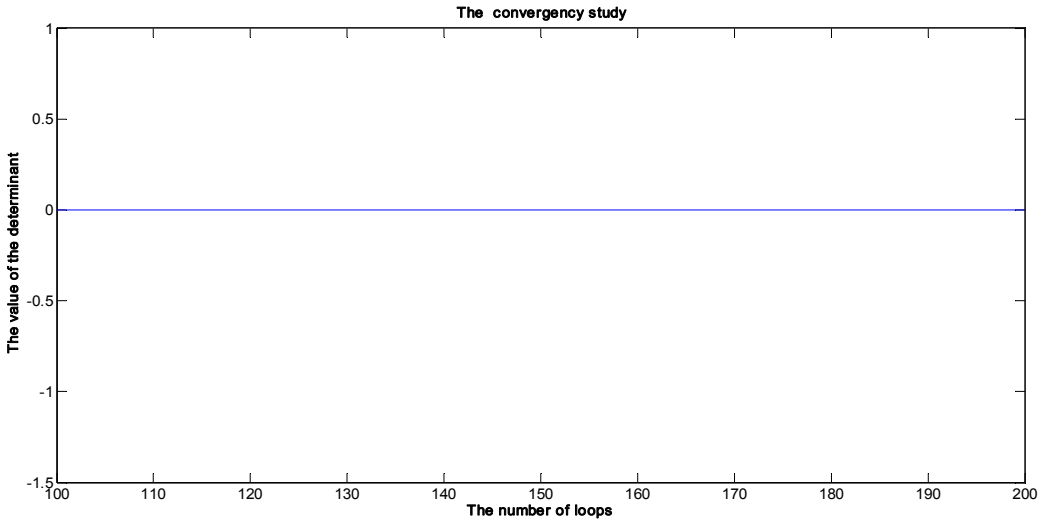

Figure 4.8 The magnified picture of figure 4.7

For another example with different parameters: when m=2, n=3, ω=1, length=2, the loop from 100:200:

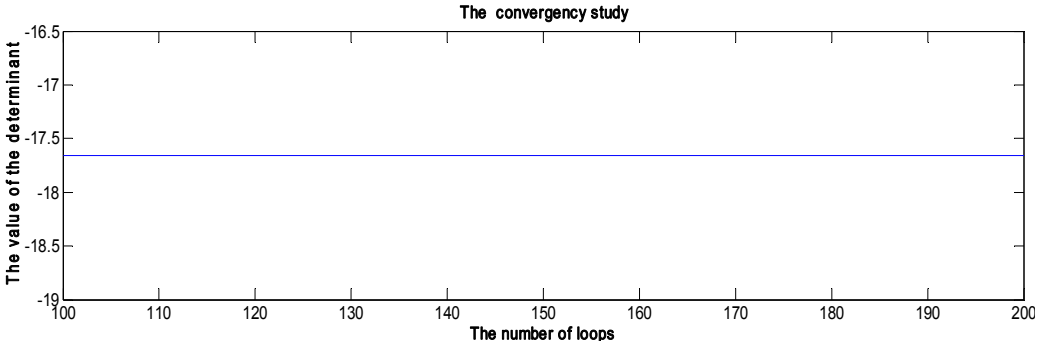

Figure 4.9 The convergency study for different parameters

These figures show that only after more than 60 loops, very good convergence could be achieved. As a safety factor applied, all results are reported for more than 500 loops.

4.5.3.2 Oscillation study

The purposes to do this study are:

i. Find the parameters to control the oscillation

ii. Discover the reasons of the oscillation

iii. Give the procedures for obtaining the natural frequency

If the material properties, geometry and the number of the loops are fixed, the controllable parameters left are the longitudinal mode number m andthe circumferential mode number n. But the longitudinal mode m is actually in the expression $\lambda = m\pi/$ lembedded in the whole theory. So the length of the hollow cylinder will be an influencing factor working with m. λ and n are the two independent parameters which will be studied.

Under the same material in the convergence study, length=10, R_i =0.6, R_o =1, loop 500, 1000 points between 0~1. Fix the circumferential mode number as n=3:

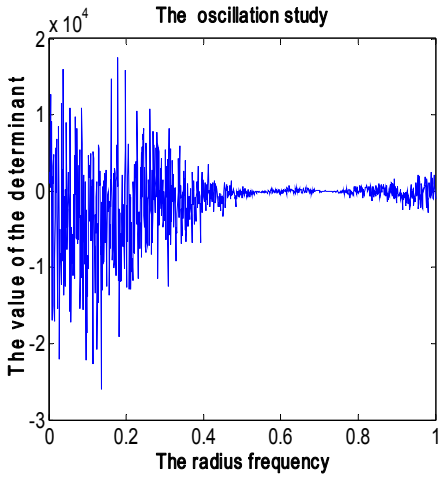

Figure 4.10 The oscillation behaviors when m=10

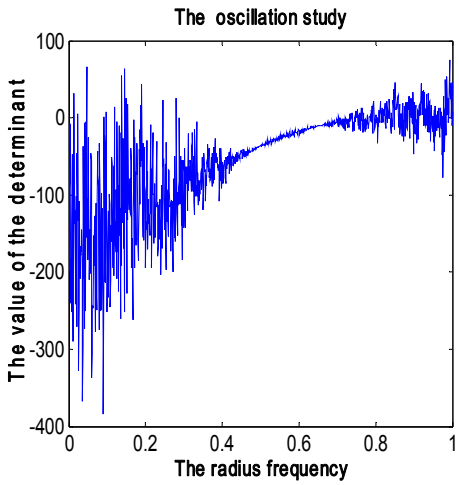

Figure 4.11 The oscillation behaviors when m=9

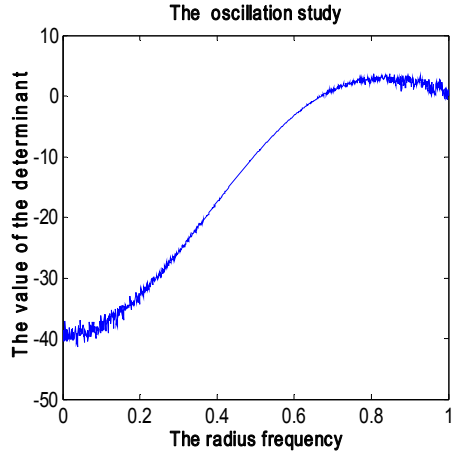

Figure 4.12 The oscillation behaviors when m=8

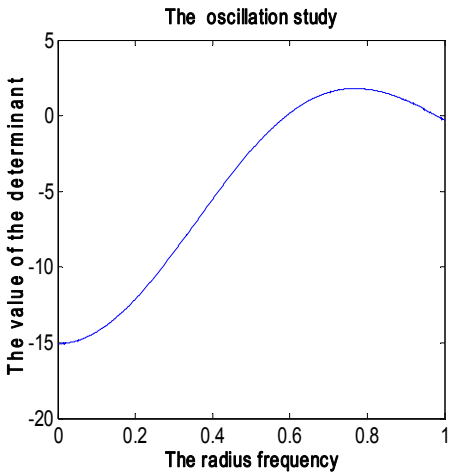

Figure 4.13 The oscillation behaviors when m=7

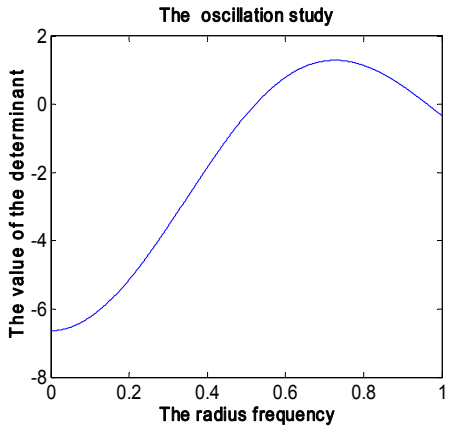

Figure 4.14 The oscillation behaviors when m=6

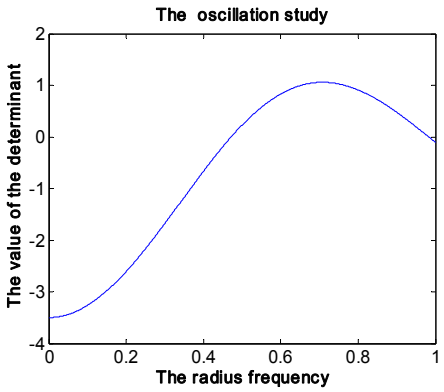

Figure 4.15 The oscillation behaviors when m=5

The oscillation behaviors by changing the longitudinal mode number m

Similar as section 4.5.2, the oscillation is gradually eliminating with m decreasing. Then test the parameter n.

When m=4 test n from 2 to 4, and 15

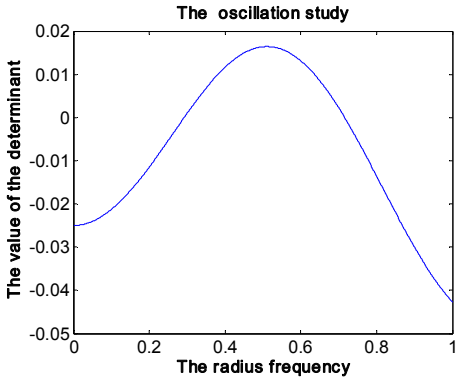

Figure 4.16 The oscillation behaviors when n=2

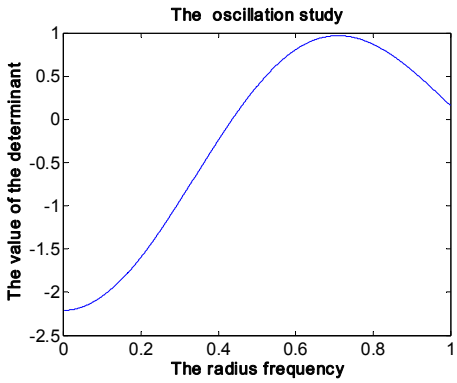

Figure 4.17 The oscillation behaviors when n=3

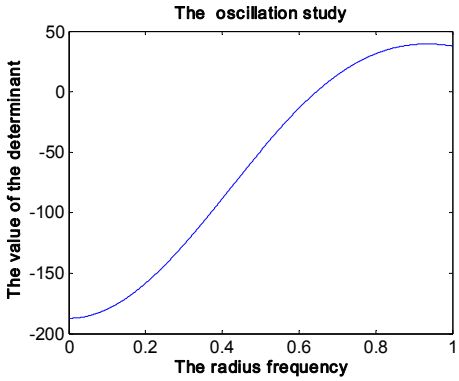

Figure 4.18 The oscillation behaviors when n=4

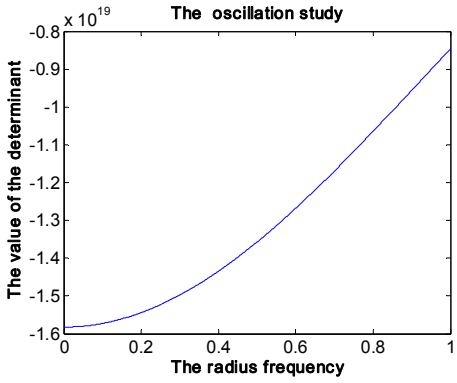

Figure 4.19 The oscillation behaviors when n=15

From the figures, the circumferential mode n will not impact the oscillation.

We will then discuss the reasons for the oscillations. From the computational point of view, the largest and most terrible noise indicates some singular points exist. In other words, the final determinant is not a continuous function with the variable ω. If the theory has a built in singularity and this singularity can't be eliminated, the theory is determined to have failed to obtain the computational results. And even if we are to be avoiding the singularity, many methods that involve numerical approximations can be used. However, fortunately, this oscillation is not the computational singularity noise. If expanding the final determinant as a function of ω, it will be an extremely high degree polynomial of ω, which looks like:

$$f(\omega) = C_1\omega^{n_1} + C_2\omega^{n_2} + C_3\omega^{n_3} \ldots + C_0 \quad (4.150)$$

where the $n_1 > n_2 > n_{3\ldots} > 0$ as integers, C_i are real constants. n_1 will be more than ten thousands when the computational loops are larger than 100. Subsequently, when $f(\omega) = 0$ for calculating the natural frequencies, the oscillating area is the range with too many solutions for this high order polynomial. The smooth area is in the range between two solutions which should be a perfect continuous function. It was proven by the figure 4.5 the smooth curve is still very smooth in the very small range with 10k points testing. It is a very important observation for assuring the accuracy of the final results. Because it is showing the power series method is not introducing "noises" or new singularities and it provides a theoretical foundation for controlling the oscillation.

Secondly we will discuss how the longitudinal mode number m influences the oscillation. As has been shown in section 4.2.1, the ω is always coming out with the Ω_1, Ω_2 and Ω_3 in the equation 4.51 to 4.53.If the final determinant expands with Ω_1, Ω_2 and Ω_3:

$$f(\omega) = C_1{\Omega_1}^{n_1}{\Omega_2}^{m_1}{\Omega_3}^{l_1} + C_2{\Omega_1}^{n_2}{\Omega_2}^{m_2}{\Omega_3}^{l_2} + C_3{\Omega_1}^{n_3}{\Omega_2}^{m_3}{\Omega_3}^{l_3} \ldots + C_0 \quad (4.151)$$

where the $n_1 + m_1 + l_1 > n_2 + m_2 + l_2 > n_3 + m_3 + l_3 \ldots > 0$, n_i, m_i and l_i are positive integers.

And all three Ω_i are in the pattern:

$$\Omega_i = D\lambda^2 + E\rho\omega^2 \tag{4.152}$$

where D and E are the constants decided by the material elasticity properties.

From the above two equations, the λ will directly impact the position of solutions ω from the second degrees of ω^2.

This influence from bundled pattern Ω_i for ω could also be seen from the variation of the density ρ as shown in the figures below:

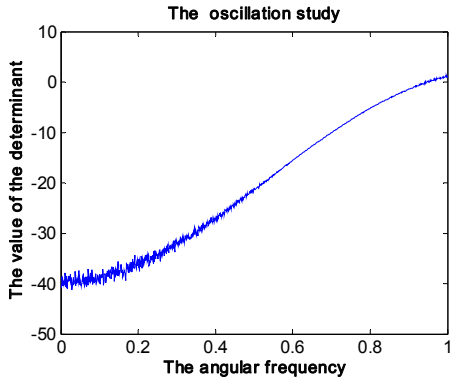

Figure 4.20 The oscillation behaviors when the density ρ=0.5

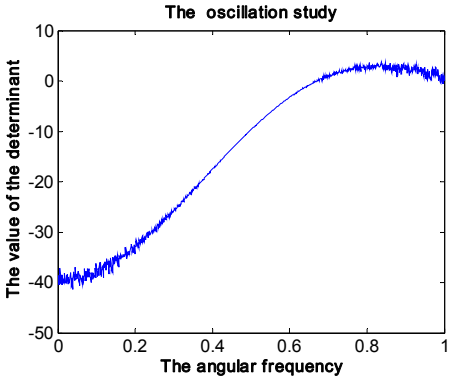

Figure 4.21 The oscillation behaviors when the density ρ=1

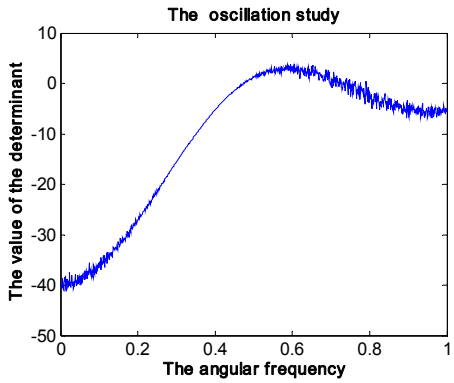

Figure 4.22 The oscillation behaviors when the density ρ=2

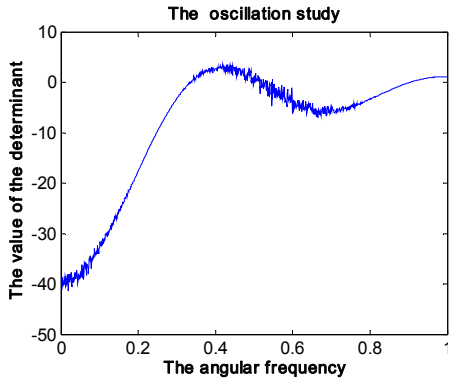

Figure 4.23 The oscillation behaviors when the density ρ=4

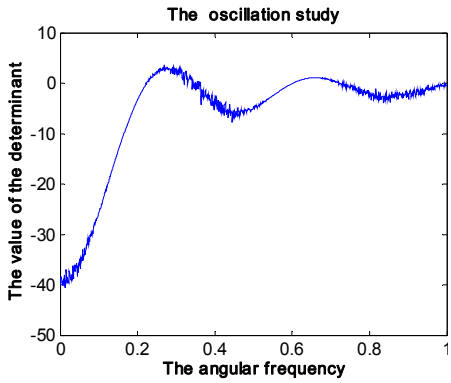

Figure 4.24 The oscillation behaviors when the density ρ=9

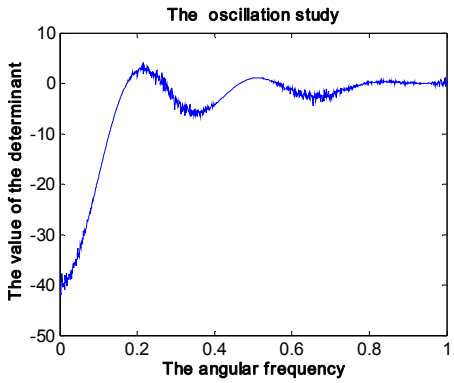

Figure 4.25 The oscillation behaviors when the density ρ=15

Figure 4.20 to Figure 4.25 are generated when m=8, n=3, l=10, R_i =0.6, R_o =1, loop=500, 1000 points between 0 and 1. The curve is compressed with the density increasing in the same frequency range (0~1), which follows the mathematical coefficient behavior for the simple polynomial as in the equation 4.150. This study for density gives another proof of the observation of the influence for the final polynomials from the bundled simple polynomialΩ_i.

From a mathematical point of view, the study of the solution behaviors of a high degree polynomial and how the coefficients in the polynomial will influence the oscillation could be interesting. And in the field of applied mathematics, with the practical meaning for finding the material and structure range in order to avoid the oscillations, it also could be a good topic for a new development of the Abel theorem, eigenvalue or stability study of ODE system.

However; as an engineering topic, because the material and structural properties are known parameters, the objective is more meaningful to find the procedures as a standard for achieving credible solutions. For example, so far for the hollow cylinder with the studied material properties and geometry, when λ<2 (m<7), the natural frequency could be accurately obtained. As summary and conclusions of the above

studies, the procedures for obtaining the exact solution of the natural frequency for the orthotropic hollow cylinders by using power series method are suggested as below:

i. Checking the material properties and mode shape numbers for making sure the calculation under real-no repeated indicial situation.

ii. Set a starting value of the natural frequency from the theories targeted for the benchamrking study.

iii. Study the convergence to decide the least loops for the series.

iv. Study the oscillation of the final determinant around the starting point.

v. Find the range of longitudinal mode m to insure no oscillation.

vi. Adjust the starting value to find two value making two final determinants one positive, and the other negative.

vii. Use bisection method to achieve the natural frequency with desired accuracy

4.5.4 The comparison with FEA

The accuracy study for quadratic solid and shell composite element in the Abaqus® is delivered by comparing the exact solutions from 3D elasticity theory discussed above. All analytical results are tested in the area with no oscillation. The material properties are the same as described in section 4.5.3. The other parameters are provided in the tables:

Table 4.2 The natural frequecy comparison with the hollow cylinder structure: outside radius 1m, inside 0.8m, length 2m

m	n	Shell quadratic Mesh:0.05m^3	Solid quadratic Mesh:0.05m^3	Frequency (Analytical)
1	3	0.33269	0.35327	0.3304015
1	2	0.35831	0.36685	0.3395532
1	4	0.43643	0.46035	0.4485577
1	5	0.5839	0.60692	0.6020427

Table 4.3 The natural frequecy comparison with the hollow cylinder structure: outside radius 1m, inside 0.7m, length 2m

m	n	Shell quadratic Mesh:0.05m^3	Solid quadratic Mesh:0.08m^3	Frequency (Analytical)
1	2	0.37923	0.393101	0.375504
1	3	0.39382	0.422478	0.410374
1	4	0.54283	0.575323	0.57093

Table 4.4 The natural frequecy comparison with the hollow cylinder structure: outside radius 1m, inside 0.6m, length 2m

m	n	Shell quadratic Mesh:0.05m^3	Solid quadratic Mesh:0.1m^3	Frequency (Analytical)
1	2	0.38772	0.405602	0.392585
1	3	0.44196	0.479939	0.471856
1	4	0.62492	0.671233	0.668397
2	2	0.722	0.743301	0.735489

Table 4.5 The natural frequecy comparison with the hollow cylinder structure: outside radius 1m, inside 0.6m, length 4m

m	n	Shell quadratic Mesh:0.05m^3	Solid quadratic Mesh:0.1m^3	Frequency (Analytical)
1	2	0.18943	0.206715	0.197188
1	3	0.37002	0.401324	0.399211
2	2	0.38959	0.405602	0.392585
2	3	0.44422	0.479939	0.471856

From the above tables, the quadratic shell element provides promising results. Solid quadratic elements are still very accurate. Generally, the solid elements are not suggested to be used for the composite or orthotropic materials, except for bulk structures. The shell elements are strongly recommended. And in the manual of Abaqus®, an accuracy study is delivered for the stresses of a statically loaded cylinder. The error for stress analyses could be 3%~15% for quadratic solid element with fine meshes by comparing with analytical results.

The difference from the 3D analyses and 2D analyses could be observed in the Table 4.4 and 4.5. As in the two dark grids, the results should be same for the same mode shape n and λ. The analytical results and 3D elements results are perfectly matched, giving the more credibility, but the 2D shell element results are showing slight differences.

4.5.5 The limitation for material properties of powerseries method

As been motioned, there are some restrictions for using the powerseries methods, for example, when $G_{rx} = G_{\theta x}$ the method could not be used due to the integer difference indicial roots. The other limitations are mainly depended on the indicial roots. And because of the complexities of indicial roots, except "when $n * \sqrt{G_{rx}/G_{\theta x}}$is integer" which been motioned in section 4.5.1 could be easily found as a rule to show the range of material properties, the general range will be many individually ranges and dependent on the mode shapes. In another word, the "traps" of material properties will not show any general properties, such as the material being more orthogonal or less orthogonal the method will be easier to success. And because of it the calculation procedures which are concluded in the end of section 4.5.3 becomes essential.

By following the calculation procedures, the real orthogonal materials could be used and calculated, such as ASTT(b)-C_2-O glass-reinforced plastic and PN-3 polyester resin. The mechanical parameters: E_r=0.42*10^4 MPa, E_θ=1.31*10^4 MPa, E_x=1.79*10^4 MPa, $v_{r\theta}$= 0.31, $v_{z\theta}$= 0.15, v_{rz}= 0.08, $G_{r\theta}$= G_{rz} =0.24*10^4 MPa, $G_{\theta z}$=0.28*10^4 MPa. The density takes as unit 1. The geometry is R_i=3m and R_o =5m, length =10m. The results are showing as table 4.6. The result shows good agreement with quadratic solid element.

Table 4.6 The natural frequecy comparison with the hollow cylinder structure for the real orthogonal material

m	n	Solid quadratic Mesh:0.5m^3	Frequency (Analytical)
1	2	13.739	13.735
1	3	24.053	24.035
1	4	36.444	36.405
2	2	26.309	26.301
2	3	32.921	32.901
3	2	40.938	40.917

CHAPTER V

CONCLUSION

The contributions of this research work could be classified into practical observations and theoretical improvements discussed as below.

5.1 Engineering contributions

The first contribution of this work in Chapter 2 is to investigate the engineering need to perform a comprehensive comparison study of the analytical and numerical vibrations of cylinders and cylindrical shells using various theories. This dissertation only focused on some of the possible benchmarks for this work. The second contribution made here is by using and developing exact 3D elasticity theory solutions, an investigation is carried out to find the capability of the commercial FEA packages for obtaining natural frequencies of certain structures: The accurate results using finite elements can be obtained with quadratic solid elements. These results are important for benchmarking purposes but require significant computational time. Thus, they may not be practical for industrial applications.

Another conclusion is that the use of an advanced shell theory may enhance the accuracy of these elements. This is verified by using such a theory with an exact solution.

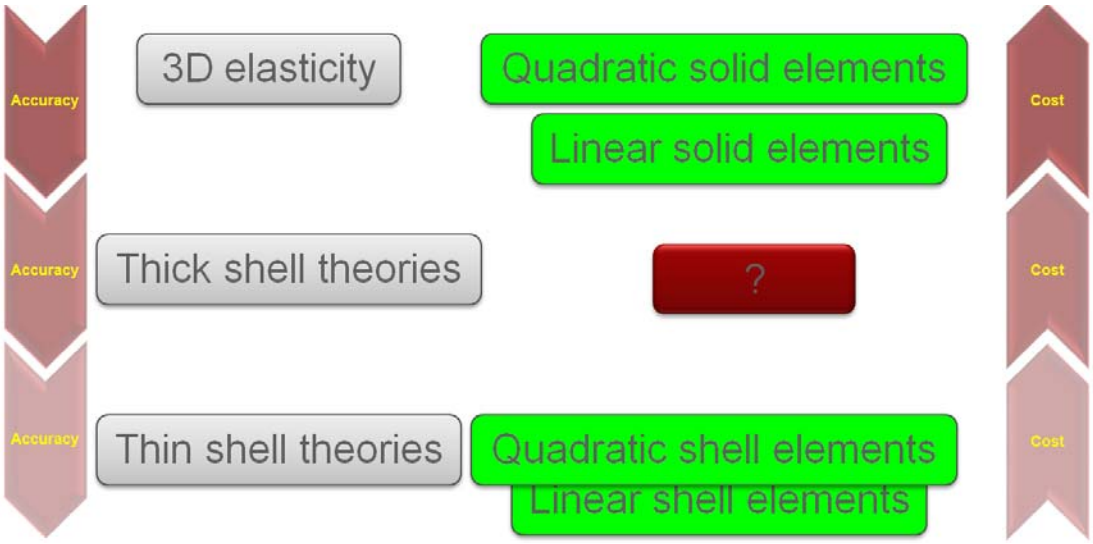

Figure 5.1 The illustration for the demanding of advanced shell theories to apply in the FEA

The point made here is illustrated in Figure 5.1. Although 3D elements can provide accurate results, they are not practical in industrial applications of thin- and thick-walled structures. Instead, shell elements are needed for such applications. However, further improvements to the shell theory used in the finite element formulation are needed to improve the accuracy of these shell elements. And the selection of the advanced shell theories should depends on benchmarking their results against those obtained using the 3D elasticity theory.

5.2 Theoretical contribution

Another finding observed in the literature review is the absence of the results of the exact solution for the free vibration analyses of orthotropic hollow cylinders. This dissertation developed the route from the foundation theory to the detailed results. The observations and developments include:

i. Derivation using the power series method solution for free vibration analyses of the orthotropic hollow cylinders with improved expressions for modern programming.

ii. Discussion of all special cases of the solutions and giving the corresponding solution methods.

iii. Providing the solution for the special case of the complex indicial roots.

iv. Detailed description and discussion of the oscillation behavior of the power series solution of this topic. In addition, giving the theoretical foundation for proving that this oscillation behavior is not ill-conditioning or singularities defects from the theory.

v. Finding the method to avoid the oscillation area and giving the procedures to obtain the credible results. In addition, verifying results against those found in previous literature and FEA.

REFERENCES

1. Qatu, MS. Vibration of laminated shells and plates. San Diego, C:Elsevier, 2004.

2. Qatu, MS. Recent research advances in the dynamic behavior of shells, part 1: laminated composite shells. Appl Mech Rev 2002; 55: 325-350.

3. Leissa, A., Vibration of Shells. Acoustical Society of America.1993.

4. Qatu, MS. Review of shallow shell vibration research. Shock Vib Dig 1992; 24: 3-15.

5. Qatu, MS. Accurate theory for laminated composite deep thick shells. Int. J. Solids and Structures 1999; 36: 2917-2941.

6. Leissa AW. Vibration of shells. NASA SP388. The Government Printing Office, Washington, DC, 1973. Republished 1993, the Acoustical Society of America.

7. Kapania, PK. Review on the analysis of laminated shells. J Pressure Vessel Tech 1989; 111: 88-96.

8. Noor AK, and Burton WS. Assessment of computational models for multilayered composite shells. Appl Mech Rev 1990; 43: 67-97.

9. Noor AK, and Burton WS, Computational models for high-temperature multilayered composite plates and shells. Appl Mech Rev 1992; 45:419-446.

10. Noor AK, Burton WS and Peters JM. Assessment of computational models for multilayered composite cylinders. Int J Solids Struct 1991; 27: 1269-1286.

11. Liew KM, Lim CW, and Kitipornchai S. Vibration of shallow shells: a review with bibliography. Appl Mech Rev 1997; 50: 431-444.

12. Soldatos KP. Mechanics of Cylindrical Shells with Non-circular Cross-Section. Appl Mech Rev, 1999; 52: 237-274.

13. Noor AK, Burton WS and Bert CW. Computational models for sandwich panels and shells. Appl Mech Rev 1996; 49: 155-200.

14. Noor AK and Venneri SL. High-performance computing for flight vehicles. Comput Syst Eng 1992; 3: 1-4.

15. Carrera E. Historical review of Zig-Zag theories for multilayered plates and shells. Appl. Mech. Rev 2003; 56:287-309.

16. Carrera E. Theories and finite elements for multilayered, anisotropic, composite plates and shells J Archives of Comput Methods Eng 2002; 9:87-140.

17. Soedel W. Vibrations of shells and plates, 3rd Edition. New York, NY: Marcel Dekker, 2004.

18. Reddy JN. Mechanics of laminated composite plates and shells: theory and analysis. Second Edition. Boca Raton, FL: CRC press, 2003.

19. Ye J. Laminated composite plates and shells: 3D modeling. London: Springer-Verlag, 2003.

20. Lee CY. Geometrically correct laminated composite shell modeling. Ikoyi, Lagos, Nigeria: VDM Verlag, 2008.

21. Shen HS. Functionally graded materials: nonlinear analysis of plates and shells. Boca Raton, FL : CRC Press, 2009.

22. Santos H, Mota Soares CM, Mota Soares CA, Reddy JN. A finite element model for the analysis of 3D axisymmetric laminated shells with piezoelectric sensors and actuators: bending and free vibrations. Comput Struct 2008; 86: 940-947.

23. Santos H, Mota Soares CM, Mota Soares CA, Reddy JN. A finite element model for the analysis of 3D axisymmetric laminated shells with piezoelectric sensors and actuators. Compos Struct 2006; 75:170-178.

24. Shakeri M, Eslami MR, Daneshmehr A. Dynamic analysis of thick laminated shell panel with piezoelectric layer based on three dimensional elasticity solution. Comput Struct2006:84; 1519–1526.

25. Malekzadeh P, Fiouz A R, Razi H. Three-dimensional dynamic analysis of laminated composite plates subjected to moving load. Compos Struct 2009; 90 (2); 105-114.

26. Saviz MR, Shakeri M, Yas MH. Electrostatic fields in a layered piezoelectric cylindrical shell under dynamic load. Smart Mater. Struct. 16 (2007. 1683-1695.

27. Toorani MH, Lakis AA. Shear deformation in dynamic analysis of anisotropic laminated open cylindrical shells filled with or subjected to a flowing fluid. Comput Methods Appl Mech Eng 2001:190; 4929-4966.

28. Dong K, Wang X. The effect of transverse shear, rotary inertia on wave propagation in laminated piezoelectric cylindrical shells in thermal environment. J Reinforc Plast Compos 2007; 26: 1523-1538.

29. Ribeiro P. On the influence of membrane inertia and shear deformation on the geometrically nonlinear vibrations of open, cylindrical, laminated clamped shells. Compos Sci Technol2009; 69: 176-185.

30. Qatu MS. Theory and vibration analysis of laminated barrel thick shells. J Vib Contr 2004; 10: 319-341.

31. Wang X, Lu G, Guillow SR. Stress wave propagation in orthotropic laminated thick-walled spherical shells. Int J Solids Struct2002:39:4027–4037.

32. Ding KW. The thermoelastic dynamic response of thick closed laminated shell. Shock and Vibration 2005; 12:283–291.

33. Ganapathi M, Haboussi M. Free vibrations of thick laminated anisotropic non-circular cylindrical shells. Compos Struct 2003; 60:125-133.

34. Ganapathi M, Patel BP, Pawargi DS. Dynamic analysis of laminated cross-ply composite non-circular thick cylindrical shells using higher-order theory. Int J Solids Struct 2002:39; 5945-5962.

35. Khare RK, Rode V. Higher-order closed-form solutions for thick laminated sandwich shells. Journal of Sandwich Structures and Materials 2005;7: 335-358.

36. Balah M, Al-Ghemady HN. Energy–momentum conserving algorithm for nonlinear dynamics of laminated shells based on a third-order shear deformation Theory. Journal of Engineering Mechanics 2005; 131:12-22.

37. Pinto Correia IF, Mota Soares CM, Mota Soares CA, Herskovits J. Analysis of laminated conical shell structures using higher order models. Compos Struct 2003; 62: 383–390.

38. Qian W, Liu GR, Chun L, Lam KY. Active vibration control of composite laminated cylindrical shells via surface-bonded magnetostrictive layers. Smart Mater Struct 2003; 12:889.

39. Lam KY, Ng TY, Qian W. Vibration analysis of thick laminated composite cylindrical shells. AIAA J 2000;38:1102.

40. Braga AMB, Rivas ACE. High-frequency response of isotropic-laminated cylindrical shells modeled by a layer-wise theory. Int J Solids Struct 2005; 42:4278–4294.

41. Basar Y, Omurtag MH. Free-vibration analysis of thin/thick laminated structures by layer-wise shell models. Comput Struct 2000;74:409-427.

42. Lee I, Oh IK, Shin WH, Cho KD, Koo KN. Dynamic characteristics of cylindrical composite panels with Co-cured and constrained viscoelastic layers. JSME International Journal, Series C: Mechanical Systems, Machine Elements and Manufacturing 2002; 45:16.

43. Moreira RAS, Rodrigues JD, Ferreira AJM. A generalized layerwise finite element for multi-layer damping treatments. Computational Mechanics 2006;37:426.

44. Oh IK. Dynamic characteristics of cylindrical hybrid panels containing viscoelastic layer based on layerwise mechanics. Compos Part B: Engineering 2007;38:159.

45. Oh IK. Damping characteristics of cylindrical laminates with viscoelastic layer considering temperature- and frequency-Dependence. Journal of Thermal Stresses 2009;32:1.

46. Oh IK, Cheng TH. Vibration analyses of cylindrical hybrid panel with viscoelastic layer based on layerwise finite elements. Key Eng Mater 2006;324-325 II:699.

47. Saravanan C, Ganesan N, Ramamurti V. Analysis of active damping in composite laminate cylindrical shells of revolution with skewed PVDF sensors/actuators. Compos Struct 2000:48; 305-318.

48. Saravanos DA, Christoforou AP. Low-energy impact of adaptive cylindrical piezoelectric–composite shells. Int J Solids Struct 2002; 39:2257–2279.

49. Shin WH, Oh IK, Han JH, Lee I. Aeroelastic characteristics of cylindrical hybrid composite panels with viscoelastic damping treatments. J Sound Vib 2006;296:99.

50. Varelis D, Saravanos DA. Coupled mechanics and finite element for nonlinear laminated piezoelectric shallow shells undergoing large displacements and rotations. Int J Numer Methods Eng 2006;66: 1211-1233.

51. Wang A, Yang G, Zhang X. Vibration and transverse stresses of laminated cylindrical shells. Chinese Journal of Applied Mechanics/ Ying Yong Li Xue Xue Bao/ 2001;18:34.

52. Ray MC, Reddy JN. Optimal control of thin circular cylindrical laminated composite shells using active constrained layer damping treatment. Smart Mater Struct 2004;13: 64–72.

53. Evseev EG, Morozov EV. Aeroelastic interaction of the shock waves with the thin-walled composite shells. Composite Shells 2001; 54:153-159.

54. Li J, Hua H. Transient vibrations of laminated composite cylindrical shells exposed to underwater shock waves. Engineering Structures 2009; 31:738-748.

55. Ruotolo R. A comparison of some thin shell theories used for the dynamic analysis of stiffened cylinders. J Sound Vib 2001;243:847.

56. Civalek Ö. Free vibration analysis of composite conical shells using the discrete singular convolution algorithm. Steel and Compos Struct 2006;6:353.

57. Civalek Ö. Numerical analysis of free vibrations of laminated composite conical and cylindrical shells: Discrete singular convolution (DSC) approach. J Comp Appl Math 2007;205:251.

58. Sakiyama T, Hu XX, Matsuda H, Morita C. Vibration of cantilevered laminated composite conical shells with twist. vol. 4. Seville, Spain: WITPress, 2002.

59. Hu XX, Sakiyama T, Matsuda H, Morita C. Vibration of twisted laminated composite conical shells. Int J Mech Sci 2002;44:1521-1541.

60. Lee YS, Choi MH, Kim JH. Free vibrations of laminated composite cylindrical shells with an interior rectangular plate. J Sound Vib 2003; 265:795-817.

61. Kim YW, Lee YS. Transient analysis of ring-stiffened composite cylindrical shells with both edges clamped. J Sound Vib 2002; 252:1-17.

62. Shang XC. An exact analysis for free vibration of a composite shell structure-hermetic capsule. Appl Math Mech (English Edition) 2001; 22:1035-1045.

63. Korhevskaya EA, Mikhasev GI. Free vibrations of a laminated cylindrical shell subjected to nonuniformly distributed axial forces. Mechanics of Solids 2006;41:130-138.

64. Toorani MH, Lakis AA. Free vibrations of non-uniform composite cylindrical shells. Nucl Eng Des 2006; 236:1748-1758.

65. Umur Y, Varlik O. Free vibrations of bonded single lap joints in composite, shallow cylindrical shell panels. AIAA journal 2005; 43:2537-2548.

66. Singh AV. Linear and geometrically nonlinear vibrations of fiber reinforced laminated plates and shallow shells. Comput Struct 2000; 76:277-285.

67. Hu HT, Ou SC. Maximizations of fundamental frequency of laminated truncated conical shells with respect to fiber orientation. Compos Struct 2001; 52:265-275.

68. Timarchi T, Soldatos KP. Vibrations of angle-ply laminated circular cylindrical shells subjected to different sets of edge boundary conditions. J Eng Math 2000; 37:211-230.

69. Topal U. Mode-frequency analysis of laminated spherical shell. In: Proceedings of the 2006 IJME.-. INTERTECH International Conference- Session ENG P501-001, Kean University, New Jersey, 19-21 October 2006.

70. Tizzi S. A Ritz procedure for optimisation of cylindrical shells, formed by a nearly symmetric and balanced angle-ply composite laminate, with fixed minimum frequency. Comput Struct 2006; 84:2159-2173.

71. Ferreira AJM, Roque CMC, Jorge RMN. Natural frequencies of FSDT cross-ply composite shell by multiquadrics. Compos Struct 2007; 77:296-305.

72. Iqbal, J and Qatu, MS. Transverse vibration of circular two-segment composite shafts. Accepted for publication. Compos Struct 2010; 92: 1126-1131.

73. Tetsuya N. Simplified analytical method for calculation of natural frequencies of laminated composite cylindrical shells using equivalent curvature. Reports of the Tokyo Metropolitan Technical College 2000; 35:25-30.

74. Zhang XM. Parametric analysis of frequency of rotating laminated composite cylindrical shells with the wave propagation approach. Comput Methods Appl Mech Eng2002; 191:2057-2071.

75. Zhao X, Liew KM, Ng TY. Vibrations of rotating cross-ply circular cylindrical shells with stringer and ring stiffener. Int J Solids Struct 2002; 39:529-545.

76. Hua L, Lam KY. Orthotropic Influence on frequency characteristics of a rotating composite laminated conical shell by the generalized differential quadrature method. Int J Solids Struct2001; 38:3996-4015.

77. Gong SW, Lam KY. Rotating multilayered cylindrical shells to impact loading. AIAA J 2003; 41:139-142.

78. Shi Y, Hong J, Wu W. Dynamic characteristic analysis of rotating composite shell. Beijing Hangkong Hangtian Daxue Xuebao/Journal of Beijing University of Aeronautics and Astronautics 2004; 30:31.

79. Huang CH, Lee YJ. Quasi-static simulation of composite-laminated shells subjected to low-velocity impact. J Reinforc Plast Compos2005;24: 763-774.

80. Kim YN, Im KH, Lee KS, Cho YJ, Kim SH, Yang IY. Experimental approach on the behavior of composites laminated shell under transverse impact loading. Rev Quant Nondestruc Analy 2005;24: 1100-1106.

81. Johnson AF, Holzapfel M. Modelling soft body impact on composite structures. Compos Struct 2003;61:103-113.

82. Johnson AF, Holzapfel M. Influence of delamination on impact damage in composite structures. Compos Sci Technol 2006;66:807-815.

83. Johnson AF, Pickett AK, Rozycki P. Computational methods for predicting impact damage in composite structures. Compos Sci Technol 2001; 61: 2183-2192.

84. Kim YN, Im KH, Yang IY. Characterization of impact damages and responses in CFRP composite shells. Kumamoto, Japan: Trans Tech Publications Ltd, 2004; 465-466:247-252.

85. Kim YN, Yang IY. Impact response and damage of composite shell with various curvatures. Jeju Island, Korea, Republic of: Trans Tech Publications Ltd, 2004; 270-273: 1911.

86. Lee YS, Ryu CH, Myung CM. Identification of impact loading characteristics of composite laminated cylindrical shells using neural networks. Prague, Czech Republic: Civil-Comp Limited 2002; 195-196.

87. Rastorguev GI, Snisarenko SI. Physical relations for problems of impact loading and unsteady deformation of composite structures. J Appl Mech Tech Phys 2009;50:155-162.

88. Smojver I, Soric J, Bathe KJ. On damage modelling of laminated composite shells subjected to low velocity impact. Computational Fluid and Solid Mechanics. Oxford: Elsevier Science Ltd, 2003,

89. Tiberkak R, Bachene M, Rechak S, Necib B. Damage prediction in composite plates subjected to low velocity impact. Compos Struct 2008; 83:73-82.

90. Zhao G, Cho CD. On Impact Damage of Composite Shells by a Low-Velocity Projectile. J Compos Mat 2004; 38: 1231-1254.

91. Zhao GP, Cho CD. Progressive damage analysis of composite shell under impact loading. Key Eng Mater 2004;274-276:111-116.

92. Zhao GP, Cho CD. Damage initiation and propagation in composite shells subjected to impact. Compos Struct 2007;78:91-100.

93. Wan ZM, Wang L, Du XW. Failure behavior of laminated composite cylindrical shells under axial impact loading. Harbin Gongye Daxue Xuebao, Journal of Harbin Institute of Technology (China)2001; 33:304-308.

94. Yang IY, Cho YJ, Kim YN, Heo U, Park SG, Im KH, Kim JH, Sim JK. The penetration characteristics of CF/epoxy curved sheller according to stacking sequence. Key Eng Mater 2006 321-323 Part 2:885-888.

95. Sahu SK, Datta PK. Research advances in the dynamic stability behavior of plates and shells: 1987-2005 - Part I: Conservative systems. Applied Mechanics Reviews 2007;60:65.

96. Yang J, Fu Y. Analysis of dynamic stability for composite laminated cylindrical shells with delaminations. Compos Struct 2007;78:309-315.

97. Birman V, Simitses GJ. Dynamic Stability of Long Cylindrical Sandwich Shells and Panels Subject to Periodic-in-time Lateral Pressure. J Compos Mat 2004; 38:591-607.

98. Darabi M, Darvizeh M, Darvizeh A. Non-linear analysis of dynamic stability for functionally graded cylindrical shells under periodic axial loading. Compos Struct 2008;83:201-211.

99. Ng TY, Lam KY, Liew KM, Reddy JN. Dynamic stability analysis of functionally graded cylindrical shells under periodic axial loading. Int J Solids Struct 2001;38:1295-1309.

100. Darvizeh M, Haftchenari H, Darvizeh A, Ansari R, Sharma CB. The effect of boundary conditions on the dynamic stability of orthotropic cylinders using a modified exact analysis. Compos Struct 2006;74:495-502.

101. Kamat S, Ganapathi M, Patel BP. Analysis of parametrically excited laminated composite joined conical-cylindrical shells. Comput Struct 2001;79:65-76.

102. Kasuya H, Yamagishi Y. An Analysis of Dynamic Stability of Cross-Ply Laminated Cylindrical Shells under Impact Hydrostatic Pressure. Zairyo/Journal of the Society of Materials Science, Japan 2003; 52:1357-1362.

103. Nemoto K, Kasuya H, Yamagishi Y. An analysis of dynamic stability of composite laminated cylindrical shells subjected to periodic external pressure. Nippon Kikai Gakkai Ronbunshu, A Hen/Trans Jpn Soc Mech Eng, Part A 2003;69:545-551.

104. Peng F, Xiang H, Fu YM. Dynamic instability of viscoelastic cross-ply laminated plates and circular cylindrical shells. Zhendong Gongcheng Xuebao/Journal of Vibration Engineering 2006;19:459.

105. Sofiyev AH. Torsional buckling of cross-ply laminated orthotropic composite cylindrical shells subject to dynamic loading. European Journal of Mechanics A/Solids 2003; 22:943–951.

106. Khdeir AA. Thermally induced vibrations of cross-ply laminated shallow shells. Acta Mechanica 2001; 151:135-147.

107. Tylikowski A. Dynamic stability of rotating composite shells with thermoactive shape memory alloy fibers. J Therm Str 1998; 21:327-339.

108. Pinto Correiaa IF, Barbosa JI, Mota Soares CA, Mota Soares CA. A finite element semi-analytical model for laminated axisymmetric shells: statics, dynamics and buckling. Comput Struct 2000; 76:299-317.

109. Wu CP, Lo JY. An asymptotic theory for dynamic response of laminated piezoelectric shells. Acta Mechan 2006; 183:177–208.

110. Prusty BG, Satsangi SK. Finite element transient dynamic analysis of laminated stiffened shells. J Sound Vib 2001;248: 215-233.

111. Park T, Kim K, Han S. Linear static and dynamic analysis of laminated composite plates and shells using a 4-node quasi-conforming shell element. Compos: Part B 2006; 37: 237-248.

112. Fares ME, Youssif YG, Alamir AE. Minimization of the dynamic response of composite laminated doubly curved shells using design and control optimization. Compos Struct 2003;59: 369-383.

113. Yang XM, Shen YP. Dynamic Instability of laminated piezoelectric shells. Int J Solids Struct 2001;38: 2291-2303.

114. Sahu SK, Datta PK. Parametric resonance characteristics of laminated composite doubly curved shells subjected to non-uniform loading. J Reinforc Plast Compos 2001;20: 1556-1576.

115. Tetsuya N, Masanori K, Kohei S. A study on vibration characteristics of laminated composite cylindrical shells. Natural frequencies of FW antisymmetrically laminated composite cylindrical shells. Trans Jpn Soc Mech Eng 2000; 66:1747-1755.

116. Lee, CY. Dynamic variational asymptotic procedure for laminated composite shells. PhD Thesis, Georgia Inst Tech, 2007.

117. Vu-Quoc L, Tan XG. Optimal solid shells for nonlinear analyses of multilayer composites. II. Dynamics. Comput Methods Appl Mech Eng2003; 192:1017-1059.

118. Birman V, Griffin S, Knowles G. Axissymmetric dynamics of composite spherical shells with active peizoelectric-composite stiffeners. Acta Mech 2000;141:71-83.

119. Lee CY, Hodges DH. Dynamic variational-asymptotic procedure for laminated composite shells—Part I: Low-frequency vibration analysis. J Appl Mech 2009; 76:77-84.

120. Tetsuya N. Natural frequencies and transverse deformations of laminated cylindrical shells. Dynamics & Design Conference 2000; 907-910.

121. Ip KH, Tse PC. Locating damage in circular cylindrical composite shells based on frequency sensitivities and mode shapes. European Journal of Mechanics A/Solids 2002; 21:615-628.

122. Ribeiro P, Jansen E. Nonlinear vibrations of laminated cylindrical shallow shells under thermomechanical loading. J Sound Vib 2008; 315:626-640.

123. Krishnamurthy KS, Mahajan P, Mittal PK. Impact response and damage in laminated composite cylindrical shells. Compos Struct 2003;59: 15-36.

124. Krishnamurthy KS, Mahajan P, Mittal RK. A parametric study of the impact response and damage of laminated cylindrical composite shells. Compos Sci Technol 2001; 61:1655-1669.

125. Liew KM, Hu YG, Zhao X, Ng TY. Dynamic stability analysis of composite laminated cylindrical shells via the mesh-free kp-Ritz method. Comput Methods Appl Mech Eng 2006;196:147-160.

126. Yang J, Fu Y. Analysis of dynamic stability for composite laminated cylindrical shells with delaminations. Compos Struct 2007; 78:309-315.

127. Zhou CT, Wang LD. Nonlinear theory of dynamic stability for laminated composite cylindrical shells. Appl Math Mech 2001;22: 53-62.

128. Ganapathi M. Dynamic stability characteristics of functionally graded materials shallow spherical shells. Compos Struct 2007;79:338-343.

129. Park T, Lee SY. Parametric instability of delaminated composite spherical shells subjected to in-plane pulsating forces. Compos Struct 2009;91:196-204

130. Sofiyev AH. The vibration and stability behavior of freely supported FGM conical shells subjected to external pressure. Compos Struct 2009; 89:356-366.

131. Tzou HS, Wang DW, Chai WK. Dynamics and distribution control of conical shells laminated with full and diagonal actuators. J Sound Vib 2002;256: 65-79.

132. Armenãkas, A.E., Gazis, D.C., Herrmann, G., 1969. Free Vibrations of Circular Cylindrical Shells. Pergamon Press Ltd., Oxford, UK.

133. Zill, D.G., Cullen, M.R. Differential Equations with Boundary-Value Problems, edition 7th, Cengage Learning, 2008

134. Timoshenko, S., Goodier, J.N., 1951. Theory of Elasticity, second ed. McGraw-Hill Book Co., Inc, New York.

135. Sokolnikoff, I.S., 1956. Mathematical Theory of Elasticity, second ed. McGraw-Hill Book Co., Inc, New York.

136. Flűgge, W., and Kelkar, V. S., 1968. The Problem of an Elastic Circular Cylinder. Int. J. Solids. Struct. 4(4), 397-420.

137. Qatu, M. S., 2004. Vibration of Homogeneous and Composite Thick Barrel Shells. J. Vib. Control. 10, 319-341.

138. Herrmann, G. Mirsky, I., 1956. Three-Dimensional and Shell Theory Analysis of Axially-Symmetric Motions of Cylinders. J. Appl. Mech. 23(4), 563-568.

139. Gazis, D.C., 1959. Three-Dimensional Investigation of the Propagation of Waves in Hollow Circular Cylinders. Part I-Analytical Foundation. J. Acoust. Soc. Amer. 31(5), 568-573.

140. Mirsky, I., 1965. Wave Propagation in Transversly Isotropic Circular Cylinders. Part I-Theory. J. Acoust. Soc. Amer. 37(6), 1016-1021.

141. Mirsky, I., 1964. Axisymmetric Vibration of Orthotropic Cylinders. J. Acoust. Soc. Amer. 36(11), 2106-2112.

142. Chou, F. H., Achenbach, J. D., 1972. Three-Dimensional Vibrations of Orthotropic Cylinders. J. Amer. Soc. Civil. Engineers. EM 4, 813-822.

143. Yuan, F. G., Hsieh, C. C., 1998. Three-Dimensional Solution of The Free Vibration Problem of Homogeneous Isotropic Cylindrical Shells and Panels. Composite Structures. 42, 153-167.

144. Soldatos, K. P., Hadjigeorgiou, V. P., 1990. Three-Dimensional Solution of The Free Vibration Problem of Homogeneous Isotropic Cylindrical Shells and Panels. J. Sound. Vib. 137(3), 369-384.

145. ABAQUS® manual, 6.9.

146. Kadi, A. S.: A Study and Comparison of the Equations of Thin Shell Theories. Ph.D. Dissertation, The Ohio State Univ., 1970.

147. Qatu, M.S., Sullivan, R.W., Wang, W., Recent research advances on the dynamic analysis of composite shells: 2000-2009, Composite Structures, Vol 93, No 1, pp 14-31,2010

148. Srinivas, S. Analysis of laminated, composite, circular cylindrical shells with general boundary conditions, NASA TR R-412, 1974

149. Shuvalov, A.L. “The Frobenius Power Series Solution For Cylindrically Anisotropic Radially Inhomogeneous Elastic Matericals”, Q. JI Mech. Appl. Math. 56 (3), 327-345, 2003